Dipl.-Ing. Marlene Petz

# Advanced Modeling of Resource Adequacy

**Doctoral thesis**
**to achieve the university degree of**
**Doctor of Technical Sciences, equivalent to the Doctor of Philosophy (PhD)**

**submitted to**
**Graz University of Technology**

Supervisor: Univ.-Prof. DDI Dr. Robert Schürhuber
Reviewer: Associate Prof. Dipl.-Ing. Dr.techn.Johann Auer

Institute of Electrical Power Systems

Graz, December 2024

# AFFIDAVIT

I declare that I have authored this thesis independently, that I have not used other than the declared sources/resources, and that I have explicitly indicated all material which has been quoted either literally or by content from the sources used. The text document uploaded to TUGRAZonline is identical to the present doctoral thesis.

Graz, 02.12.2024

Signature

# Contents

# List of Figures

# List of Tables

# Acknowledgement

Sieben Jahre nach der Erstellung des ersten probabilistischen Lastdeckungsmodells innerhalb der Abteilung für Versorgungssicherheit der Austrian Power Grid AG (APG) darf ich ein paar Dankesworte an die Wegbegleiter meiner vertiefenden Arbeit auf diesem Gebiet richten.

Initialer Dank gebührt meinem Kollegen vom belgischen Übertragungsnetzbetreiber ELIA, Daniel Huertas Hernandez, welcher mich vom Öffnen des ersten Modells bis zum heutigen Tag begleitet, unterstützt, gefordert und gefördert hat. Sehr bald begannen wir gemeinsam mit der Weiterentwicklung des Modells aber auch des Tools Antares mit Unterstützung von RTE. Ein besonderer Dank gilt hier den französischen Kollegen für die Aufnahme und Berücksichtigung des Feedbacks aus meiner Arbeit, sowie rte international für die Umsetzung der Entwicklungen im Tool. Der Austausch auf internationaler Ebene, mit Experten auf dem Gebiet, war stets ein großer Motivator während meiner Arbeit im Bereich System Adequacy sowie auf dem Weg zur Vollendung dieser Arbeit.

Besonders bedanken möchte ich mich bei meinem Team (APG System Adequacy Team), welches mich bei der Beschreibung der detaillierten Modellierung unterstützt, Weiterentwicklungen publiziert, und vor allem während meiner Bildungskarenz das Tagesgeschäft innerhalb der APG betreut hat. Gregorio, Alex, Anna und Simon, DANKE für eure Unterstützung und die vielen schönen gemeinsamen Jahre!

Ganz besonders möchte ich mich bei meinem persönlichen APG-Mentor Georg Achleitner bedanken. Georg du hast mir auf jedem Schritt meiner Karriere die richtigen Fragen gestellt, damit ich die Folgeschritte selbst veranlassen konnte. Ich danke dir Georg für die Einleitung meiner Dissertation „Advanced Modeling of Resource Adequacy“, zur Herstellung des Kontaktes mit Univ.-Prof. DDI Dr. Robert Schürhuber sowie deiner persönlichen Begleitung.

Besonderer Dank gebührt meinem betreuenden Professor des Instituts für elektrische Anlagen und Netze der Technischen Universität Graz Herrn Univ.-Prof. DDI Dr. Robert Schürhuber. Robert, du hast mich über die gesamte Laufzeit dieser Dissertation in regelmäßigem Austausch gefordert, meine Arbeit inhaltlich begleitet, ausführlich kommentiert und auf das abschließende Niveau gebracht. Vielen Dank dafür.

Ebenfalls bedanken möchte ich mich bei Associate Prof. Dipl.-Ing. Dr.techn. Johann Auer für den Review meiner Arbeit. Hans hat mich bereits durch mein Bachelor- und Masterstudium an der TU Wien begleitet, es freut mich, dich in meinem aktuellen akademischen Werk als Reviewer zu haben.

Acknowledgement

Bereits seit den ersten Studientagen an der TU Wien begleitet mich Lukas Schwalt als einer meiner engsten Freunde durch alle Prüfungen und Lebensabschnitte. Richtig gute Freunde über einen so langen Zeitraum an meiner Seite zu wissen, ist neben der Gesundheit, eines meiner wichtigsten Lebensgüter!

Abschließend möchte ich den größten Dank an meine Familie richten: meine Mama, mein Papa, mein Bruder Thomas und ganz besonders mein Freund Andreas. Ihr habt in den letzten Monaten Außerordentliches geleistet!

Liebe Mama, lieber Papa ihr habt mir mein Studium ermöglicht, welches mich an jenen Punkt meiner beruflichen Karriere brachte, wo ich heute stehe, und meine Dissertation einreiche. Euch beiden möchte ich diese Arbeit widmen!

# Abstract


The European energy system is changing. Thermal power plants are being decommissioned, the generation of renewable energies is being accelerated by subsidies from individual member states, and at the same time, grid expansion must be driven forward to support these changes. Probabilistic resource adequacy assessments have been established in Europe as a tool for evaluating the security of supply within a country and as a way of determining a possible starting point for the introduction of capacity markets.

In this thesis, the development of the methodology of probabilistic resource adequacy assessments, is discussed. Particular emphasis is placed on the further development of the models for developing the representation of hydropower. The calculations are carried out in Antares[1], a tool for efficiently performing probabilistic resource adequacy assessments.

In this paper, models with different pre-optimization processes for hydropower are discussed, as well as the introduction of water values and a detailed representation of swell power. Finally, the correct representation of short-term storage, which is used for closed-cycle pumped storage, is described and the representation for possible flexibility on the demand side is derived from this. In this context, large batteries participating on the market and the flexible components of electric vehicles and heat pumps are modeled.

The results of this work show a comparison of model results with historically measured values for the utilization of hydropower. The improved pre-optimization of hydropower from reservoirs in Austria can achieve a reduction of the deviation of the annual energy for turbines from 2.4 % to 0.1 %. For the annual pumping energy, a deviation of 13.5 % from historical measurements for pumped storage remains. Further improvement in the modeling of pumped storage power plants can be achieved by considering cascades of hydro power plants individually. In this work, the individual modeling of the hydropower cascade Kaprun is discussed. It leads to a 10 % higher pumping behavior compared to aggregated modeling, which is common in European calculations. The explicit modeling of swell power is also discussed in this work and implemented in a geographically reduced model (3 country nodes). The explicit modeling of swell power in the geographically reduced model leads to an improvement of up to 37 %. in the adequacy indicators. In a final step, an approach for modeling short-term storage is discussed that can also be applied to flexible demand components. In an academic approach, different penetration rates of batteries and flexible shares of heat pumps and electric vehicles are discussed. When the values for batteries published in the Austrian grid infrastructure plan [2] in combination with a flexible share of 50 %of heat pumps and electric vehicles are introduced, a 45 % reduction in the adequacy indicators can be achieved.

# Kurzfassung

Das europäische Energiesystem befindet sich im Wandel. Thermische Kraftwerke werden stillgelegt, die Erzeugung erneuerbarer Energien wird durch Subventionen einzelner Mitgliedstaaten beschleunigt und gleichzeitig muss der Netzausbau vorangetrieben werden. Probabilistische Abschätzungen der Angemessenheit der Resourcen haben sich in Europa als Instrument zur Bewertung der Versorgungssicherheit eines Landes sowie als Möglichkeit zur Bestimmung eines Ausgangspunkts für die Einführung von Kapazitätsmärkten etabliert.

In der vorliegenden Arbeit wird die Weiterentwicklung der Methodik probabilistischer Abschätzungen der Angemessenheit der Resourcen erörtert. Besonderes Augenmerk wird auf die Weiterentwicklung der Modelle zur Darstellung der Wasserkraft gelegt, die in Antares [1], einem Tool zur effizienten Durchführung probabilistischer Simulationen, durchgeführt werden. Es werden Modelle mit unterschiedlichen Voroptimierungsprozessen für Wasserkraft diskutiert, gefolgt von der Einführung von Wasserwerten und einer detaillierten Darstellung der Schwellkraft. Schließlich wird die korrekte Darstellung für Kurzzeitspeicher, die für Pumpspeicher mit geschlossenem Kreislauf verwendet wird, beschrieben und daraus die Darstellung für mögliche Flexibilität auf der Lastseite abgeleitet.

Die Ergebnisse dieser Arbeit zeigen einen Vergleich von Modellergebnissen mit historisch gemessenen Werten für die Nutzung von Wasserkraft. Durch die verbesserte Voroptimierung der Wasserkraft aus Stauseen in Österreich kann eine Reduzierung der Abweichung der Jahresenergie für Turbinen von 2.4 % auf 0.1 % erreicht werden. Für die jährliche Pumpenergie verbleibt eine Abweichung von 13.5 % von historischen Messungen für Pumpspeicher. Eine weitere Verbesserung der Modellierung von Pumpspeicherkraftwerken kann durch die individuelle Berücksichtigung von Kaskaden von Wasserkraftwerken erreicht werden. In dieser Arbeit wird die individuelle Abbildung der Kraftwerkskette Kaprun erörtert. Sie führt zu einem um 10 % höheren Pumpverhalten im Vergleich zur aggregierten Modellierung, die in europäischen Berechnungen üblich ist. Die explizite Modellierung von Schwellkraft wird in der Arbeit diskutiert und in einem geographisch reduzierten Modell (3 Länderknoten) durchgeführt. Die explizite Modellierung von Schwellkraft im reduzierten Modell führt zu einer Verbeseserung der Lastdeckungsindikatoren um bis zu 37 %. In einem letzten Schritt wird ein Ansatz zur Abbbildung von Kurzzeitspeichern diskutiert, der auch auf flexible Lastkomponenten angewendet werden kann. In einem akademischen Ansatz werden unterschiedliche Durchdringungsraten von marktteilnehmenden Batterien und flexible Anteile von Wärmepumpen und E-mobilität diskutiert. Bei Einführung der im österreichischen Netzinfrastrukturplan [2] veröffentlichten Werte für Batterien und einem flexiblen Anteil von Wärmepumpen und E-mobilität von 50 % kann eine Reduktion der Angemessenheitsindikatoren im europäischen Modell um 45 % erreicht werden.

# Abbreviations

| | |
|---|---|
| APG | Austrian Power Grid |
| APS | Annual Pump Storage |
| BHS | Battery Home Storage |
| BZR | Bidding Zone Review |
| CEP | Clean Energy for all Europeans package |
| CL | Closed Loop |
| CONE | Cost Of New Entry |
| CRM | Capacity Remuneration Mechanism |
| CY | Climate Year |
| DC | Data Center |
| DPS | Daily Pump Storage |
| DSR | Demand Side Response |
| EENS | Expected Energy Not Supplied |
| ENTSO-E | European Network of Transmission System Operators for Electricity |
| ERAA | European Resource Adequacy Assessment |
| EV | Electronic Vehicle |
| EVA | Economic Viability Assessment |
| GUI | Graphical User Interface |
| HP | Heat Pump |
| LCV | Light Commercial Vehicle |
| LLD | Loss of Load Duration |
| LOLE | Loss of Load Expectation |
| LOLP | Loss of Load Probability |
| LP | Linear Programming |
| MAF | Mid Term Adequacy Forecast |
| MCY | Monte Carlo Year |
| MILP | Mixed Integer Linear Programming |
| MS | Member State |
| NECP | National Energy and Climate Plans |
| NGC | Net Generation Capacity |
| NRA | National Regulatory Authorities |
| NTC | Net Transfer Capacity |
| OL | Open Loop |
| PCI | Project of Common Interest |
| PECD | Pan European Climate Database |
| PEMMDB | Pan European Market Modelling Database |
| PLEF | Pentalateral Energy Forum |
| POD | Proper Orthogonal Decomposition |

| | |
|---|---|
| PSP | Pump Storage Plant |
| PV | Photovoltaic |
| RA | Resource Adequacy |
| RC | Remaining Capacity |
| RES | Renewable Energy Source |
| SDS | Sustainable Development Scenario |
| ROR | Run Of River |
| RS | Reliability Standard |
| RSC | Regional Security Coordinator |
| RTE | Réseau de Transport d'Electricité |
| SMHI | Swedish Meteorological and Hydrological Institute |
| SO&AF | System Outlook and Adequacy Forecast |
| SoC | State of Charge |
| SOR | Summer Outlook Report |
| STA | Short Term Adequacy Assessment |
| SVD | Singular Value Decomposition |
| TSO | Transmission System Operator |
| TYNDP | Ten Year Network Development Plan |
| UCED | Unit Commitment and Economic Dispatch |
| VOLL | Value Of Lost Load |
| WOR | Winter Outlook Report |
| WPS | Weekly Pump Storage |

# 1 Introduction

The entire electricity generation mix in Europe is undergoing radical change: Thermal power plants, which are capable of generating band energy, are leaving the market due to phase-out programs for coal and nuclear energy. Non-dispatchable and volatile renewable energies are entering the market and need to be transmitted via the grid infrastructure. In the analysis to assess the adequacy of resources, an attempt is made to assess for each hour of the given target year whether the forecast demand can be covered by the available generation plus import capacities and storage technologies. When assessing the adequacy of resources, the representation of the future transmission grid (380 and 220 kV) is greatly reduced and replaced by an aggregated connection between two neighboring Member States (MS) by hourly values, the so-called Net Transfer Capacities (NTC). These assessments are carried out annually in order to monitor Europe-wide developments with regard to the development of the generation mix and developments on the electricity demand side. These assessments are carried out centrally by the European Network of Transmission System Operators for Electricity (ENTSO-E) in cooperation with the Transmission System Operators (TSOs) of the European Member States, which closely monitor and scrutinize the results of these processes. The results of the processes are of political importance and can trigger measures in the various Member States, such as the establishment of capacity remuneration mechanisms (CRM) after certain thresholds of the reliability standards (RS) of a Member State are exceeded.

Between 2017 and 2019, various developments were made to the resource adequacy assessment procedures required under the Clean Energy for All Europeans package (CEP) [3]. Firstly, Article 23 of Regulation 943 - the Electricity Regulation [4]: This article concerns the annual European process, i.e. the European Resource Adequacy Assessment (ERAA), and forces it to assess target years from two to ten years into the future. This assessment is carried out using a probabilistic, flow-based approach and an economic assessment of the power plant fleet is carried out for each scenario. Secondly, Regulation 941 - the Risk Preparedness Regulation [5]: This regulation concerns the short-term and seasonal adequacy processes, namely the winter and summer outlook (WOR, SOR) and the short-term adequacy process (STA). These processes also include a probabilistic adequacy assessment using the model established under the ERAA, which is updated by the TSOs using the latest available input data.

The above-mentioned regulations triggered methodologies, which were created and established by ENTSO-E together with TSO experts [6],[7],[8]. The methodological framework of future adequacy processes serves as basis for the development work performed within this thesis to gain knowledge regarding the advanced modeling of resource adequacy.

## 1.1 Research Scope

The first focus of this work is to further develop the representation of hydropower plants in resource adequacy assessments. To account for stochastic uncertainties, the assessments are performed on the basis of hundreds of Monte Carlo simulations. To reflect the volatile behavior of renewable generation and the temperature dependency on the demand side, climate-related generation and demand time series are merged with unplanned outages. This results in several hundred Monte Carlo samples. Since running several hundred simulations involves very long computing times, some simplifications are accepted in the representation of hydropower generation in the simulation.

The limitations of the simplified representation of hydropower (e.g. aggregation of generation types in one cluster per country node, addition of swell and run-of-river generation in the same cluster) were strongly questioned by the TSOs. Specifically for Austria, the Austrian TSO Austrian Power Grid AG (APG) questioned the aggregation of swell and run-of-river generation in a time series. This aggregation took place after the introduction of a new Europe-wide database format for European market modeling. This work examines the effects of certain simplifications in the mapping of hydropower and proposes improvements to the modeling.

Especially due to the hydro storage potential within Austria, a proper representation is of importance to avoid overestimation of flexibility resulting from simplified hydro representation.

As a second focus area of this thesis, the development of future additions to the electric load is presented in chapter 3.2, since these additions will provide a certain amount of flexibility to the future generation fleet. Therefore, joint investigations together with the Austrian Institute of Technology were triggered to estimate future penetration rates of heat pumps (HPs), electric vehicles (EVs) and batteries. In a second step, a modeling approach was investigated using these technologies together with their available storage potential within the European modeling framework but using a geographically reduced test model. This geographically reduced test model enables methodological investigations by executing calculations with reduced calculation time due to the smaller geographical scope.
The following list provides an overview of topics covered in the various chapters of the thesis:

- **Chapter 2:** introduction towards the overall topic of resource adequacy, highlighting the overall process landscape as well as details on the methodology
- **Chapter 3:** description of the input data used for adequacy processes
- **Chapter 4:** elaboration of the advanced modeling approaches for hydro representation
- **Chapter 5:** modeling approach of future additions to the load
- **Chapter 6:** results following the newly developed modelling approaches within this thesis

## 1.2 Research Question

This study addresses the following questions and examines improvements to existing approaches:

**Table 1.1:** Research questions

| Question | Chapter | Title |
|---|---|---|
| What are the current limitations on the hydro representation within the modeling framework of European Resource Adequacy Assessments? | 4 | New Concepts on Hydro Storage Representation within Antares |
| Which tool specific improvements can be developed? | 4 | New Concepts on Hydro Storage Representation within Antares |
| Which impact do the different representations have on the hourly dispatch? | 6 | Modeling and Results |
| Which additional storage components can be added to the generation system? | 5 | Investigations on additional storage and flexibility components |
| Which flexibility options do these additional components provide? | 6 | Modeling and Results |

## 1.3 Scientific Publications

In the course of the time during which this work was written, the progress of research was presented in several conference papers and a journal article. A Master thesis served as supporting work for the methodological development of the hydropower representation within the framework of the European Resource Adequacy Assessments. Joint research work was carried out with the Austrian Institute of Technology with regard to demand development. The results are also presented in conference and journal articles.

### Conferences

M. Petz, G. Achleitner, R. Schürhuber „Advanced modelling of generation adequacy in Europe"; 54$^{\text{th}}$ International Universities Power Engineering Conference 3 – 6 September 2019, Bucharest, Romania.

M. Petz, G. Achleitner „Generation Adequacy – Lastdeckungsanalysen: Derzeitige Aufgaben des Übertragungsnetzbetreibers und zukünftige Herausforderungen basierend auf den Forderungen des Clean Energy Packages“; 16. Symposium Energieinnovation 12 – 14 February 2020, Graz, Austria.

M. Petz, G. Achleitner, B. Mihic, R. Schürhuber „Resource Adequacy Methodologies in the European framework - how to take flexibilities into account in future modelling of resource adequacy?”; CIRED Workshop 22 – 23 September 2020, Berlin, Germany.

M. Petz, D. Meier, J. Hierzer, K. Misak, A. Bres, J. Spreitzhofer „Entwicklung zukünftiger Lastkomponenten und deren mögliche Auswirkung auf die Lastdeckungssituation in Österreich am Beispiel des Wärmepumpenzuwachses bis 2030“; 12. Internationale Energiewirtschaftstagung an der TU Wien, 09 September 2021, Wien, Austria.

M. Petz, G. Achleitner, B. Mihic, R. Schürhuber „Resource Adequacy Methodologies – future flexibility options added to Austria’s generation fleet and its impact on adequacy”; CIRED 2021 Conference 20 – 23 September 2021, Geneva, Switzerland.

M. Petz, G. Achleitner, B. Mihic, R. Schürhuber „Modelling of Resource Adequacy in the Mid Term Adequacy Forecast using a new Europe wide database format – impact on hydro usage and its flexibility”; CIGRE SEERC 29 November 2021, Vienna, Austria.

**Journals**

M. Petz, D. Meier, J. Hierzer, G. Achleitner, A. Bres, J. Spreitzhofer „Wärmpumpenzuwachs in Österreich bis 2030 und dessen Auswirkung auf Lastprofile – Sensitivitäten am Beispiel eines Testmodells für europäische Lastdeckungsanalysen“, e & i Elektrotechnik und Informationstechnik, Springer-Verlag, Wien, Austria, 2021.

**Supportive Thesis**

G. Iotti “Hydropower Modelling in Mid-Term Adequacy Forecasts in the peculiar case of Austria”, Politecnico de Milano, Milano, Italy, 2020.

S. Bauchinger “Vergleich unterschiedlicher Modellierungsansätze zur Abbildung von Lauf- und Schwellkraft in europäischen Lastdeckungsanalysen”, Vienna University of Technology, Vienna, Austria, 2022.

S. Bürbaum “Enhanced representation of hydro generation in resource adequacy models - using the example of power plant cascade Kaprun”, Vienna University of Technology, Vienna, Austria, 2023.

# 2 Current Methodology

The following chapter provides an overview of the methodology used to assess resource adequacy in the electricity sector. It begins with an overview of the history of European litigation and the current legal landscape, followed by the definition of probabilistic adequacy assessments using Monte Carlo simulations. The indicators used to assess resource adequacy, namely Loss of Load Expectation, LOLE, [LOLE] = h/a, and Expected Energy Not Supplied, EENS, [EENS] = MWh/a, are described and the optimization problem is specified.

As far as the adequacy of the system in the electricity sector is concerned, the distinction between resource adequacy and transmission adequacy needs to be clarified:

**Transmission Adequacy Assessments** are carried out for a period of up to 20 years in the future, identifying bottlenecks in the European grid infrastructure and providing potential projects of common interest (PCIs) from each TSO to increase the reliability of the grid infrastructure of the future. The best-known procedure in the European framework is the Ten-Year Network Development Plan (TYNDP) [9].

**Resource Adequacy Assessments** aim to determine whether the future demand for electricity can be met at every hour of a future target year by the available generation within a country and by possible import and storage capacities. The adequacy indicators Loss of Load Expectation (LOLE) as well as Expected Energy not Supplied (EENS) are used to determine the scarcity situation in the individual Member States (MS).

## 2.1 European process history

Until 2016, ENTSO-E carried out the assessment of resource adequacy using a deterministic approach in which only one hour per week was analyzed. Every Wednesday at 7 p.m. was considered: For each generation type, the total installed generation power was recorded and possible generation outages and the availability of renewables were taken into account. The minimum demand, downward reserve requirements and the need for pumped storage power were recorded and evaluated. The remaining capacity (RC) per country was calculated, taking into account cross-border electricity flows between two countries using Net Transfer Capacities (NTC) time series in hourly resolution [10]. Figure 2.1 shows the evolution over time of the of mid-term resource adequacy assessments, which aim to assess the adequacy of resources for the upcoming decade, using different target years and methodologies.

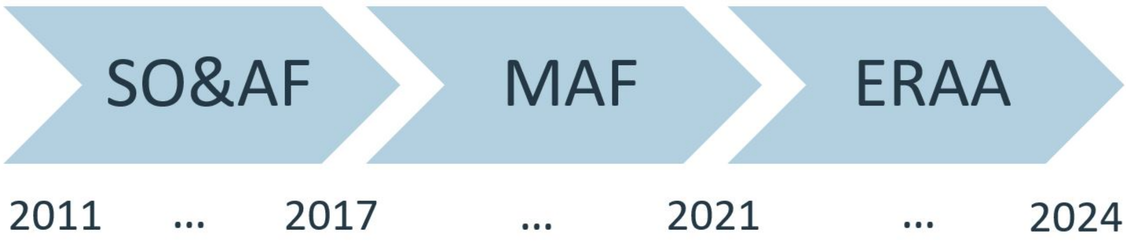


**Figure 2.1:** Historical development of the Mid-term Adequacy Forecasts products

For the semi-annual interim report entitled **System Outlook and Adequacy Forecast** (SO&AF) the data for the 3$^{rd}$ Wednesday in January at 7 p.m. and the 3$^{rd}$ Wednesday in July at 11 a.m. were collected. This report covered power plant generation as well as some operational restrictions (e.g. maintenance work). The SO&AF was the very first report that assessed resource adequacy for the mid-term time horizon up to 10 years in the future following a deterministic calculation [10].

As more and more highly volatile renewable resources entered the market, the purely deterministic approach was not considered sufficient anymore. As of 2018 an advanced approach takes into account the stochastic uncertainty resulting from volatile renewable generation using Monte Carlo simulations.

The first process to follow this Monte Carlo approach and carry out stochastic resource adequacy assessments was the **Mid-Term Adequacy Forecast** (MAF) [11]. This process developed over the period between 2017 and 2020 and was the successor of the System Outlook and Adequacy Forecast (SO&AF). In 2021, the MAF process was replaced by the **European Resource Adequacy Assessment** (ERAA).

With the entry-into-force of the Electricity Regulation in 2019, high political pressure was put on the European Resource Adequacy Assessment. The ERAA process follows requirements of Article 23 of the Electricity Regulation 2019/943, so that the assessment [4]:

- identifies resource adequacy concerns by assessing the overall adequacy of the electricity system to meet current and projected electricity demand at Union, Member State and bidding zone level
- covers each year within a period of 10 years from the date of assessment
- is conducted by ENTSO-E, which also drafts a methodology that is submitted to the Electricity Coordination Group; the TSOs must provide ENTSO-E with the relevant input data
- is carried out on annual basis
- is based on a transparent methodology

Following the above listed requirements from the regulation, the ENTSO-E methodology drafted in 2019 foresees that the process [6]:

- is carried out at the level of each bidding zone (at least all Member States)
- is based on central reference scenarios for projected demand and supply, including an economic assessment of the likelihood of retirement, mothballing, new build of generation assets and measures to reach energy efficiency and electricity interconnection targets, as well as appropriate sensitivities on extreme weather events, hydrological conditions, wholesale prices and carbon price developments
- contains separate scenarios to consider the likelihood of resource adequacy concerns occurring following the implementation of different capacity mechanism designs
- considers the contribution of all resources, including existing and future opportunities for generation, energy storage, sectoral integration, demand response and imports and exports and their contribution to flexible grid operation
- includes variants with and without existing or planned capacity mechanisms
- is based on a market model using the flow-based approach (where applicable)
- applies probabilistic calculations
- applies a single modeling tool
- includes indicators 'loss of load expectation' and 'expected energy not served'
- identifies the sources of possible resource adequacy concerns, be it a network constraint, a resource constraint or both
- takes into account real network development
- ensures that the national characteristics of generation, demand flexibility and energy storage as well as the availability of primary resources and the level of interconnection are properly taken into account

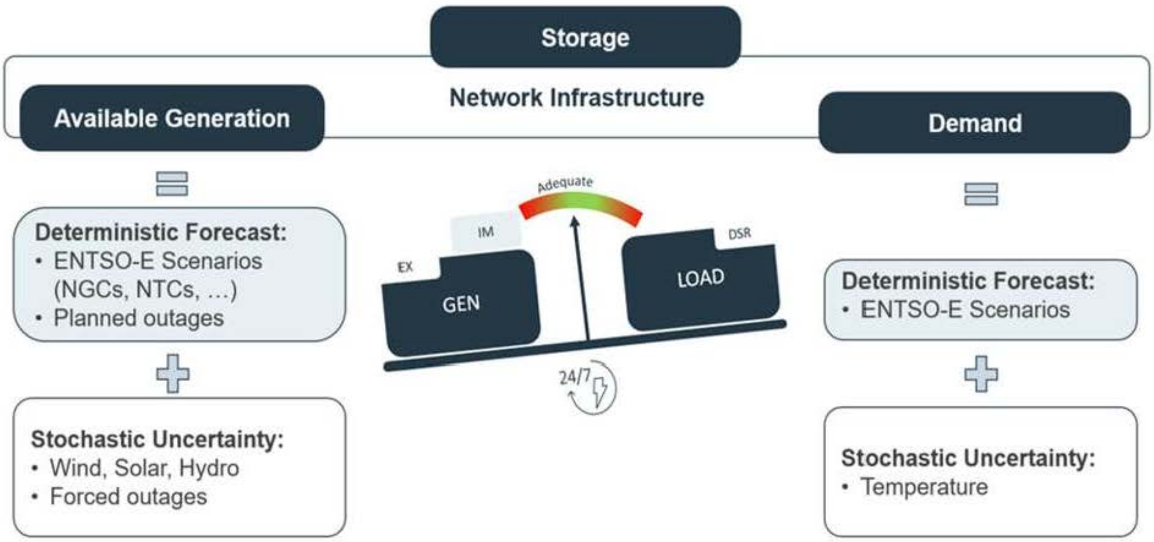


**Figure 2.2:** Resource adequacy assessment methodology following the ENTSO-E approach [11]

Figure 2.2 shows the basic structure of resource adequacy assessments, which take into account:

- TSO deterministic input variables (net generation capacity, net transmission capacity, planned outages)
- centrally generated climate year dependent stochastic input data for renewable generation
- centrally generated climate year dependent stochastic demand projections

In order to reflect stochastic uncertainties (climate variables, unplanned outages), a probabilistic approach using Monte Carlo simulations is used to assess the adequacy of resources, the details of which are described in chapter 2.3.

## 2.2 European process landscape

The European process landscape ranges from long-term investment decisions with time horizons of up to 20 years into the future to day-to-day business, where the short-term adequacy process (STA) is located. Figure 2.3 provides an overview of the European adequacy processes, ranging from long-term investments such as the Ten-Year Network Development Plan (TYNDP) to medium-term policy (ERAA), seasonal outlooks (SOR) and short-term adequacy processes (STA).

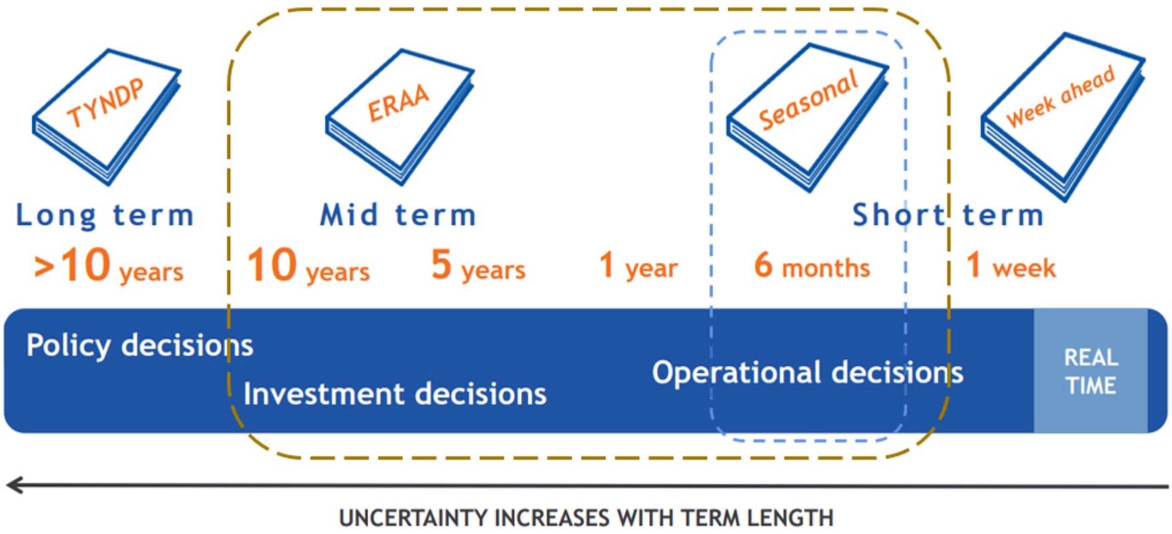


**Figure 2.3:** European processes for adequacy assessments [12]

- **Short Term Adequacy (STA)** processes operate close to the real-time time horizon and are executed in a TSO's operations control center. The STA process performs daily calculations with a rolling forecast window of one week in advance to analyze the adequacy of resources for the next seven days. For this process, forecast data for renewable energy, hydropower and electricity demand are taken from the near-real-time processes (Day Ahead Congestion Forecast also known as DACF, and Intraday Congestion Forecast, also known as IDCF). The input data is transferred using automatic routines and the adequacy calculation is carried out centrally. The individual results of the process are returned to the TSOs and load coverage is indicated by the indicators EENS and LOLE. The remaining capacity (RC) per hour is reported and can be extracted for each country individually.

- **The Seasonal Outlook Report (SOR)** is a semi-annually calculated process whose forecast is aimed at the next six months, with ENTSO-E asking the TSOs to provide input data twice a year. In exceptional cases, such as the gas crises in 2022, additional data is collected. The calculation of the seasonal outlook partly follows the methodology developed for the ERAA, whereby probabilistic assessments with 35 historical climate years and generation capacities provided by the TSOs form the base model. An NTC representation is used for cross-border exchanges. The LOLE and EENS adequacy indicators are the result of the report.

- **The European Resource Adequacy Assessment (ERAA)** focuses on the midium-term time horizon and is carried out once a year with focus on the next ten years. The target methodology is to forecast each of the ten years. In the 2021 - 2023 ERAA editions, only two to four years are assessed in the 10-year time frame and the results are given in LOLE and EENS. This probabilistic annual calculation is the central adequacy procedure of ENTSO-E and its results are used in many Member States to assess the need for capacity remuneration mechanisms.

- **Ten Year Network Development Plan (TYNDP):** This process is not a resource adequacy process as its main objective is the adequacy of transmission capacity. For the sake of completeness, it is listed in the overview in order to have all ENTSO-E system development products at a glance.

While Mid Term Adequacy Forecast (MAF) processes were carried out using five different modeling tools (PLEXOS [13], GRARE [14], ANTARES [1], BID3 [15], PowerSym [16]), whose results were first compared with each other and in a second step the averaged results of the five tools were published in the MAF report, the ERAA methodology stipulates that only results of one tool are published by ENTSO-E. For the ERAA 2021 process, PLEXOS and ANTARES provided results, with only the PLEXOS results being published in the ERAA 2021 report. For the ERAA 2022 and 2023 editions, the officially published results are obtained with PLEXOS, which has been specified as the official ENTSO-E modeling tool.

Antares users such as the French, Belgian and Austrian TSOs (RTE [17], ELIA [18] and APG [19]) create Antares models based on ERAA input data and use them for national activities, such as the ELIA Adequacy and Flexibility study for Belgium 2024 -2034 [20] or Les bilans prévisionnels from RTE [21]. Methodological developments in the ERAA process also result from national studies carried out by RTE and ELIA.

This thesis addresses the development needs identified in a comparison of the hydropower representation between the MAF 2018 and MAF 2019 methodologies, which was conducted as part of a master's thesis focusing on the Antares representation [22]. The approaches described in this thesis follow the probabilistic methodology used in the MAF 2019 and later ERAA editions. The following methodological developments discussed in this thesis have been incorporated into the ERAA model:

- ERAA 2021: split between run-of-river and swell power (see chapter 4.4)
- ERAA 2021: new representation for short cycle pumped storage plants (see chapter 4.3)
- ERAA 2021: implementation of market participating batteries (see chapter 5.1)
- ERAA 2022: implicit demand side response (iDSR) resulting from heat pumps and electric vehicles (see chapter 5.2)
- ERAA 2022: implementation of water values (see chapter 4.2)

As a by-product of the developments in the modeling of hydropower with short cycle storage, a possible approach for modeling flexible demand components was introduced in the framework of ERAA 2022. The developments discussed in this thesis are the result of discussions between the R&D work of the French TSO and experts from the Austrian and Belgian TSOs.

In ERAA 2024, the TSOs using Antares perform a parallel calculation stream with the aim of providing Antares results alongside the official PLEXOS ERAA 2024 report. The official PLEXOS ERAA 2024 model is created by ENTSO-E staff together with the TSOs using PLEXOS (e.g. TenneT [23], 50Hertz [24], PSE [25], Terna [26], Eirgrid [27]). The calculation is shared between the TSOs and the ENTSO-E in order to obtain the results in a reasonable calculation time (two weeks calculation time for four target years).

Article 20 of the Electricity Regulation [4] provides that Member States monitor resource adequacy in their territory on the basis of existing European processes and, where appropriate, supplement them with national studies. The work carried out as part of this thesis helps to guide decisions and developments towards a possible National Resource Adequacy Assessment (NRAA) in Austria.

In addition to the ENTSO-E process landscape, the Pentalateral Energy Forum (PLEF) consortium was founded. Within the PENTA region, which includes Belgium, the Netherlands, France, Luxembourg, Germany, Austria and Switzerland, transmission system operators, national regulatory authorities (NRAs) and Member State (MS) representatives work closely together to assess the regional impact of resource adequacy concerns. Therefore, a Pentalateral Energy Forums' report based on ENTSO-E input data,was prepared in 2015 [28], 2018 [29] and 2020 [30], providing a detailed assessment for the PENTA region.

As the ERAA is the most advanced and methodologically strongest assessment, the representatives of the PENTA countries have decided to refrain from individual regional assessments and to support the ERAA process with additional studies that provide further insights into the input data and the improvement of the methodology, at least for the PENTA countries [31].

## 2.3 Monte Carlo Simulations

A Monte Carlo simulation approach is used to reflect the stochastic uncertainty resulting from the climate-dependent time series of renewable generation and temperature-dependent demand on the one hand and the unplanned outages of generation and cross border interconnection on the other. Within the ERAA methodology, these Monte Carlo simulations are derived by a combination of $M$ climate-dependent input time series (1982 - 2016) from renewable generation and demand, which are combined in a second step with $N$ unplanned forced outage patterns for thermal units and cross border interconnections. The number of unplanned outages varies between 10 to 20 and is chosen to ensure model convergence. For the MAF processes, the convergence of the different tools was compared using the coefficient of convergence ($\upsilon$), while an acceptable low number of unplanned forced outage patters was selected for the later ERAA editions due to the increased model complexity.

The convergence of the overall model is assessed on the basis of results of the entire geographical scope using the EENS indicator, whereby the coefficient of variation ($\upsilon$) is calculated as follows:

$\upsilon = \frac{\sqrt{\mathrm{Var(EENS)}}}{\mathrm{EENS}}$, with $\mathrm{Var(EENS)} = \frac{\mathrm{Var(ENS)}}{N}$

where

| | |
|---|---|
| $\upsilon$ | coefficient of variation |
| Var(EENS) | variance of the expectation estimate |
| EENS | Expected Energy Not Served |
| ENS | Energy not supplied in a given Monte Carlo Year |
| $N$ | Number of Monte Carlo Simulations considered |

Figure 2.4 shows the development of the coefficient of variation with an increasing number of Monte Carlo simulations performed. It can be assumed that no significant changes in $\upsilon$ are to be expected with a further increase in the number of Monte Carlo samples. The interpretation of the figure leaves the leeway to carry out between 10 to 20 random draws for unplanned outages.

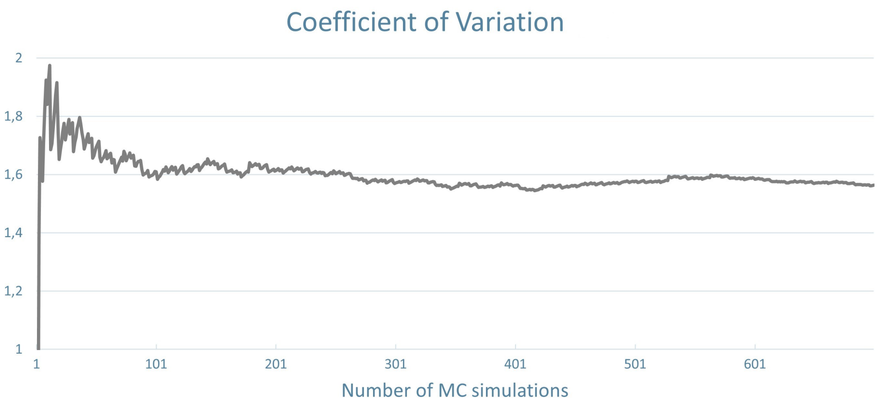


**Figure 2.4:** Evolution of the coefficient of variation ($\upsilon$) with increasing number of Monte Carlo Samples [11]

In both the MAF processes and in ERAA 2021, a subset of $M = 35$ historical climate years (1982 - 2016) is used and merged with a set of $N = 20$ random draws for unplanned outages. This results in 700 Monte Carlo simulations. When introducing higher complexity, such as a flow-based representation for cross-border capacities, the number of $N$ is reduced to 10.
In the course of process development, the number of $N$ decreased from originally $N = 30$ in the MAF process to $N$=20 in early the ERAA 2021 process and is now $N = 10$ in the latest processes, in which a flow-based representation is also available.

Figure 2.5 illustrates the sampling of $M$ climate-dependent input time series with $N$ random draws for unplanned outages according to the ERAA methodology [6].

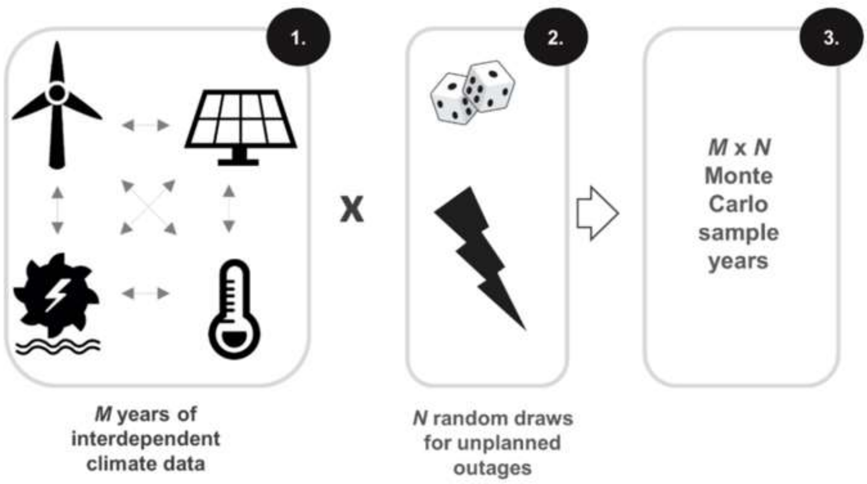


**Figure 2.5:** Sampling of the Monte Carlo time series [32]

For each Monte Carlo set, a full economic simulation is performed in which marginal costs are calculated as a part of a cost minimization problem (Unit Commitment and Economic Dispatch – UCED approach) formulated as a large scale mixed integer linear programming (MILP) problem. Details about the methodology can be found in chapter 2.5.

## 2.4 Adequacy Indicators

As several hundred result time series are evaluated, a statistical approach is used to provide adequacy indicators for each bidding zone. The average over all Monte Carlo samples and all hours of a simulated target year is calculated. These averages provide an overview of the results in the different Member States, which is typically used in discussions with stakeholders (ministries, regulators, etc.). Percentile values, namely P5 and P95, are also available in the appendix of the adequacy reports, while the focus of the comparison of results in the ERAA report and in this thesis remains on the mean values.

In probabilistic adequacy assessments, two main indicators are used to benchmark results:

**Expected Energy Not Served, EENS [EENS] = GWh/a**: is the expected energy that is not supplied by a generating system because demand exceeds the available generation and import capacity within a year, as an average over all Monte Carlo samples performed [33].

$$\mathrm{EENS} = \frac{1}{N} \cdot \sum_{i=1}^{N} \mathrm{ENS}_i \tag{2.1}$$

| | |
|---|---|
| ENS | the energy that is not served in a bidding zone for a single Monte Carlo sample because the demand within the bidding zone exceeds the available resource capacity plus possible imports. |
| EENS | Expected Energy Not Served in a single bidding zone is the mathematical average of the calculated ENS over the total number of Monte Carlo samples |
| $N$ | number of Monte Carlo simulations considered |
| $i$ | index variable - Monte Carlo simulations |

A loss of load event is an hour in a particular Monte Carlo simulation in which the demand exceeds the available generation and import capacity.

**Loss Of Load Expectation, LOLE, [LOLE] = h/a:** is the number of hours in a given period (e.g. a year) in which the available generation plus imports cannot cover the demand within a bidding zone.

$$\text{LOLE} = \frac{1}{N} \cdot \sum_{i=1}^{N} \text{LLD}_i \tag{2.2}$$

| | |
|---|---|
| LOLE | Loss of Load Expectation is the average of the Loss of Load Duration over the total number of Monte Carlo samples. |
| LLD | Loss of Load Duration is the number of hours per year in which the bidding zone is affected by ENS during a single Monte Carlo simulation. The LLD can only be specified as an integer number of hours, as the calculation is carried out in hourly resolution. It does not provide a statement about the severity of an event. |
| $N$ | number of Monte Carlo simulations considered |
| $i$ | index variable - Monte Carlo simulations |

Loss of Load Expectation is a value that is generally used to compare the results of individual bidding zones, but does not provide a statement about the depth or severity of the scarcity event. LOLE and EENS should therefore be interpreted in conjunction.

## 2.5 Optimal unit commitment and economic dispatch (UCED)

Once the total amount of Monte Carlo samples is determined, the optimization problem of the adequacy simulations follows a total cost minimization approach, which is performed for each Monte Carlo sample and provides results for each hour of the evaluated target year. In this chapter, first the overall cost minimization problem is formulated following an optimal unit commitment and economic dispatch (UCED) approach. Then, the specifics of the Antares tool are explained, which applies different methods to pre-optimize hydropower plants, followed by the description of the Antares optimization problem.

The optimization attempts to find the most cost effective solution on a weekly basis that provides hourly results according to an optimal Unit Commitment and Economic Dispatch approach. The objective of the UCED problem is to find the optimal power dispatch to meet the hourly electricity demand, taking into account hard and soft technical constraints. Hard constraints must always be met, while soft constraints can be violated with high penalty costs. As described by Wood, et al. [34], the problem is formulated as follows:

Assuming there are a number of subsets of the full set of $N_{\text{gen}}$ generating units that would satisfy the expected demand, which of these subsets should be used to minimize operating cost?

Tools for solving a unit commitment problem are priority list schemes, dynamic programming (DP) or lagrange relaxation (LR) or a mixed integer linear problem (MILP). The solution of an MILP approach in the pan-European electricity system leads to an enormous computational effort without a feasible solution being found. In order to simplify the MILP solution attempt, several assumptions and restrictions are made that lead to a simplification of the models and a reduction of the MILP to linear programming (LP). Tool-specific heuristics are also applied and discussed (see chapter 2.6.1). In the MAF and ERAA calculations, certain technical constraints of thermal units are relaxed so that a simplified optimization problem can be solved using a pure linear programming (LP) approach.

**MILP problem formulation**

A Mixed Integer Linear Problem in its basic formulation is defined as follows [35]:

Objective function with the aim to minimize overall costs

$\min \mathbf{c}^{\mathsf{T}} \cdot \mathbf{x}$

subject to

$\mathbf{A}_{\mathrm{neq}} \cdot \mathbf{x} \leq \mathbf{b}_{\mathrm{neq}}$

$\mathbf{A}_{\mathrm{eq}} \cdot \mathbf{x} = \mathbf{b}_{\mathrm{eq}}$

$\mathbf{l}_{\mathrm{b}} \leq \mathbf{x} \leq \mathbf{u}_{\mathrm{b}}$

where

| | |
|---|---|
| $\mathbf{c}^{\mathsf{T}}$ | column vector of constants |
| $\mathbf{x}$ | column vector of unknown variables |
| $\mathbf{A}_{\mathrm{neq}}$ | inequality system matrix |
| $\mathbf{A}_{\mathrm{eq}}$ | equality system matrix |
| $\mathbf{b}_{\mathrm{neq}}$ | inequality vector of constants (known) |
| $\mathbf{b}_{\mathrm{eq}}$ | equality vector of constants (known) |
| $\mathbf{l}_{\mathrm{b}}$ | vector of lower bound |
| $\mathbf{u}_{\mathrm{b}}$ | vector of upper bound |

The objective function describes the overall optimization problem (minimizing total generation costs) taking into account a number of constraints, which are specified below in more details.

### 2.5.1 Thermal generation

Transforming the MILP formulation described above into a thermal generation fleet that attempts to answer the UCED question, the problem is as follows [34]:

1. Introduce a set of Boolean support variables:

Define $\mathrm{U}_{i,t}$ as $\mathrm{U}_{i,t} = 0$ if the unit $i$ is offline during the period $t$

Define $\mathrm{U}_{i,t}$ as $\mathrm{U}_{i,t} = 1$ if the unit $i$ is online during the period $t$

| | |
|---|---|
| $t$ | period of assessment $(1 \ldots T)$ |
| $i$ | index variable $(1 \ldots N_{\text{gen}})$ |
| $\mathrm{U}_{i,t}$ | Boolean variable indicating if the unit $i$ is in operation $(\mathrm{U} = 1)$ or offline $(\mathrm{U} = 0)$ during period $t$ |

2. Introduce the objective function as follows:

$$\min \sum_{t=1}^{T} \sum_{i=1}^{N_{\text{gen}}} [\mathrm{C}_i(\mathrm{P}_{i,t}) + \mathrm{C}_{\text{start}\,i,t}] \cdot \mathrm{U}_{i,t} = \mathrm{C}(\mathrm{P}_{i,t}, \mathrm{U}_{i,t})$$

| | |
|---|---|
| $t$ | period of assessment $(1 \ldots T)$ |
| $T$ | upper time bound of period of assessment |
| $i$ | index variable $(1 \ldots N_{\text{Gen}})$ |
| $N_{\text{Gen}}$ | number of generating units in the system |
| $\mathrm{C}_i(\mathrm{P}_{i,t})$ | cost of the unit $i$ during period $t$ |
| $\mathrm{C}(\mathrm{P}_i,\mathrm{U}_i)$ | total system costs |
| $\mathrm{C}_{\text{start},i,t}$ | start-up costs result from a certain amount of energy that must be expended to bring the unit on-line |
| $\mathrm{P}_{i,t}$ | electrical power output of the unit $i$ during period $t$ |
| $\mathrm{U}_{i,t}$ | Boolean variable indicating if unit $i$ is on $(\mathrm{U} = 1)$ or offline $(\mathrm{U} = 0)$ during period $t$ |

3. Introduce additional constraints which need to be respected:

Loading constraint: $\mathrm{P}_{\text{load,t}} - \sum_{i=1}^{N_{\text{gen}}} \mathrm{P}_{i,t} \cdot \mathrm{U}_{i,t} = 0,\ \text{for } i = 1 \ldots N_{\text{gen}} \ \text{ and } \ t = 1 \ldots T$

Unit limits: $\mathrm{U}_{i,t} \cdot \mathrm{P}_{\text{i,min}} \leq \mathrm{P}_{i,t} \leq \mathrm{U}_{i,t} \cdot \mathrm{P}_{\text{i,max}}, \ \text{ for } \ i = 1 \ldots N_{\text{gen}} \ \text{ and } \ t = 1 \ldots T$

| | |
|---|---|
| $t$ | period of assessment $(1 \ldots T)$ |
| $T$ | upper time bound of period of assessment |
| $i$ | index variable $(1 \ldots N_{\text{Gen}})$ |
| $N_{\text{Gen}}$ | number of generating units in the system |
| $\mathrm{P}_{i,t}$ | electrical power output of the unit $i$ during period $t$ |
| $\mathrm{U}_{i,t}$ | Boolean variable indication if unit $i$ is on $(\mathrm{U} = 1)$ or offline $(\mathrm{U} = 0)$ during period $t$ |
| $\mathrm{P}_{\text{load,t}}$ | total system load which needs to be covered |
| $\mathrm{P}_{\text{i,max}}$ | maximum electrical power output of the unit $i$ |
| $\mathrm{P}_{\text{i,min}}$ | minimum electrical power output of the unit $i$ |

The above restrictions lead to the existence of integer variables that describe the *on* and *off* state of the thermal units and define the minimum operating hours of each thermal unit.

Within the optimization the following constraints must be respected:

As the temperature and pressure of thermal power plants have to be changed slowly, a certain amount of energy is required to start up the plant. This amount of energy is not stated in MW, but is taken into account as the start-up costs of a unit. The maximum amount of start-up costs results from a cold start, when a unit was completely shut down, and can be correspondingly lower if a unit has only recently been shut down and is still close to operating temperature. If a unit has been shut down for some time, there are two different approaches to bring it back up to operating temperature:

- **cooling:** allows the unit's boiler to cool down and return to operating temperature in good time before commissioning
- **banking:** the boiler must be supplied with sufficient energy to maintain the operating temperature

Up to a certain amount of hours, the start-up costs for banking are lower than the start-up costs of cooling.

The following additional constraints for thermal power plants are taken into account when calculating resource adequacy:

- **forced outage rate:** likelihood of an unplanned outage
- **must run profiles in MW:** during certain periods, specific units can call up a must-run status, i.e. the units are always dispatched in full or in part according to their must-run profile supplied as an hourly profile
- **minimum stable level in MW:** minimal operation level of a unit
- **derating profiles in MW:** user inputs with hourly restrictions for individual units or a group of units
- **planned outages:** The planned shutdowns of generation units are usually planned months or years in advance and made available via the input data collection
- **Start-up time in hours:** time interval required to bring a unit from zero to its minimum stable level

whereas additional constraints added to the MILP problem, such as

- **ramping up and down rates:** thermal units cannot change their output power more than a certain amount within a given time frame
- **unit minimum up- time:** once the unit is up and running it should not immediately be turned off
- **unit minimum down- time:** once the unit is down it should not be immediately be turned on
- **transmission security constraints:** constraints that force a dispatch of generation in a way that no transmission lines are overloaded
- **spinning reserve constraints:** reserve power supply that remains online but unloaded an is ready to respond rapidly in the event of a shortfall.
- **air quality constraints:** limits on emissions from fossil-fired plants
- **generator fuel limit constraints:** Certain units have limitations on the amount of fuel available or have a requirement to burn a certain amount of fuel
- **crew constraints:** if a plant consists of several units, multiple units cannot be turned on at the same time since there are not enough crew members

are not considered in the resource adequacy calculations.

### 2.5.2 Hydro generation

As part of the optimization approach for the adequacy simulations, run of river generation is scheduled at hourly zero costs and thus deducted from the demand profile.

The available energy from hydropower storage units is the result of the pre-optimization step for hydropower and is transferred to the solver as a daily hydropower energy quantity. These hydropower energy lots are included in the optimization problem together with the thermal properties and must take into account the various thermal boundary conditions formulated above.

The loading constraints and unit constraints introduced in the MILP formulation above are extended to consider hydrological units and to include the cost of hydro units in the minimization function. The advanced hydro-optimization approach described in this thesis calculates a value for each filling level of a hydro reservoir (so-called water values) using Bellman's optimality principle. The presentation of this approach is elaborated in the chapter 2.6.2.

### 2.5.3 Wind generation

As part of the optimization approach for the adequacy simulations, wind generation is scheduled at hourly zero costs and thus deducted from the demand profile.

### 2.5.4 Photovoltaic generation

As part of the optimization approach for the adequacy simulations, photovoltaic generation is scheduled at hourly zero costs and thus deducted from the demand profile.

The UCED optimization of the resource adequacy simulations follows a perfect market forecast: all available capacity types are known in advance with perfect accuracy, no deviations between forecast and realization are expected, this also implies a perfect allocation of storage capacities within the year.

## 2.6 Antares Optimization

The Antares simulator is an open-source tool developed by the French TSO RTE [17], allowing the user to enter and update input data by a Graphical User Interface (GUI). The input data can be provided by direct input via the GUI. Due to the large amount of input data for a pan-European model, automated input routines help to store a large amount of input data in .txt files that serve a defined folder structure. A typical simulation follows several consecutive steps [36]:

1. input data provision by the user (via GUI or scripting routines for large amount of input data)
    a) ready-made time series by the user
    b) providing stochastic modeling parameters to let the simulator generate time series (via the time-series generator)
2. setting the sampling preferences (e.g. number of Monte Carlo years, sampling approach)
3. core optimization (hydro energy manager & unit commitment optimizer)
4. exporting routines to analyze the results

Figure 2.6 illustrates the above-mentioned steps that the Antares simulator follows to carry out adequacy simulations.

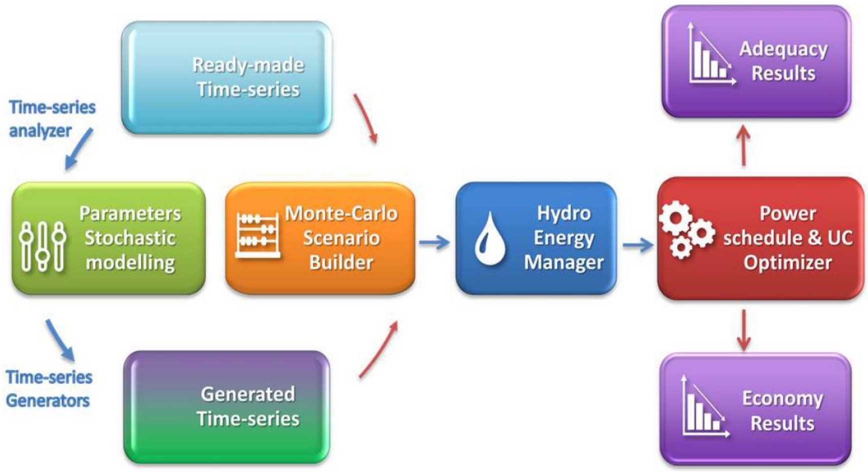


**Figure 2.6:** Antares Simulator overview [36]

This chapter explains details of the hydro energy manager (dark blue box in Figure 2.6), which performs the hydro pre-allocation, followed by the overall Antares solution for solving the unit commitment (red box in Figure 2.6). The hydro pre-allocation is used to break down the hydropower information provided by the TSO (e.g. time series for hydro inflows and minimum and maximum filling levels) into monthly or daily energy quantities that are later used in the unit allocation phase (red box in Figure 2.6 - power schedule & UC Optimizer).

While generation from run of river units is generally provided by hydro inflow time series in hourly resolution, which are dispatched at zero cost immediately, for hydro storage basins the pre-allocation is performed based on a net load proportional heuristic as described in chapter 2.6.1. Net load in this case is understood as the total load of a bidding zone from which renewable generation such as run of river, wind, PV, biomass, biogas, waste, geothermal as well as must-run thermal generation is subtracted. After the Antares tool was improved (version 7), the hydro pre-optimziation can be also carried out with a dynamic programming approach, which is explained in more detail in chapter 2.6.2.

### 2.6.1 Hydro pre-allocation using net load proportional heuristic

In accordance with the ENTSO-E guidelines for data collection [37], TSOs provide minimum and maximum filling levels of the hydro reservoir in weekly resolution (Figure 2.7) together with the hydro inflows to the hydro reservoir for all climate years. The Antares pre-allocation of hydropower is used to break down the hydropower information by the TSOs (hydro inflows and reservoir minimum and maximum filling levels) into the relative hydropower quantities (monthly and daily energy lots), which are then used in the unit commitment phase.

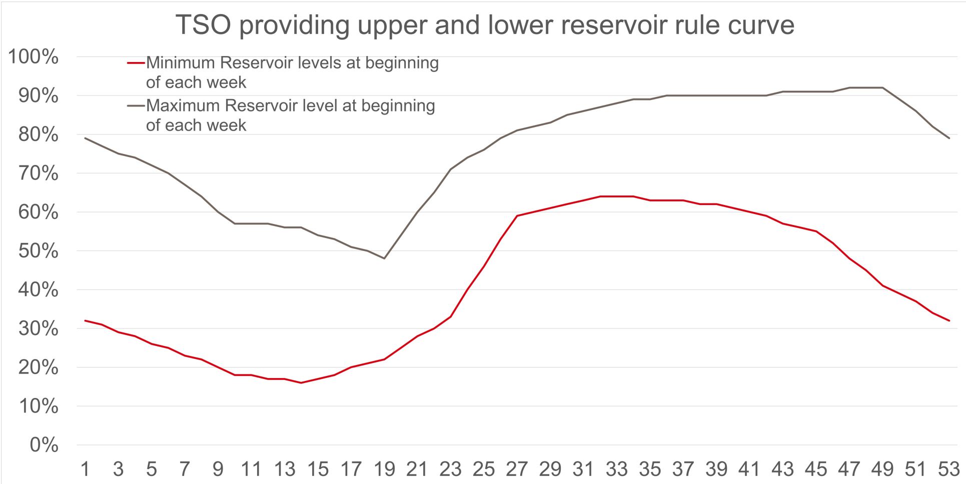


**Figure 2.7:** Minimum and maximum trajectories of the hydro reservoir provided by the Austrian TSO, example of Austrian input data for ERAA 2022

Alternatively TSOs provide deterministic filling levels of the hydro reservoir per climate year (Figure 2.8) on a scale between 0 % to 100 %. These are used together with the hydro inflows, to determine the monthly energy available for the tool to be used within the given month.

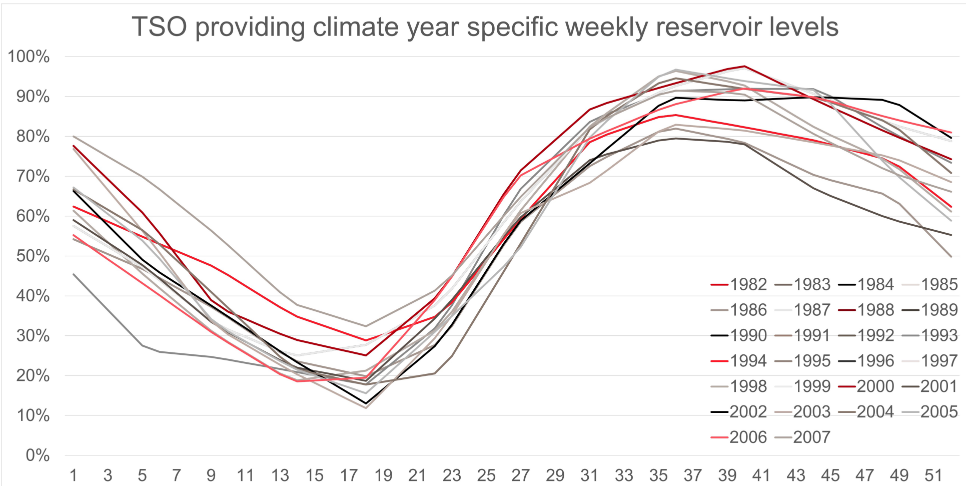


**Figure 2.8:** Climate year specific weekly filling levels of the hydro reservoir provided by TSOs - as provided by APG in the MAF calculations

Available input from TSO side can look as follows:

- deterministic predefined monthly hydro storage energy values (generation time series for hydro storage generation) which need to be used within the specified month derived from the climate year dependent hydro reservoir level rule curves as shown in Figure 2.8 and the corresponding hydro inflows.

- hydro inflows in combination with weekly minimum and maximum reservoir levels (Figure 2.7) which are used to determine the monthly energy values by using the reservoir management functionality of Antares

By using the internal reservoir management functionality of Antares, the hydro energy to the bidding zone is allocated based on the expected inflows and reservoir level rule curve constraints, pro-rate to the net load, which is defined as follows [36]:

Net load for a bidding zone $z$ is defined as: $\mathbf{L}_z^* = \mathbf{L}_z - \mathbf{M}_z$

where

| | |
|---|---|
| $z$ | bidding zone $z \in Z$ |
| $Z$ | total number of areas (bidding zones) in the system |
| $\mathbf{M}_z$ | 35 climate-dependent hourly time-series of accumulated must run generation of all kinds for bidding zone $z$, $\mathbf{M}_z \in \mathbb{R}$ $(35 \times 8760)$ |
| $\mathbf{L}_z$ | 35 climate-dependent time series of natural load for bidding zone $z$, $\mathbf{L}_z \in \mathbb{R}$ $(35 \times 8760)$ |
| $\mathbf{L}_z^*$ | 35 climate-dependent time series of net load for bidding zone $z$, $\mathbf{L}_z^* \in \mathbb{R}$ $(35 \times 8760)$ |

The must-run generation from renewables and thermal must-run ($\mathbf{M}_z$) is deducted from the natural load ($\mathbf{L}_z$) of the bidding zone.

After the deduction of the must-run generation from the load of the bidding zone the net load ($\mathrm{L}_z^*$) is weighted by a hydro allocation matrix $\mathrm{A}^\intercal$, which indicates to which extent the hydropower storage generation of the bidding zone $z$ depends on the local demand and must-run generation within the bidding zone. All matrices used are of the size of $(35 \times 8760)$ reflecting 35 climate dependent input time series in hourly resolution.

Weighted load for a bidding zone $z$ is defined: $\mathbf{\Lambda}_z = \mathbf{A}^\intercal \mathbf{L}_z^*$

where

| | |
|---|---|
| $z$ | bidding zone $z \in Z$ |
| $Z$ | total number of areas (bidding zones) in the system |
| $\mathbf{L}_z^*$ | 35 climate-dependent time series of net load for bidding zone $z$, $\mathbf{L}_z^* \in \mathbb{R}$ $(35 \times 8760)$ |
| $\mathbf{\Lambda}_z$ | 35 climate-dependent time series of weighted load for bidding zone $z$, $\mathbf{\Lambda}_z \in \mathbb{R}$ $(35 \times 8760)$ |
| $\mathbf{A}^\intercal$ | inter-area hydro-allocation matrix is a weight given to the load of an area, $\mathbf{A}^\intercal \in \mathbb{R}$ $(35 \times 8760)$ |

The inter-area hydro-allocation matrix $\mathbf{A}^\intercal$ can in extreme cases consist of:

- $\mathbf{A}^\intercal$ being the identity matrix: Monthly and weekly hydropower storage energy profiles of each zone $z$ depend only on the local demand and must-run generation in $z$

- $\mathbf{A}^\intercal$ with a main diagonal of zeros: Monthly and weekly hydropower storage energy profiles of each zone $z$ do not depend at all on the local demand and must-run generation in $z$

Once the weighted load is determined for each node, Antares applies a two-step heuristic. In a first step, the monthly pre-allocation is performed by either using the reservoir management functionality ($\mu = 1$) or not ($\mu = 0$). The result of this monthly pre-allocation is then applied to the daily pre-allocation.
Figure 2.9 illustrates the four steps that the Antares tool completes to decompose the hydro inflows entered by the user:

1. hydro inflows are allocated to monthly hydro energy lots according to a net load proportional heuristic of Antares using the reservoir management functionality ($\mu = 1$), or

2. monthly hydro energy lots are provided by the user (Antares does not perform the monthly pre-allocation - reservoir management functionality is off ($\mu = 0$))

3. daily hydro energy lots are retrieved according to the net load proportional heuristic

4. daily hydro energy lots retrieved after the daily pre-allocation are transferred to the power scheduler and Unit Commitment optimizer as input for the main Antares optimization problem (see chapter 2.6.3).

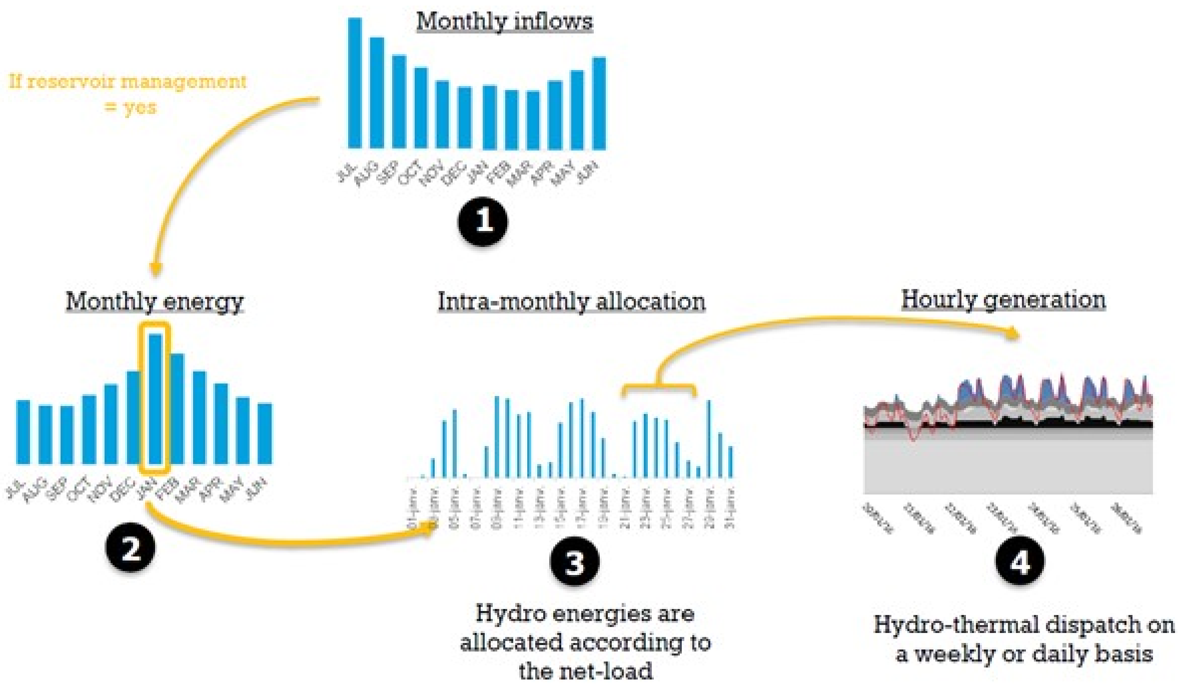


**Figure 2.9:** Four steps of the hydro pre-allocation of Antares [36]

While the first step (monthly pre-allocation) can be selected by the user (reservoir management functionality on ($\mu = 1$) or off ($\mu = 0$)), the daily pre-allocation is applied by the tool by default. Depending on which of the functions is used, the input data must be provided in different formats:

- reservoir management parameter set to **OFF** ($\mu = 0$), where the user must provide monthly energy targets, which are allocated and treated as fixed daily energy lots. These energy lots must be consumed within the respective month; it is not possible to redistribute them to another month. The distribution from monthly to daily energy is based on the Antares heuristic. This approach was used for Austrian hydropower plants up to MAF 2019.

- reservoir management parameter set to **ON** ($\mu = 1$), where the user must provide input data in the form of natural hydro inflows into the hydro reservoirs, which are summed up to an annual inflow and used by the tool together with minimum and maximum trajectories of the hydro reservoir. This approach has been used for Austrian hydropower plants since the MAF 2020.

The following parameters are introduced and help to decompose either annual energy lots into monthly or monthly energy lots into daily energy lots:

inter-monthly generation breakdown $\alpha = \frac{\log(\mathrm{GEN}_{\mathrm{RES,M}})}{\log(\mathrm{Load}_{\mathrm{M}})}$

inter-daily generation breakdown $\beta = \frac{\log(\mathrm{GEN}_{\mathrm{RES,D}})}{\log(\mathrm{Load}_{\mathrm{D}})}$

where

| | |
|---|---|
| $\mathrm{GEN}_{\mathrm{RES,M}}$ | historic measured generation of the reservoir of the month M |
| $\mathrm{Load}_{\mathrm{M}}$ | historic measured net residual loads of the month M |
| $\mathrm{GEN}_{\mathrm{RES,D}}$ | historic measured generation of the reservoir of the day D |
| $\mathrm{Load}_{\mathrm{D}}$ | historic measured net residual loads of the day D |

Both parameters are introduced when breaking down monthly or daily energy lots according to the Antares heuristic. The parameters are derived from historic measured values of reservoir generation and net load of a bidding zone. The use of the parameter depends on whether the user wants to use the reservoir management functionality ($\mu = 1$) or not ($\mu = 0$) and use the follow load parameter ($\varphi = 1$) or not ($\varphi = 0$). Figure 2.10 displays the selectable parameters and the monthly and daily energy allocation according to the selected parameter.

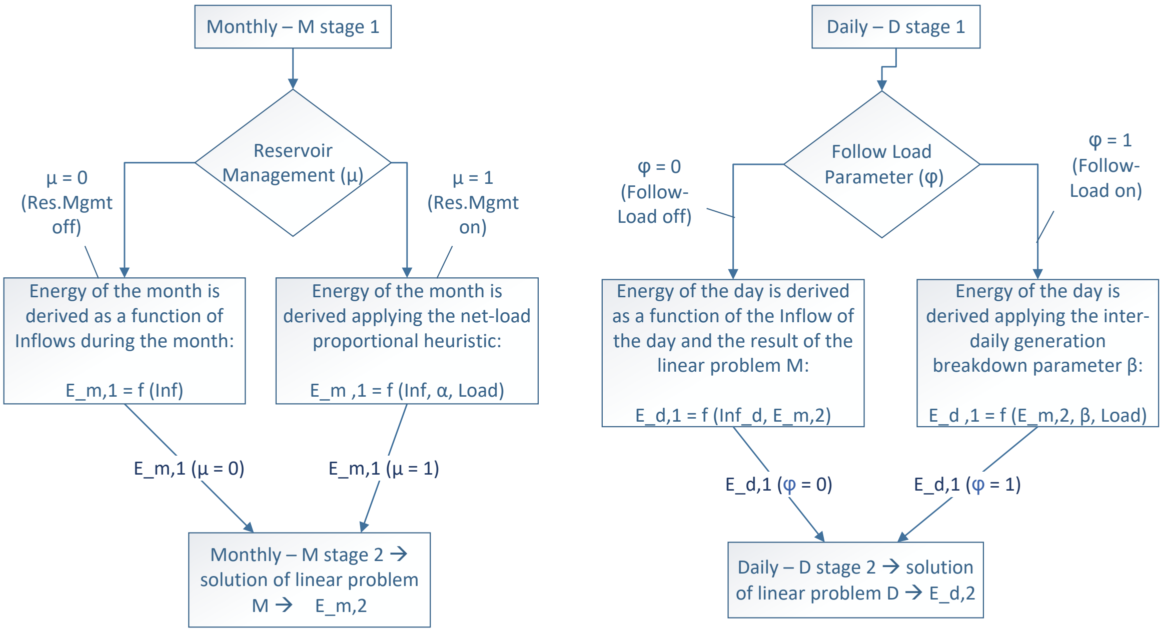


**Figure 2.10:** Monthly and daily hydro allocation [36]

### 1. M-Stage: monthly pre-allocation

The aim of this phase is to allocate the hydro inflows provided by the user to hydro energies per month to be used by the tool. The algorithm starts with setting the initial conditions:

Begin if $(\mu = 0)\,\{S_{t,min} \leftarrow 0; S_{t,max} \leftarrow \Sigma; S_0 \leftarrow \Sigma/2\}$

where

| | |
|---|---|
| $\mu$ | reservoir management parameter |
| $\Sigma$ | reservoir size, $[\Sigma] = \mathrm{MWh}$ |
| $\mathrm{S}_{\mathrm{t,max}}$ | reservoir maximum level at the end of time step $t$, $[\mathrm{S}_{\mathrm{t,max}}] = \mathrm{MWh}$ |
| $\mathrm{S}_{\mathrm{t,min}}$ | reservoir minimum level at the end of time step $t$, $[\mathrm{S}_{\mathrm{t,min}}] = \mathrm{MWh}$ |
| $\mathrm{S}_0$ | initial reservoir level at the beginning of the first day of the hydro year, $[\mathrm{S}_0] = \mathrm{MWh}$ |

To set the initial condition under the assumption that the reservoir management functionality is not used ($\mu = 0$), the minimum level of the reservoir at the end of day $d$ is set to 0; the maximum level of the reservoir at the end of day $d$ is set to the reservoir size ($\Sigma$) and the initial reservoir level at beginning of the first day is set to half of the reservoir size ($\Sigma/2$). Setting the initial reservoir level at the beginning of the year at half of the reservoir size is an arbitrary decision and was already made at the beginning of the probabilistic adequacy calculations, which apply to the entire European perimeter.

Figure 2.11 illustrates the reservoir constraints, which are later used as either hard constraints to be respected within each step of the optimization and the soft constraints, reservoir minimum and maximum trajectories.

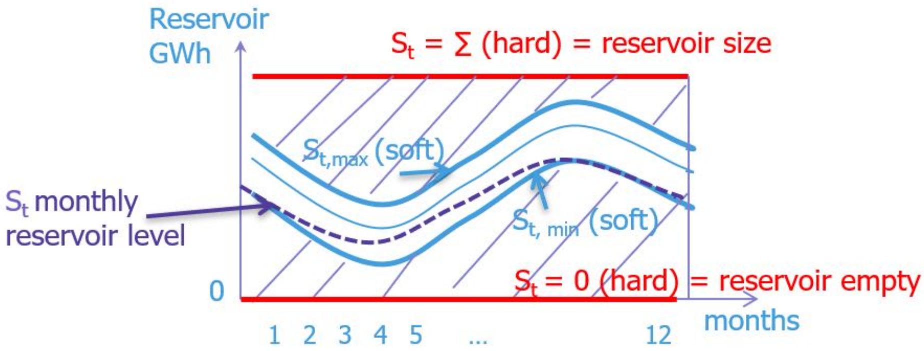


**Figure 2.11:** Reservoir level constraints (hard and soft) [38]

**M1 - applying the heuristic using the inter-monthly generation breakdown parameter:**

If the reservoir management functionality is used ($\mu = 1$) and the parameter for following the load ($\varphi = 1$) is activated, the heuristic applies the inter-monthly generation breakdown parameter $\alpha$ to determine the energy target of the months as follows:

if $(\mu = 1 \text{ and } \varphi = 1) : \text{for } (m : 1, \ldots 12) : \left\{ E_{m,1} \leftarrow \Lambda_m^\alpha \frac{\sum_m \mathrm{Inf}_m}{\sum_m \Lambda_m^\alpha} \right\}$

where

| | |
|---|---|
| $\mu$ | reservoir management parameter |
| $\varphi$ | follow-load parameter |
| $\alpha$ | inter-monthly generation breakdown parameter |
| $\Lambda$ | time-series of weighted Load |
| $\mathrm{E}_{m,1}$ | optimal energy to generate in month $m$, at the end of stage 1 of the pre-allocation, $[\mathrm{E}_{m,1}] = \mathrm{MWh}$ |
| $\mathrm{Inf}_m$ | natural inflow of energy to the reservoir during month $m$, $[\mathrm{Inf}_m] = \mathrm{MWh}$ |

If the reservoir management functionality ($\mu = 0$) and the parameter for following the load ($\varphi = 0$) are not used, the monthly energy targets are provided by the user as total inflows for the month. These inflows are summed up and the total energy of the month results as the sum of all inflows within the month. In addition, these monthly energy quantities must be consumed in the respective month and cannot be carried over to a later month.

else $(\mu = 0 \text{ and } \varphi = 0) : \text{for } (m : 1, \ldots 12) : \{E_{m,1} \leftarrow \mathrm{Inf}_m\}$

where

| | |
|---|---|
| $\mathrm{E}_{m,1}$ | optimal energy to generate on month $m$, at the end of stage 1 of the pre-allocation, $[\mathrm{E}_{m,1}]$ = MWh |
| $\mathrm{Inf}_m$ | natural inflow of energy to the reservoir during month $m$, $[\mathrm{Inf}_m]$ = MWh |

**M2 - solution of the linear problem M:** for $(m : 1, \ldots 12) : E_{m,2} \leftarrow$ solution of the linear problem M where $\mathrm{E}_{m,2}$ is the energy to generate on month $m$, at the end of stage 2 of the pre-allocation. For each month an optimal Energy generation $\mathbf{E}_t$ as well as an optimal Reservoir level at the end of each month $\mathbf{S}_t$ is assessed through the following optimization and highlighted as decision variables in bold:

**Optimization Problem M**

$$\min_{\mathbf{E}_t,\mathbf{S}_t} \left(\mathrm{C}_\Delta\ \Delta + \mathrm{C}_\Psi\ \Psi + \sum_t (\mathrm{C}_\mathrm{D}\ \mathrm{D}_t + \mathrm{C}_{\mathrm{V}+}\ \mathrm{V}_{t+} + \mathrm{C}_{\mathrm{V}\text{-}}\ \mathrm{V}_{t-})\right)$$

with

$$\mathrm{V}_{t-} = \mathrm{S}_{\mathrm{t,min}} - \mathbf{S}_\mathrm{t}$$

$$\mathrm{V}_{t+} = \mathbf{S}_\mathrm{t} - \mathrm{S}_{\mathrm{t,max}}$$

$$\mathrm{D}_t = \mathbf{E}_t - \mathrm{E}_{m,1}$$

$$\Delta = \max_{(m:1\ldots12)} (\mathrm{D}_t)$$

$$\Psi = \max_{(m:1\ldots12)} (\mathrm{V}_{t-})$$

where

| | |
|---|---|
| $\mathbf{E}_t$ | optimal generation on time step $t$ as an output of the hydro pre-allocation phase, $[\mathbf{E}_\mathrm{t}]$ = MWh |
| $\mathbf{S}_t$ | optimal reservoir level at the end of time step $t$ as an output of the hydro pre-allocation phase, $[\mathbf{S}_\mathrm{t}]$ = MWh |
| $\Delta$ | maximum deviation throughout the month |
| $\Psi$ | maximum violation of lower rule curve throughout the period |
| $\mathrm{D}_t$ | deviation (absolute difference) between the target reached ($E_t$) and initial aim ($\mathrm{E}_{m,1}$) |
| $\mathrm{V}_{t+}$ | amplitude of the violation of the upper rule curve at time step $t$ |
| $\mathrm{V}_{t-}$ | amplitude of the violation of the lower rule curve at time step $t$ |
| $t$ | time variable used for months $m$ $(1, \ldots 12)$ |
| $\mathrm{C}_\Delta$ | costs resulting from deviating from the generation objective assessed in stage 1 of the monthly pre-allocation |
| $\mathrm{C}_\Psi$ | costs resulting from violating the lower rule curve throughout the period |
| $\mathrm{C}_\mathrm{D}$ | costs resulting from the deviation between the target reached ($E_t$) and the initial aim ($\mathrm{E}_{m,1}$) |
| $\mathrm{C}_{\mathrm{V}+}$ | costs resulting from violating the upper rule curve at time step $t$ |
| $\mathrm{C}_{\mathrm{V}\text{-}}$ | costs resulting from violating the lower rule curve at time step $t$ |

subject to

**reservoir hard constraints:**

| | |
|---|---|
| $\mathbf{S}_t \geq 0$ | reservoir level $\mathrm{S}_t$, $[\mathrm{S}_t] = \mathrm{MWh}$, always has to be positive |
| $\mathbf{S}_t \leq \Sigma$ | reservoir level $\mathrm{S}_t$ always has to stay below the reservoir size $\Sigma$ |

**energy conservation:**

| | |
|---|---|
| $\mathbf{E}_t = \mathrm{S}_{t-1} - \mathrm{S}_t + \mathrm{Inf}_t$ | optimal energy generation $\mathrm{E}_t$ at time step $t$ results as the delta of the reservoir level (the reservoir level at the previous time step $\mathrm{S}_{t-1}$ minus the optimal reservoir level $\mathrm{S}_t$ at the end of time step $t$) plus the natural inflow $\mathrm{Inf}_t$ on time step $t$; in the first equation $\mathrm{S}_{t-1}$ is either the initial stock $\mathrm{S}_0$ or the final stock of the previous year (hydro hot start) |
| $\sum_t \mathbf{E}_t = \sum_t \mathrm{E}_{m,1}$ | sum of the optimal generation $\mathbf{E}_t$ at time step $t$ equals the sum of the generation objectives $(\mathrm{E}_{m,1})$ assessed in the first step for time step $t$ |

**reservoir soft constraint:**

| | |
|---|---|
| $\mathbf{E}_t \leq \mathrm{E}_{m,1} + \mathrm{D}_t$ | the optimal generation $\mathbf{E}_t$ stays lower or equal to the generation objective assessed in the first step $\mathrm{E}_{m,1}$ plus the deviation between target reached and initial aim $\mathrm{D}_t$ for the time step $t$ |
| $\mathbf{E}_t \geq \mathrm{E}_{m,1} - \mathrm{D}_t$ | the optimal generation $\mathbf{E}_t$ has to stay greater or equal to the generation objective assessed in the first step $\mathrm{E}_{m,1}$ minus the deviation between target reached and initial aim $\mathrm{D}_t$ on time step $t$ |
| $\mathrm{V}_{t-} \geq \mathrm{S}_{t,min} - \mathbf{S}_t$ | amplitude of the violation of the lower rule curve $\mathrm{V}_{t-}$ has to stay greater or equal the minimum reservoir level $\mathrm{S}_{t,min}$ minus the optimal reservoir level $\mathbf{S}_t$ at the end of time step $t$ |
| $\mathrm{V}_{t+} \geq -\mathrm{S}_{t,max} + \mathbf{S}_t$ | amplitude of the violation of the upper rule curve $\mathrm{V}_{t+}$ has to stay greater or equal the negative value of the maximum reservoir level $-\mathrm{S}_{t,max}$ plus the optimal reservoir level $\mathbf{S}_t$ at the end of time step $t$ |
| $\Psi - \mathrm{V}_{t-} \geq 0$ | maximum violation of the lower rule curve $\Psi$ throughout the period $t$ has to stay greater or equal to the amplitude of the violation of the lower rule curve $\mathrm{V}_{t-}$ at time step $t$ |

**2. T-Stage: daily pre-allocation**

This stage aims to mitigate the previous calculated monthly profile to obtain a feasible hydro daily energy target, compatible as much as possible with reservoir rule curves.

**T1 – applying Antares heuristic using the inter-daily generation breakdown parameter:**

$$\text{if } (\varphi = 1) : \text{for } (d : 1, \ldots 31) : \left\{ \mathrm{E}_{d,1} \leftarrow \Lambda_d^{\beta} \frac{\mathrm{E}_{m,2}}{\sum_{d \in m} \Lambda_d^{\beta}} \right\}$$

where

$\Lambda$ time-series of weighted Load
$\mathrm{E}_{d,1}$ optimal energy to generate on day $d$, at the end of stage 1 of the pre-allocation
$\mathrm{E}_{m,2}$ optimal energy to generate on month $m$, at the end of stage 2 of the pre-allocation

If the follow-load parameter is activated ($\varphi = 1$), the heuristic applies the inter-daily generation breakdown parameter $\beta$ to determine the energy target for the day.

else $(\varphi = 0)$ : for $(d : 1, \ldots 31)$ : $\left\{ E_{d,1} \leftarrow \mathrm{Inf}_d \frac{E_{m,2}}{\sum_{d \in m} \mathrm{Inf}_d} \right\}$

where

$\mathrm{E}_{d,1}$ optimal energy to generate on day $d$, at the end of stage 1 of the pre-allocation
$\mathrm{E}_{m,2}$ optimal energy to generate on month $m$, at the end of stage 2 of the pre-allocation
$\mathrm{Inf}_d$ natural inflow of energy to the reservoir on day $d$

If the follow-load parameter is deactivated ($\varphi = 0$), the daily energy targets are calculated by multiplying the inflow of the day by the energy target of the respective month divided by the sum of all daily inflows of that month.

**T2 - solution of the linear problem $\mathbf{T}(m)$:**

for $(m : 1, \ldots 12)$ : $\mathrm{E}_{d \in m,2} \leftarrow$ solution of the linear problem $\mathrm{T}(m)$ where $\mathrm{E}_{d \in m,2}$ is the energy to generate on day $d$, at the end of stage 2 of the pre-allocation

In the following optimization problem the time variable $t$ is used as index for the daily optimization problem. Days of the month result as 28, 29, 30 or 31 depending on the month and type of year.

**Optimization Problem T**

$$\min_{\mathbf{E}_t, \mathbf{S}_t, \mathbf{O}_t} \left( \mathrm{C}_\Delta\ \Delta + \mathrm{C}_\mathrm{Y}\ \mathrm{Y} + \mathrm{C}_\Psi\ \Psi + \sum_t (\mathrm{C}_\mathrm{D}\ \mathrm{D}_t + \mathrm{C}_{\text{V-}}\ \mathrm{V}_{t-} + \mathrm{C}_\mathrm{O}\ \mathbf{O}_t + \mathrm{C}_\mathrm{S}\ \mathbf{S}_t) \right)$$

with

$\mathrm{V}_{t-} = \mathrm{S}_{\mathrm{t,min}} - \mathbf{S}_\mathrm{t}$
$\mathrm{D}_t = \mathrm{E}_{d,1} - \mathbf{E}_t$
$\Delta = \max_{d:1,\ldots 31} (\mathrm{D}_t)$
$\Psi = \max_{d:1,\ldots 31} (\mathrm{V}_{t-})$

where

| | |
|---|---|
| $\mathbf{E}_t$ | optimal generation on time step $t$ as an output of the hydro pre-allocation phase, $[\mathbf{E}_\mathrm{t}] =$ MWh |
| $\mathbf{S}_t$ | optimal reservoir level at the end of time step $t$ as an output of the hydro pre-allocation phase, $[\mathbf{S}_\mathrm{t}] =$ MWh |
| $\mathbf{O}_t$ | overflow from the reservoir on day $d$, at the end of the daily pre-allocation (inflow in excess to an already full reservoir), $[\mathbf{O}_\mathrm{t}] =$ MWh |
| $t$ | time variable used for days of a month $d$ (28, 30 or 31) |
| $\Delta$ | maximum deviation throughout the period |
| Y | generation deficit at the end of the period, as compared to the objective aimed at |
| $\Psi$ | maximum violation of lower rule curve throughout the period |
| $\mathrm{D}_t$ | deviation (absolute difference) between the target reached and initial aim |
| $\mathrm{V}_{t-}$ | amplitude of the violation of the lower rule curve at time step $t$ |
| $\mathrm{C}_\Delta$ | costs resulting from deviating from the generation objective assessed in stage 1 of the daily pre-allocation |
| $\mathrm{C}_\mathrm{Y}$ | costs resulting from a generation deficit at the end of the period, as compared to the objective aimed at |
| $\mathrm{C}_\Psi$ | costs resulting from the maximum violation of the lower rule curve throughout the period |
| $\mathrm{C}_\mathrm{D}$ | costs resulting from the deviation (absolute difference) between the target reached and initial aim |
| $\mathrm{C}_{\mathrm{V}\text{-}}$ | costs resulting from the violation of the lower rule curve at time step $t$ |
| $\mathrm{C}_\mathrm{O}$ | costs resulting from letting the reservoir overflow |
| $\mathrm{C}_\mathrm{S}$ | costs resulting from the deviation of the end of period targeted reservoir level |

subject to
**reservoir hard constraints:**

| | |
|---|---|
| $\mathbf{S}_t \geq 0$ | reservoir level $\mathbf{S}_t$ always has to be positive |
| $\mathbf{S}_t \leq \Sigma$ | reservoir level $\mathbf{S}_t$ always has to stay below the reservoir size |
| $\mathbf{E}_t \geq 0$, $\mathbf{E}_t \leq \mathrm{E}_{t,max}$ | optimal generation $\mathbf{E}_t$ has to stay greater or equal zero and the optimal generation $\mathbf{E}_t$ has to stay lower or equal the maximum generation $\mathrm{E}_{t,max}$ at time step $t$ |

**energy conservation:**

| | |
|---|---|
| $\mathbf{E}_t = \mathrm{S}_{t-1} - \mathbf{S}_t + \mathrm{Inf}_t - \mathbf{O}_t$ | the optimal generation $\mathbf{E}_t$ at time step $t$ results as the delta between two consecutive reservoir levels (the reservoir level at the previous time step $\mathrm{S}_{t-1}$ minus the optimal reservoir level $\mathbf{S}_t$ at the end of time step $t$) plus the inflow $\mathrm{Inf}_t$ minus the overflow $\mathbf{O}_t$; where in the first equation the reservoir level at the previous time step $\mathrm{S}_{t-1}$ is either the starting stock used in $M$ or the final stock of the previous month $D_{m-1}$ |

| | |
|---|---|
| $\sum_t \mathbf{E}_t + \mathrm{Y}_m =$ | sum of the optimal generation $\mathbf{E}_t$ plus the generation deficit $\mathrm{Y}_m$ at the end of time step $t$, |
| $\sum_t \mathrm{E}_{d,1} + \mathrm{Y}_{m-1}$ | equals the sum of the generation objective assessed in the first stage ($\mathrm{E}_{d,1}$) plus the generation deficit $\mathrm{Y}_{m-1}$ at the end of the previous time step $m-1$, as compared to the objective aimed at $\mathrm{Y}_{m-1}$ |

**reservoir soft constraints:**

| | |
|---|---|
| $\mathbf{E}_t \leq \mathrm{E}_{d,1} + \mathrm{D}_t$ | the optimal generation $\mathbf{E}_t$ stays lower or equal to the generation objective assessed in the first step $\mathrm{E}_{d,1}$ plus the deviation between target reached and initial aim $\mathrm{D}_t$ for the time step $t$ |
| $\mathbf{E}_t \geq \mathrm{E}_{d,1} - \mathrm{D}_t$ | the optimal generation $\mathbf{E}_t$ has to stay greater or equal to the generation objective assessed in the first step $\mathrm{E}_{d,1}$ minus the deviation between target reached and initial aim $\mathrm{D}_t$ on time step $t$ |
| $\mathrm{V}_{t-} + \mathbf{S}_t \geq \mathrm{S}_{t,min}$ | amplitude of the violation of the lower rule curve $\mathrm{V}_{t-}$ plus the reservoir level $\mathbf{S}_t$ remains greater or equal to the minimum reservoir level $\mathrm{S}_{t,min}$ at the end of time step $t$ |
| $\Delta - \mathrm{D}_t \leq \mathrm{E}_{d,1}$ | maximum deviation throughout the period $\Delta$ minus the deviation (absolute difference) between target reached and initial aim $\mathrm{D}_t$ stays lower or equal the generation objective assessed in the first stage ($\mathrm{E}_{d,1}$) for time step $t$ |
| $\Psi - \mathrm{V}_{t-} \geq 0$ | maximum violation of the lower rule curve throughout the period $\Psi$ stays lower or equal the amplitude of the violation of the lower rule curve $\mathrm{V}_{t-}$ throughout the period |

When optimizing monthly or daily hydro energies, costs are minimized in a way that enforces a logical hierarchy: Allowing the reservoir to overflow is worse than violating the minimum and maximum filling levels of the reservoir, which in turn is worse than deviating from the generation targets assessed in stage 1 ($\mathrm{E}_{m,1}$ or $\mathrm{E}_{d,1}$).

The costs used in the equations listed above are hard-coded in Antares and result from empirical tests based on the hypothesis to follow the above hierarchy (overflowing the reservoir is worse than violating the minimum and maximum reservoir filling levels is worse than deviating from the targets assessed in stage 1).

A further limitation of Antares is evident in the definition of the daily optimization, since Antares can only penalize either the violation of the upper rule curve or the overflow. For this reason, there is no term in the second optimization for violating the maximum filling levels of the reservoir.

### 2.6.2 Hydro pre-allocation using water values

The pre-allocation of monthly and daily hydro energy using Antares heuristic, as described in chapter 2.6.1, has two major disadvantages:

1. If the reservoir management function of Antares is not used, the user must enter monthly quantities of hydro energy that must be used in that month - in the event of extreme weather situations such as cold spells, drought, etc., water cannot be stored for a later month in which hydro energy is required in greater quantities.

2. If the reservoir management function of Antares is used, extreme situations can also be taken into account, as the amounts of energy from hydropower can be used during the whole

year, with the applied heuristics being load-proportional. This load-proportionality has the disadvantage, that the net load is calculated by subtracting the must-run generation from the load, which is why perfect knowledge of the must-run units (including generation from renewable sources) is expected.

In the specific case of Austria, the feed-in from hydropower plants does not follow any kind of load-proportional behavior, but rather follows market prices, which are also very often influenced by the impact of renewable energy from neighboring countries (e.g. wind and solar production from Germany). Therefore, the heuristic approach of Antares for modeling the adequacy of resources using a net load proportional method was questioned. For this purpose, various investigation steps and model test calculations were carried out, which are discussed in chapter 6.1.

In Antares version 7, a functionality for determining the specific costs for each reservoir level [%] and each day of the year was introduced, which is referred to in this thesis as *water value functionality*. This functionality enables the inclusion of hydropower generation in the merit order list and thus the scheduling in the main optimization at a specific cost. The water values result from a calculation that is performed on the overall model prior to the main optimization: RTE has developed an R-based application that performs the calculation of water values for a bidding zone and a reservoir type using a dynamic programming (DP) approach in advance of an Antares adequacy calculation [38].

The idea of dynamic programming is that the original problem is divided into a series of sub-problems that are individually easier to solve than the original problem. This principle was investigated by various researchers after the Second World War. In 1954, Richard Bellman introduced the concept of dynamic programming, in which the division of a main problem into various sub-problems is applied [39].

The basic description of dynamic programming and Bellman's principle of optimality as used for the water value calculations are explained below [39]. The variables introduced in this chapter only apply to this chapter and are adapted from the usual designations in the literature.

**1. The basic problem:**

Dynamic programming deals with sequential decision-making processes, which are models of dynamic systems under the control of a decision-maker. At each state in which a decision can be made, the decision maker selects an action from a set of alternatives that depends on the current state of the system. This action leads to costs or rewards and a transition to a new state. The goal is to choose a sequence of actions, called a *policy*, that optimizes the performance of the system (e.g. minimize the costs or maximize the rewards) over the whole horizon.

The planning horizon consists of $n$ periods. The state of the underlying system at the beginning of period $j$ (or at the end of period $j-1$) is described by the state variable $x_j$. At the beginning of period 1, the system is in the given initial state $x_1 = x_a$. During the period $j$, an action $u_j$ is selected from an action space $U_j(x_j)$ depending on the state $x_j$, which triggers a transition to a new state $x_{j+1} = f_j(x_j, u_j)$ depending on the previous state $x_j$ and the action $u_j$. Cost

$g_j(x_j, u_j)$ arises. The possible states $x_{j+1}$ at the end of a period $j$ should belong to a state space $X_{j+1}$. At the beginning of period 1 let $X_1 = \{x_a\}$.

The problem is formulated as:

$$
\begin{aligned}
\min \sum_{j=1}^{t} g_j(x_j, u_j) \\
s.t. \\
x_{j+1} = f_j(x_j, u_j)(j = 1...n) \\
x_1 = x_a \\
x_{j+1} \in X_{j+1}(j = 1...n) \\
u_j \in U_j(x_j)(j = 1...n)
\end{aligned}
\tag{2.3}
$$

where

| | |
|---|---|
| $n$ | periods of the planning horizon |
| $x_j$ | state variable - state of the underlying system at the beginning of period $j$ |
| $x_1$ | initial state of the period at the beginning of period 1 |
| $u_j \in U_j(x_j)$ | action selected from an action space $U_j(x_j)$ |
| $x_{j+1} = f_j(x_j, u_j)$ | transition to a new state depending on the previous state $x_j$ and action $u_j$ |
| $g_j(x_j, u_j)$ | costs arising from the action and the previous state |

A sequence of actions ($u_1$,...,$u_n$) is called a policy. A policy that satisfies the constraints of the objective function and minimizes the objective is called an optimal policy.

**2. Bellman's Equation and Principle of Optimality:**

If we take the functions $f_j$ and $g_j$, the state and action spaces $X_{j+1}$ and $U_j$ for $j = 1, ..., n$ and the problem from 1., its solutions depend only on the initial state $x_1$. This optimization problem is called $P_1(x_1)$.
The corresponding problem that covers the periods $j, j+1, ..., n$ for $1 < j \leq n$ and that depends on the initial state $x_j$ is called $P_j(x_j)$.

with:

| | |
|---|---|
| $(u_j^*, u_{j+1}^*, ..., u_n^*)$ | optimal policy for the problem $P_j(x_j)$ |
| $v_j^*(x_j)$ | minimum cost for the problem $P_j(x_j)$ |
| $(u_{j+1}^*, ..., u_n^*)$ | optimal policy for problem $P_{j+1}(x_{j+1}^*)$ |
| $x_{j+1}^* := f_j(x_j, u_j^*)$ | initial state |
| $v_{j+1}^*(x_{j+1}*)$ | costs |

If there were a better policy $(u^+_{j+1}, ..., u^+_n)$ for the problem $P_{j+1}(x^*_{j+1})$ with smaller costs $v^+_{j+1}(x_{j+1}*)$, then $(u^*_j, u^+_{j+1}, ..., u^+_n)$ would be a better policy for $P_j(x_j)$ with costs

$$g_j(x_j, u^*_j) + v^+_{j+1}(x_{j+1}*) < g_j(x_j, u^*_j) + v^*_{j+1}(x_{j+1}*) = v^*_j(x_j)$$

which contradicts to the optimality of $v^*_j(x_j)$. The following applies:

$$v^*_j(x_j) = g_j(x_j, u^*_j) + v^+_{j+1}(x_{j+1}*) = \min_{u_j \in U_j(x_j)} \left\{ g_j(x_j, u_j) + v^*_{j+1}\left[f_j(x_j, u_j)\right] \right\} \tag{2.4}$$

Bellman's principle of optimality is described by the fact that a part of an optimal policy (with respect to a fixed initial state) is an optimal policy for the respective sub-problem.

The formulation for $P_1(x_1)$ and $P_j(x_j)$ according to Bellman's optimality principle with the following definitions

| | |
|---|---|
| $(u^*_1, \ldots u^*_j, \ldots, u^*_n)$ | optimal policy for the problem $P_1(x_1)$ |
| $x^*_j$ | state at the beginning of period $j$ |
| $(u^*_j, \ldots, u^*_n)$ | optimal policy for problem $P_j(x^*_j)$ |

can be expresses in such a way that the decisions in periods $j, \ldots n$ of the n-period problem $P_1(x_1)$ are independent of the decisions in periods $1, \ldots j-1$ given the state $x_j$ is given at the beginning of the period $j$.

The function $v^*_j$, defined on the state space $X_j$ is called the *value function* $(1 \leq j \leq n+1)$ for $j = n+1$: $v^*_{n+1}(x_{n+1}) := 0 \; for \; x_{n+1} \in X_{n+1}$

Bellman's equation is formulated for $j = 1, \ldots n$: $v^*_j(x_j) = g_j(x_j, u^*_j) + v^+_{j+1}(x_{j+1}*) = \min_{u_j \in U_j(x_j)} \left\{ g_j(x_j, u_j) + v^*_{j+1}\left[f_j(x_j, u_j)\right] \right\} (x_j \in X_j, 1 \leq j \leq n)$

Bellman's equation connects two consecutive value functions $v^*_j$ and $v^*_{j+1}$ and enables the calculation of the function $v^*_j$ if the function $v^*_{j+1}$ is known. The Bellman equation can be transferred to maximize the objective function by replacing *min* by *max*.

In the following example the value function $v^*_j(\mathrm{S}_j)$ is calculated using the Bellman equation applying the maximum function and changing the state variable $x_j$ to the reservoir level $\mathrm{S}_j$.

Figure 2.12 shows one transition path for the value function $v^*_j(\mathrm{S}_j)$ that is determined as the maximum of the value functions of a previous state $v^*_{j+1}$ (green dots) plus the transition gain $g_j(S_j, u_j)$ shown in blue arrows between two time steps. The value functions of the previous state $v^*_{j+1}$ (green dots) were determined in the same way as the given value function $v^*_j(\mathrm{S}_j)$, in the previous iteration.

$$v^*_j(\mathrm{S}_j) = \max_{u_j \in U_j(\mathrm{S}_j)} \left\{ g_j(\mathrm{S}_j, u_j) + v^*_{j+1}\left[f_j(\mathrm{S}_j, u_j)\right] \right\} (\mathrm{S}_j \in \Sigma_j, 1 \leq j \leq n)$$

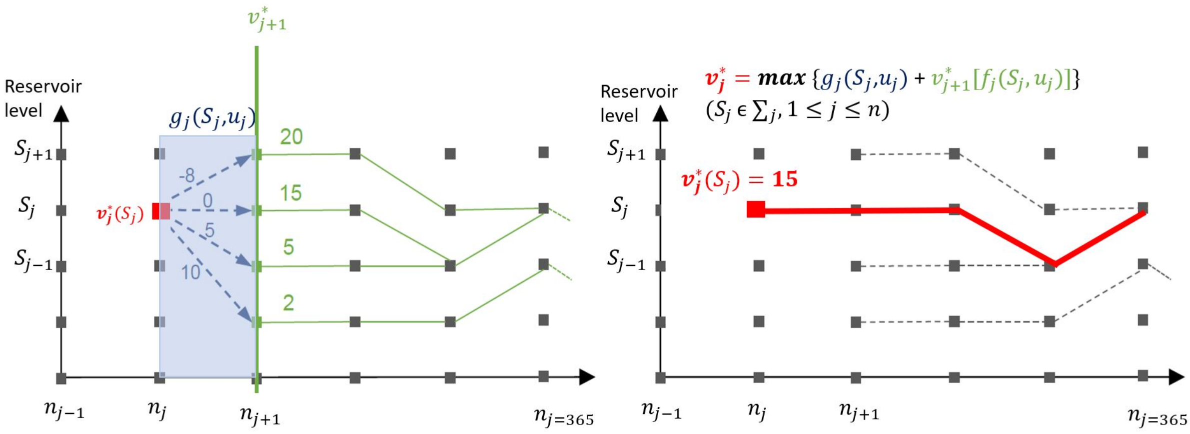


**Figure 2.12:** Bellman values using transition gains [38]

The optimal trajectory is determined by a backward recursive approach, where the initial state (starting point) is the reservoir level of the last day of the year, set manually at 50 % as an arbitrary choice. The transition gain $g_j(\mathrm{S}_j, u_j)$ is calculated as follows: the turbined energy from one reservoir level to another ($\mathrm{E}_j$) is multiplied by the marginal costs ($\mathrm{C}_{\mathrm{marg}}$) determined in a co-optimization. There, the optimizer decides whether or not to use the hydro storage power based on the production level of the thermal units and their costs at that time. If the value of water use at this time is lower than the marginal costs resulting from the thermal units, the optimizer decides to use water from the storage. However, if the value of water use at this time is higher than the marginal costs, the optimizer decides to use the thermal units. The marginal costs that arise in this co-optimization are referred to as $\mathrm{C}_{\mathrm{marg}}$ and are introduced above to describe the transition gain $g_j(\mathrm{S}_j, u_j)$. Figure 2.13 displays the determination of the marginal costs and the transition gain when using the Antares algorithm.

In the present example, the time resolution is in days ($n_{j=365}$) but it can also be in a different resolution (e.g. in weeks of the year $n_{j=52}$).

In the given example, the maximum of the four blue arrows (possible transition gains $g_j(\mathrm{S}_j, u_j)$) plus the green dots (value function of the previous state ($v^*_{j+1}$)) is calculated to determine the value function $v^*_j(\mathrm{S}_j)$ (see Figure 2.12):

$$v^*_j(\mathrm{S}_j) = \max\,((20-8), (15+0), (5+5), (2+10)) = \max\,(12, 15, 10, 12) = 15$$

In the example displayed in Figure 2.12, the optimal value function $v^*_j(\mathrm{S}_j)$ is 15. The same procedure is applied for each reservoir filling level in each time step.

The translation of the Bellman's optimality principle described above raises the question of whether one should use the water in a reservoir at the time of decision making and make money at that time, or whether one should save the water for later, keeping the hope of a future financial gain. Figure 2.13 supports the idea of determining the water value ($\omega$) for a reservoir state that consists of two different value functions:

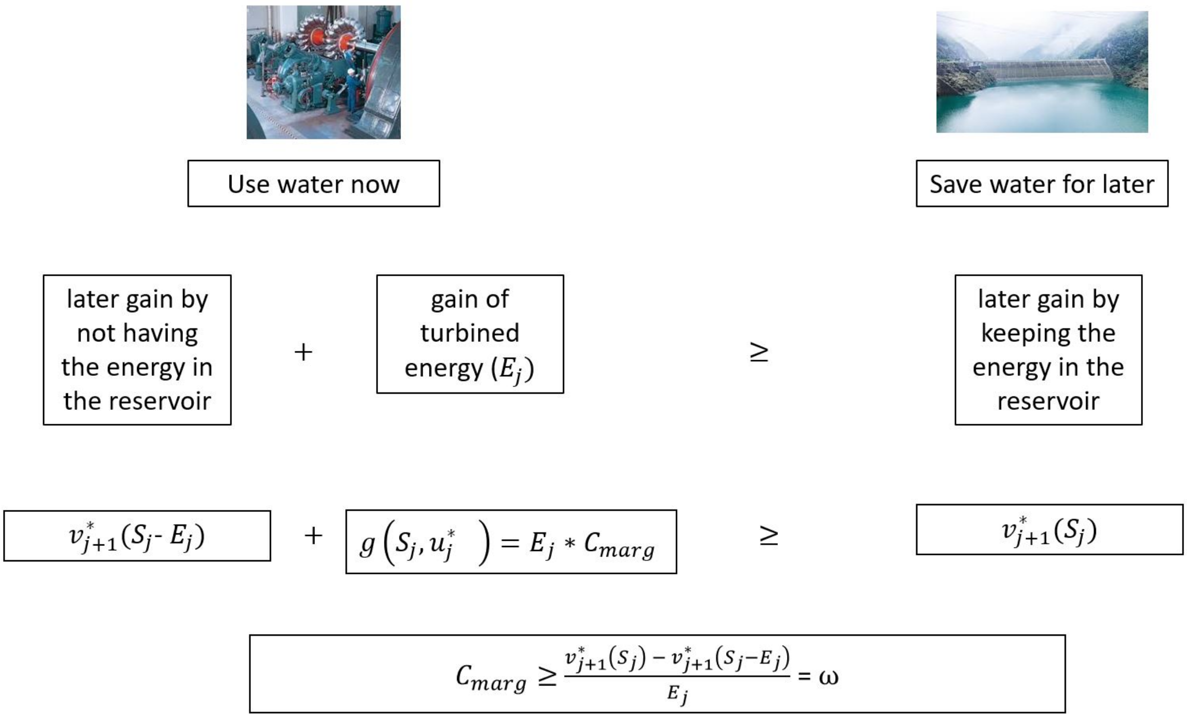


**Figure 2.13:** Determining the water value used by Antares according to Bellman's optimality principle [38]

where

| | |
|---|---|
| $v^*_{j+1}(\mathrm{S}_j)$ | value function of keeping the water in the reservoir |
| $v^*_{j+1}(\mathrm{S}_j - \mathrm{E}_j)$ | value function of releasing the water from the reservoir |
| $g(\mathrm{S}_j, u^*_j)$ | gain of the energy turbined $\mathrm{E}_j$ using an optimal policy $u^*_j$ |
| $\mathrm{S}_j$ | state of the reservoir (reservoir level) - state of the underlying system at the beginning of period $j$ |
| $\mathrm{C}_{\mathrm{marg}}$ | marginal costs available as input to the calculation determined from a parallel co-optimization |
| $\mathrm{E}_j$ | Energy turbined at timestep $n_{j+1}$ |
| $\omega$ | water value $\omega$ |

The determination of the value of water utilization (water value $\omega$) at time $n_{j+1}$ is obtained from the difference between the value function for the storage of water in the reservoir $v^*_{j+1}(\mathrm{S}_j)$ and the value function of the reservoir after the release of energy $v^*_{j+1}(\mathrm{S}_j - \mathrm{E}_j)$ divided by the total turbined energy $\mathrm{E}_j$ in the time step $n_{j+1}$.

An additional level of complexity arises from the fact that 35 different climate years are used for the resource adequacy calculations. Therefore, the determination of the water values matrix $\Omega \in \mathbb{R}$ (365 × 100) described above must be carried out for each climate year, resulting in 35 water value matrices. These still need to be post-processed, as only one water value matrix $\Omega \in \mathbb{R}$ (365 × 100) can be transferred to Antares.

The following section explains how the averaged water values are determined.

### 3. Transferring the approach into multiple Monte Carlo simulations

As already introduced in the context of the ERAA methodology for considering stochastic uncertainties due to renewable energy production or temperature-dependent load time series, the model is based on 35 historical climate data sets. In combination with the unplanned outages, several hundred Monte Carlo simulations are carried out. To take these stochastics into account when calculating the Bellman variables and the shadow prices of the storage levels, the following approaches can be used:

1. **Average of Grids:** Depending on the number of climate years selected (in ERAA $N = 35$) the algorithm is performed for every Monte Carlo year's scenario. After the value functions have been calculated for every day of the year and every storage filling level ($\Omega \in \mathbb{R}$ (365 × 100)) for every Monte Carlo year, the average value for each value function is calculated based on all $N = 35$ scenarios:

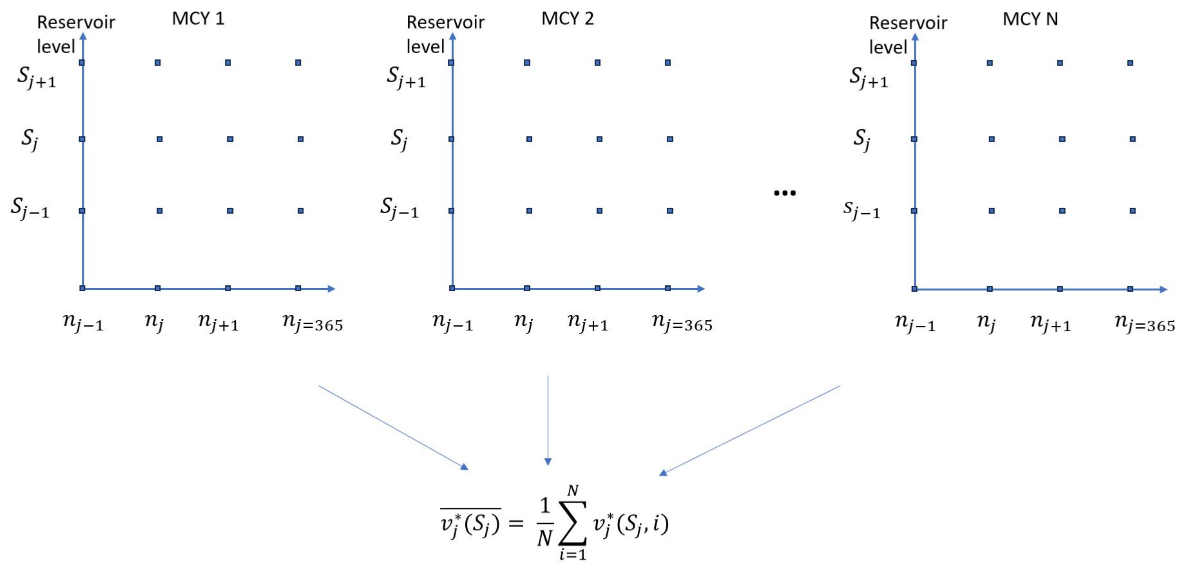


**Figure 2.14:** Average of grids aggregation [38]

where

| | |
|---|---|
| $N$ | number of Monte Carlo years (scenarios) executed |
| $i$ | index variable running through the Monte Carlo years executed |
| $v_j^*(\mathrm{S}_j, i)$ | value function of the state (Reservoir level) $\mathrm{S}_j$ of the Monte Carlo year $i$ |
| $\overline{v_j^*(\mathrm{S}_j, i)}$ | average value of all value functions of the Reservoir level $\mathrm{S}_j$ |

2. **Grid of Means:** In contrast to the Average of Grids approach, the Grid of Means defines a vector $\overline{v_{j+1}^*(\mathrm{S}_j)}$ for each time discretization step (in our case for each day), which contains all value functions of this time step, where each of the values is calculated as an average over all the $N$ Monte Carlo scenarios. This vector ($1 \times 100$) containing all the average values of the $N = 35$ Monte Carlo scenarios, serves as the basis for the next step.

   Figure 2.15 displays the creation of the vector $\overline{v_{j+1}^*(S_j)}$ with the size of $(1 \times 100)$ containing the average values over all Monte Carlo simulations per filling level.

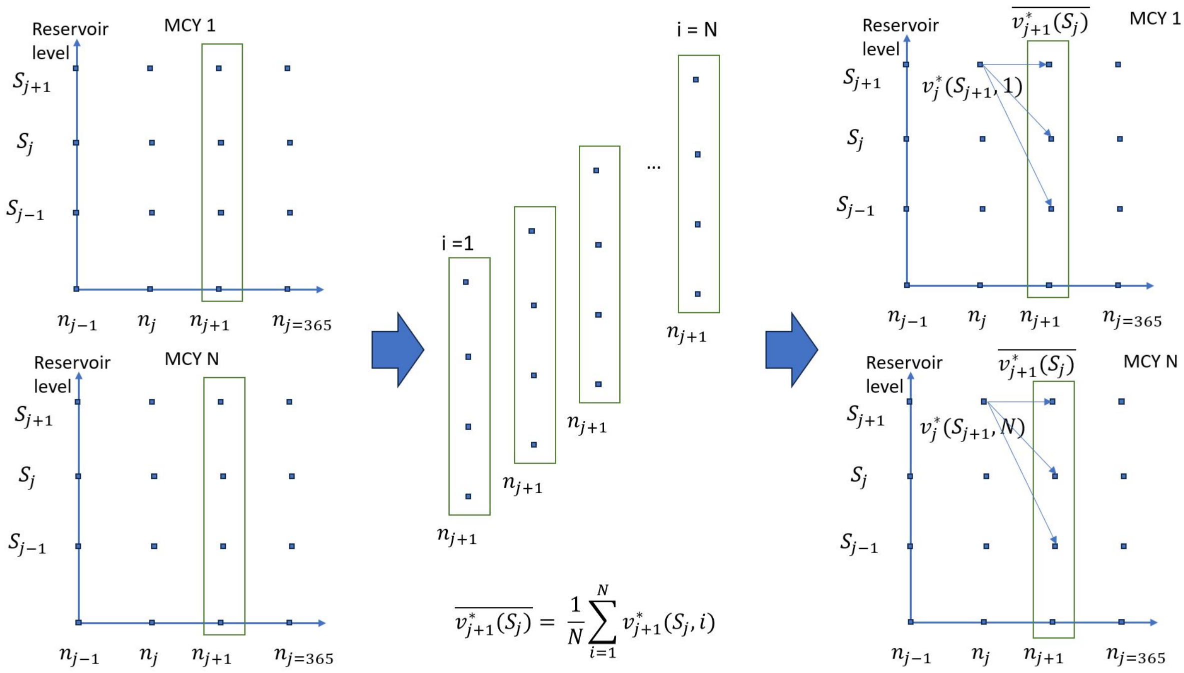


**Figure 2.15:** Grids of means aggregation [38]

The mathematical formulation for the grid of means approach looks as follows:

$$\overline{v_j^*(S_j)} = max\left\{g_j(S_j, u_j^*) + \overline{v_{j+1}^*(S_j)}\right\}$$

3. **Grid of Quantiles:** This approach follows exactly the scheme of the grid of means, for each time discretization step (each day) there is a vector $\overline{v_{j+1}^*(S_j)}$ ($1 \times 100$) that contains all value functions of this time step. Each of the values is calculated as a quantile over

each of the $N$ scenarios. The user defines the quantile which has to be calculated for all $N$ in this time step. This vector, which contains all the value functions, serves as the basis for the next step.

The mathematical formulation for the grid of quantiles approach looks as follows:

$$\overline{v_j^*(S_j)} = max\left\{g_j(S_j, u_j^*) + \overline{v_{j+1}^*(S_j)}\right\},$$

Considering the three approaches described above, the *Average of Grids* approach can be applicable in fully deterministic approaches.
The *Grid of means* approach is mathematically quite sound, but does not take into account the handling of extreme situations (e.g. weather, drought, etc.). The average value is calculated over all Monte Carlo simulations for the respective discretization step (days).

The application of the *Grid of Quantiles* approach allows the user to specify the quantile value to be used. In this way, the user also has the opportunity of defining a specific group of extreme values to be excluded from the calculation. In this way, it is also possible to exclude outliers from the calculation.

### 2.6.3 Antares Main Optimization

The formulation of the Antares optimization problem is publicly available on the RTE Antares website [1]. The formulation of the main optimization problem solved by the Antares optimization engine remains the same for the different versions of Antares used in this work.

The following general notations apply, where the generic optimization problem is denoted $P_k$, where $k$ is an index comprising all weeks of all Monte Carlo years. It is assumed that the actual conditions exactly match all standard forecasts. Demand is met by optimal generation dispatch.

| | |
|---|---|
| $k$ | optimization periods (weeks $k = 52$) over which $P_k$ is defined |
| $t \in T$ | individual time step $t$ in hours of any optimization period $k$ (hours of the week $T =$ 168 hours) |
| $G(N, L)$ | definition of the system consisting of nodes and links |
| $N$ | total amount of bidding zones in the system (one node per country and large countries split in multiple bidding zones, e.g. Sweden, Norway and Italy) $N = 51$ |
| $n \in N$ | nodes used to represent bidding zones, which contain all market information |
| $\ell \in L$ | links used to connect two nodes |
| $L$ | total amount of links connecting all country nodes in the system ($L = 152$ connecting country nodes and a subset of supportive nodes) |
| $u_\ell \in N$ | energy flow direction upstream of a link $\ell$ indicating a country is importing from the neighboring node |
| $d_\ell \in N$ | energy flow direction downstream of a link $\ell$ indicating a country is exporting to the neighboring node |
| $L_n^+ \subset L$ | set of links whose $n$ is the upstream vertex |
| $L_n^- \subset L$ | set of links whose $n$ is the downstream vertex |

Figure 2.16 depicts the notation described for connection of nodes (representing bidding zones) and energy flow directions defined on the links between two nodes (bidding zones). The upstream energy flow is defined as the flow direction coming from the outside and running into the node ($u_{\ell_1}$), while the downstream energy flow is the energy flow leaving the country node ($u_{\ell_1}$).

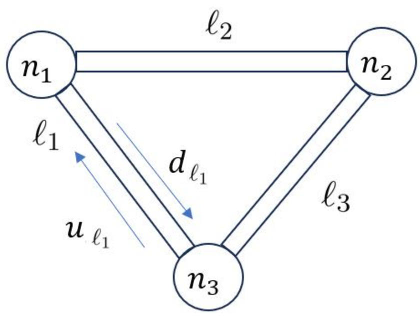


**Figure 2.16:** Graphical representation of nodes and lines

The formulation of the problem is described below, $k$ is implicit in all subsequent notations. The decision variables **E** and **M** apply for each dispatched generation type, are described below and highlighted in bold.

### Objective function

$$\min_{\mathbf{E},\mathbf{M}} (\mathrm{C}_{\mathrm{total}}),$$

with

$$\mathrm{C}_{\text{total}} = \mathrm{C}_{\text{transmission}} + \mathrm{C}_{\text{hydro}} + \mathrm{C}_{\text{thermal}} + \mathrm{C}_{\text{unsupplied}} + \mathrm{C}_{\text{spillage}}$$

where

| | |
|---|---|
| $\mathbf{E}$ | energy output in hourly resolution for all different generation types |
| $\mathbf{M}$ | number of thermal units switching their operational state |
| $\mathrm{C}_{\text{total}}$ | cost of the overall dispatch |
| $\mathrm{C}_{\text{transmission}}$ | transmission costs |
| $\mathrm{C}_{\text{hydro}}$ | costs for hydropower |
| $\mathrm{C}_{\text{thermal}}$ | costs for thermal power |
| $\mathrm{C}_{\text{unsupplied}}$ | costs for unsupplied energy |
| $\mathrm{C}_{\text{spillage}}$ | costs for spilling energy |

with

$$\mathrm{C}_{\text{transmission}} = \sum_{\ell \in L} (\mathrm{C}_\ell^+ \cdot \mathbf{E}_\ell^+ + \mathrm{C}_\ell^- \cdot \mathbf{E}_\ell^-)$$

where

| | |
|---|---|
| $\mathrm{C}_\ell^+$ | transmission cost through $\ell$, upstream direction |
| $\mathrm{C}_\ell^-$ | transmission cost through $\ell$, downstream direction |
| $\mathbf{E}_\ell^+$ | energy flow through $\ell$, upstream direction |
| $\mathbf{E}_\ell^-$ | energy flow through $\ell$, downstream direction |
| $L_n^+ \subset L$ | set of links whose $n$ is the upstream vertex |
| $L_n^- \subset L$ | set of links whose $n$ is the downstream vertex |

with

$$\mathrm{C}_{\text{hydro}} = \sum_{n \in N} \sum_{\sigma \in \Sigma} \omega_\sigma \cdot \mathbf{E}_\sigma$$

where

| | |
|---|---|
| $\mathrm{C}_{\text{hydro}}$ | costs for hydropower |
| $\sigma \in \Sigma$ | reservoirs connected to node $n$ |
| $\omega_\sigma$ | water value for energy outputs from reservoir $\sigma$ |
| $\mathbf{E}_\sigma$ | energy output from reservoir $\sigma$ |

with

$$\mathrm{C}_{\text{thermal}} = \sum_{n \in N} \sum_{\theta \in \Theta_n} (\mathrm{U}_\theta \cdot \mathbf{E}_\theta + \mathrm{C}_\theta^+ \cdot \mathbf{M}_\theta^+ + \mathrm{C}_\theta^- \cdot \mathbf{M}_\theta^- + \mathrm{C}_\theta \cdot \mathbf{M}_\theta)$$

where

| | |
|---|---|
| $C_{\text{thermal}}$ | thermal costs |
| $\theta \in \Theta_n$ | thermal clusters (sets of identical units with same characteristics) installed in node n |
| $U_\theta$ | Boolean variable indicating if a unit is in operation ($U_\theta = 1$) or offline ($U_\theta = 0$) in $\Theta$ |
| $\mathbf{E}_\theta$ | energy output from cluster (set of identical units with same characteristics) $\Theta$ |
| $C_\theta^+$ | start up cost of a single unit in cluster $\Theta$ |
| $\mathbf{M}_\theta^+$ | number of units changing from state *off* to state *on* in cluster $\Theta$ |
| $C_\theta^-$ | shutting down cost of a single unit in cluster $\Theta$ |
| $\mathbf{M}_\theta^-$ | number of units changing from state *on* to state *off* in cluster $\Theta$ |
| $C_\theta$ | costs for a running unit in $\Theta$: cost independent from output level (i.e. no load heat cost) |
| $\mathbf{M}_\theta$ | number of running units in cluster $\Theta$ |

with

$$C_{\text{unsupplied}} = \sum_{n \in N} \delta_n^+ \cdot \mathbf{E}_n^+$$

where

| | |
|---|---|
| $C_{\text{unsupplied}}$ | costs for unsupplied energy |
| $\delta_n^+$ | normative unsupplied energy value in node $n$ (value of lost load - VOLL = 15.000 €/MWh) |
| $\mathbf{E}_n^+$ | unsupplied energy in the nominal state |

with

$$C_{\text{spillage}} = \sum_{n \in N} \delta_n^- \cdot \mathbf{E}_n^-$$

where

| | |
|---|---|
| $C_{\text{spilled}}$ | costs for spilled energy |
| $\delta_n^-$ | normative spilled energy value in node $n$ (value of wasted energy in €/MWh), this value reflects a specific penalty that should be added to the cost function for each wasted MWh for any type of generation |
| $\mathbf{E}_n^-$ | spilled energy in the nominal state |

All above listed costs are input by the user:

- for thermal units a general set of costs per generation type exists and are unique for all bidding zones. For each ERAA process those are aligned with latest assumptions applied in the TYNDP as well as some economic studies executed.

- for unsupplied and spilled energy costs are also defined by the user and handed to Antares as generic parameters

**Subject to the following constraints related to the nominal system state**

- **Balance between load and generation**

$$\forall n \in N, \qquad \sum_{\ell \in L_n^+} \mathbf{E}_\ell - \sum_{\ell \in L_n^-} \mathbf{E}_\ell = (\mathbf{E}_n^+ + \sum_{\sigma \in \Sigma} \mathbf{E}_\sigma + \sum_{\theta \in \Theta_n} \mathbf{E}_\theta) - (\mathbf{E}_n^- + \mathrm{Load}_n)$$

on each node the unsupplied energy is bounded by the positive demand:

$$\forall n \in N, \qquad 0 \leq \mathbf{E}_n^+ \leq \max\ (0, \mathrm{Load}_n)$$

on each node the spilled energy is bounded by the overall generation of the node (must-run + dis-patchable energy):

$$\forall n \in N, \qquad 0 \leq \mathbf{E}_n^- \leq -\min\ (0, \mathrm{Load}_n) + \sum_{\sigma \in \Sigma} \mathbf{E}_\sigma + \sum_{\theta \in \Theta_n} \mathbf{E}_\theta$$

where

| | |
|---|---|
| $L_n^+ \subset L$ | set of links whose $n$ is the upstream vertex |
| $L_n^- \subset L$ | set of links whose $n$ is the downstream vertex |
| $\mathbf{E}_n^+$ | unsupplied energy in the nominal state |
| $\sigma \in \Sigma$ | reservoirs connected to node $n$ |
| $\mathbf{E}_\sigma$ | energy generated from reservoir $\sigma$ |
| $\theta \in \Theta_n$ | thermal clusters (sets of identical units) installed in node $n$ |
| $\mathbf{E}_\theta$ | energy generated from cluster $\Theta$ |
| $\mathbf{E}_n^-$ | spilled energy in the nominal state |
| $\mathrm{Load}_n$ | demand expressed in node $n$ (including must-run generation) |

- **flows on the grid**

Flows are bound by the sum of an initial capacity provided by the TSO via NTC hourly values:

$$\forall \ell \in L, \qquad 0 \leq \mathbf{E}_\ell^+ \leq \mathrm{NTC}^+$$
$$\forall \ell \in L, \qquad 0 \leq \mathbf{E}_\ell^- \leq \mathrm{NTC}^-$$
$$\forall \ell \in L, \qquad \mathbf{E}_l = \mathbf{E}_\ell^+ - \mathbf{E}_\ell^-$$

where

| | |
|---|---|
| $\forall l \in L$ | edges of G(N,L) |
| $\mathbf{E}_\ell^+$ | energy flow through $\ell$, all upstream vertices summarized |
| $\mathbf{E}_\ell^-$ | energy flow through $\ell$, all downstream vertices summarized |
| $\mathbf{E}_\ell$ | total energy flow through $\ell$ |
| $\mathrm{NTC}^+$ | positive maximum energy flow allowed between two nodes provided as NTC value by the TSO |
| $\mathrm{NTC}^-$ | negative maximum energy flow allowed between two nodes provided as NTC value by the TSO |

- **binding constraints**

  In the problem formulation, the modeling of the power system requires the introduction of diverse linear binding constraints between the system variables throughout the grid, expressed either in terms of hourly power, daily or weekly energies.

  The constraints are applied either on flows on a link or constraints placed on the output of a thermal unit.

  $$\forall b \in B_h, \qquad l^b \leq \sum_{j \in J} \kappa (\mathrm{E}_e)^o_{\uparrow} \leq u^b$$

  $$\forall b \in B_d, \forall k \in \{0, \dots 6\} \qquad l^b \leq \sum_{j \in J} \kappa \sum_{t \in 1,\dots 24} (\mathrm{E}_e)^o_{\uparrow(24k+t)} \leq u^b$$

  $$\forall b \in B_w, \qquad l^b \leq \sum_{j \in J} \kappa \sum_{t \in T} \mathrm{E}_{e_t} \leq u^b$$

  where

  | | |
  |---|---|
  | $j \in J$ | set of all grid interconnections and thermal clusters ($J = L \cup \Theta$) |
  | $b \in B$ | binding constraint |
  | $B_h \subset B$ | subset of B containing the binding constraints between hourly powers |
  | $B_d \subset B$ | subset of B containing the binding constraints between daily energies |
  | $B_w \subset B$ | subset of B containing the binding constraints between weekly energies |
  | $\kappa$ | weight of $e$ (either flow within $e$ or output from $e$) in the expression of constraint $b$ |
  | $o$ | time offset of $e$ (either flow within $e$ or output from $e$) in the expression of constraint $b$ |
  | $u^b$ | upper bound of binding constraint $b$ |
  | $l^b$ | lower bound of binding constraint $b$ |

- **hydro reservoir energy output**

  hydro energy produced throughout the optimization period is bounded

  $$\forall n \in N, \forall \sigma \in \Sigma, \qquad \mathrm{E}_{\min,\sigma} \leq \textstyle\sum_{t \in T} \mathrm{E}_{\sigma_t} \leq E_{max,\sigma}$$

where

| | |
|---|---|
| $E_{max,\sigma}$ | nominal maximum energy output from $\sigma$ throughout the optimization period |
| $E_{min,\sigma}$ | nominal minimum energy output from $\sigma$ throughout the optimization period |
| $E_{\sigma}$ | hydro energy output from reservoir $\sigma$ |

- **thermal units**

  The power output is bounded by must-run commitments and power availability

  $$\forall n \in N, \forall \theta \in \Theta_n, \qquad P_{min,\theta} \leq P_{\theta} \leq P_{max,\theta}$$

  the number of running units is bounded

  $$\forall n \in N, \forall \theta \in \Theta_n, \qquad M_{min,\theta} \leq M_{\theta} \leq M_{max,\theta}$$

  the energy output remains within limits set by minimum stable power and maximum capacity thresholds

  $$\forall n \in N, \forall \theta \in \Theta_n, \qquad l_{\theta} M_{\theta} \leq E_{\theta} \leq u_{\theta} M_{\theta}$$

where

| | |
|---|---|
| $P_{max,\theta}$ | maximum power output from cluster $\theta$ (depending on unit availability) |
| $P_{min,\theta}$ | minimal power output demanded from cluster $\theta$ (depending on unit availability) |
| $M_{max,\theta}$ | maximum number of running units in cluster $\theta$ |
| $M_{min,\theta}$ | minimum number of running units in cluster $\theta$ |
| $E_{\theta}$ | maximum energy output from $\theta$ throughout the optimization period |
| $M_{\theta}$ | number of running units in a cluster |
| $l_{\theta}$ | unit in $\Theta$ minimum stable power output when running |
| $u_{\theta}$ | unit in $\Theta$ maximum net power output when running |

## 2.7 Methodological Limitations in ERAA

The ERAA 2021 report contains an extensive list of methodological limitations, a subset of which, mainly relating to the Economic Dispatch, is summarized below [12]:

- the model is built on an NTC basis, while the final methodology for the regions where a flow-based market coupling approach is available, requires such an approach in the ERAA model. All calculations performed in this thesis are based on the ERAA 2021 methodology and use a cross-border NTC representation. The NTC representation for the Austrian bidding zone is considered to be very optimistic, which is why further investigations into the cross-border representation using flow-based domains are carried in recent ERAA publications [40].

- balancing reserves are taken into account by adding fixed demand profiles or deducting from maximum capacities of hydro power plants providing reserves
- no sectoral integration exists
- it is assumed that forced outages do not affect planned outages
- no random outage draws are considered for RES
- internal grid limitations are not taken into account within a bidding zone
- thermal and grid assets are not affected by climate conditions
- the market price cap is not dynamically modeled and is assumed to be the same for all regions (equal to a proxy of the Value of Lost Load = 15 000 €/MWh)[1]. The VOLL is an economic input parameter for unsupplied energy. Since the entry into force of the electricity regulation [4], Member States are required to carry out individual studies to calculate the value of lost load (VOLL) and the cost of new entry (CONE). These economic parameters are used in the Economic Viability Assessment of the ERAA, which is not carried out in this thesis. The proxy of VOLL of 15 000 €/MWh is used in the adequacy calculations in this thesis.
- Demand Side Response (DSR) is only modeled as demand reduction

In the context of this work, all test models are based on a representation of bidding zones at Member State level (e.g. in the geographically reduced trilateral test model there are three nodes that represent Austria, Switzerland and Italy North). Countries such as Italy, Norway and Sweden are divided into several bidding zones. All nodes are connected via network transfer capacities (NTCs), which are provided by the TSOs in hourly resolution. For the studies in this thesis that compare adequacy indicators, a test models is used in which a geographically reduced area is evaluated using the ERAA 2021 methodology. A full-scale European model is used for hydropower investigations in which the hourly dispatch is compared. Only results of individual climate years are extracted in hourly resolution and compared against each other.

Two main components of the ERAA methodology are excluded in this thesis: the flow-based representation of cross-border electricity exchange and the economic viability assessment (EVA). The EVA assessment is integrated into the ERAA process from ERAA 2022 and determines the viability of generation units in the European power plant fleet. Units that are identified as non-viable are then deducted for the adequacy assessment. All modeling conducted as part of this work is based on the MAF or ERAA 2021 methodology and some of the developments made in this work are then transferred to the Antares ERAA 2022 and 2023 models.

[1]As the price cap for the real market wholesale day ahead coupling (SDAC) in 2021 was 3000 €/MWh, a sensitivity was carried out in the ERAA 2021 using the lower price cap.

# 3 Input Data

For each country node in the resource adequacy assessment, a thorough preparation of the input data is the first step in the modeling process. Each TSO has the task of providing the best possible estimate of its future power plant fleet in accordance with the National Energy Climate Plans (NECPs). Such a plan is available for Austria from the Federal Minstry for climate Action, Energy, Mobility, Innovation and Technology [41]. To simplify data collection, a European database is available to support the collection of input data by the TSOs. This database is called the Pan European Market Modelling Database (PEMMDB) and is used for all ENTSO-E processes – from resource adequacy assessments over transmission adequacy studies (TYNDP) and market studies such as the Bidding Zone Review (BZR).
In addition to collecting estimates from TSOs on net installed generation capacity, ENTSO-E works closely with climate institutions and universities. The Technical University of Denmark (DTU) provides the climate database used in this process, namely the Pan European Climate Database (PECD) [42]. This climate database contains capacity factors for photovoltaic and wind generation per node for the historical climate years 1982 to 2016. The representation within resource adequacy assessments defines a node to represent a Member State, despite for bigger countries like Norway, Sweden, Italy, the country is split in several bidding zones. The hourly PECD wind and PV load factors are used to multiply the installed capacities per bidding zone and thus obtain hourly production time series for renewable generation. Climate variables such as temperature, irradiance, wind speed, etc. are also required for the creation of demand time series. All variables are provided for the climate years 1982 to 2019 for each bidding zone. This chapter provides an overview of the input data used and their preparation for the assessment of resource adequacy.

## 3.1 Electricity Generation

The ERAA process provides assessments to evaluate the adequacy of resource up to ten years into the future, for which the ENTSO-E collects the yearly evolution of installed capacities of the various types of generation for the upcoming decade.

### 3.1.1 Renewable Energy Sources (RES)

The following installed capacities are available in PEMMDB format for electricity generation from renewables. These follow the TSOs' best estimates for future climate targets:

**Wind**

- onshore
- offshore

**Photovoltaic**

- Concentrating Solar Power (CSP)
- solar rooftop
- solar photovoltaic farms

**Other renewables**

- small biomass
- geothermal
- marine
- waste
- not defined or splitting not known

To obtain the 35 climate-dependent hourly input time series for wind and PV production for each target year and country node, the following is performed:

For photovoltaic generation, the installed capacity from the PEMMDB is multiplied by the PECD capacity factors for photovoltaic (rooftop and farm systems) and solar CSP generation in hourly resolution. In a second step, these two time series are aggregated. For wind generation, the installed capacities are multiplied by the PECD capacity factors for onshore and offshore wind generation. The final 35 climate-dependent wind and PV time series are then entered into the scenario builder of the modeling tool. Time series for other renewables are created according to the TSO's specifications by either providing hourly load factors (not climate year dependent) or assuming an availability of 100 % in case the TSO does not provide load factors.

No additional planned or unplanned outages are explicitly modeled for RES, as these are already included in the hourly time series provided by the meteorological institution. The provided load factors already contain a share for non-availability of wind or PV production. RES power is fed into to the system with zero cost and curtailed when demand is low [12].

### 3.1.2 Hydro

Since the introduction of a new database format (PEMMDB 3.0), the collection of input data for hydropower generation follows a different approach than in MAF 2017 and 2018. A detailed assessment of the differences between the PEMMDB 2.0 and PEMMDB 3.0 database and its impact on the hydropower modeling approach is discussed in a master thesis [22] and serves as a starting point for the developments described in this thesis.

The following classification of hydropower plants is available in PEMMDB 3.0 format [43]. The information on the turbine and pump power is recorded at power plant level, while the storage size is provided in aggregated form per storage type:

1. **Run of River and Swell (ROR and Swell)**

   This category includes hydropower plants on rivers that utilize the large flow rates of water (i.e. Danube power plant Altenwörth 328 MW [44]). Most of these large plants have no connected reservoirs. There are hydropower plants on individual rivers in Austria (i.e. Drau, Enns) that can impound water. These reservoirs have a maximum storage capacity of 24 hours. Power plants that utilize the damming potential of a river are referred to as swell power plants ($\text{Reservoir}_{\text{capacity}}$ / $\text{turbine}_{\text{capacity}} \leq 24$ hours). In the previous PEMMDB 2.0 format, this category was divided into pure run of river and swell units, while in the new database format both types are merged into one category called run of river and swell.

   For Austria, this **merge has a significant impact on the flexibility of hydropower** and is explained in more detail in chapter 4.4. As a result of the research work carried out, APG requested ENTSO-E in 2020 to subdivide this category again for future data collection in order to take this type of generation into account properly.

2. **Traditional Reservoir (TR)**

   Hydropower plants that utilize the potential energy of stored water in large reservoirs with natural inflow but without pumping capacities belong to this category. Their storage capacity is greater than 24 hours ($\text{Reservoir}_{\text{capacity}}$/ $\text{turbine}_{\text{capacity}} > 24$ hours), i.e. the total time to empty a reservoir extends over a longer period (e.g. week, month, year). The traditional reservoirs are located in the Austrian Alps, which offer a large storage potential. An example of a traditional reservoir in Austria is the hydropower plant Gerlos with a total turbine power of 200 MW [45].

3. **Open Loop PSP reservoir (OL PSP)**

   Plants in this category have a reservoir that is fed by natural inflows and supply pumped energy. This category is of great interest to Austria, as the storage potential of the Alps can be used like a huge green battery. One of the largest pumped storage power plants in Austria is the Malta-Reißeck power plant group in the south of Austria [46]. In this thesis the power plant group Kaprun located in Salzburg is used for detailed modeling and explained in chapter 4.5.

4. **Closed Loop PSP reservoir (OL PSP)**

   Hydropower plants in this category are pumped storage power plants with reservoirs without natural inflows. The water is stored in two basins (upper and lower basin) and the water is turbined and pumped between the two basins. There is no closed loop pump storage plant in Austria in 2024; a project with a turbine and pump power of 300 MW [47] is planned. One example from the German power plant portfolio is the Goldisthal pumped storage power plant with a turbine and pump power of 1 GW [48].

A round-trip efficiency of 75% is assumed for all pumping units.

Table 3.1 provides an overview of the input data collected for each of the four hydro categories [12]. The distinction according to the resolution of the available data is divided into daily (D) and weekly (W) information, availability (*) and non-availability(-), red colored entries are not used in the process.

**Table 3.1:** Hydro data availability and resolution in the PEMMDB 3.0 database format - used in ERAA 2021 [12]

| [MW/GWh] | Run of River &Swell | Trad. Reservoir | Open Loop PSP | Closed Loop PSP |
|---|---|---|---|---|
| Hydro Inflows | D | W | W | - |
| max. power output | D | W | W | W |
| min. power output | D | W | W | W |
| max. generated energy | - | W | W | W |
| min. generated energy | - | W | W | W |
| max. pumping power | - | - | W | W |
| min. pumping power | - | - | W | W |
| max. pumped energy | - | - | W | W |
| min. pumped energy | - | - | W | W |
| Deterministic Reservoir Level | - | W | W | - |
| max. Reservoir Level | - | W | W | - |
| min. Reservoir Level | - | W | W | - |
| Reservoir Size | * | * | * | * |
| Installed Capacity | * | * | * | * |

D: Daily
W: Weekly
- : not available
* : available

**Hydrological inflow** data are provided centrally by the Swedish Meteorological and Hydrological Institute (SMHI) [49] for inflows from river and reservoirs for the historical years 1982 to 2017 This data is also referred to as the “PECD Hydro database”. For Austria, the inflows provided by the SMHI for rivers correspond very well with the historically observed inflow values, while for reservoirs the inflows from SMHI do not correlate with historical data collected by the Austrian TSO. APG therefore provides the historical inflows for the reservoirs in Austria directly to ENTSO-E. As historical data is only available up to 2010, the years between 1982 and 2010 are provided with a transfer function that correlates the available inflow information from 2010 to 2017 with the earlier years.

For run of river power plants, the inflows are dispatched immediately, while the inflows for reservoirs are aggregated into monthly energy quantities and pre-optimized with the help of tool-specific heuristics, as explained in chapter 2.6. According to the main optimization algorithm, these energy quantities can then be released or stored for later use. If the hourly inflows exceed the dispatch requirement or the maximum storage level trajectories, these can be spilled accordingly.

**Minimum and maximum power output** refer to specific technical, operational or statistically derived limits that restrict the flexibility of hydropower generation. If those are not explicitly provided by the TSO, they are assumed as 0 for minimum power and installed capacity for maximum power.

**Minimum and maximum generation energy constraints** are used to represent weekly limitations to the energy output. The total generation over a whole week has to be lower or higher to the maximum or minimum energy constraint of the respective week.

**Maximum pumping power** – the maximum power output of a pumping unit used in adequacy simulations.

**Reservoir level constraints** are provided by the TSOs in weekly resolution. For APG, Austria's historical reservoir levels are measured and the minimum and maximum values per week are extracted. These are used by the modeling tools as hard constraints at the beginning of each week. The solution often ends in infeasibility as the solver sets the initial reservoir level at the beginning of a week without sufficient flexibility. Therefore, these constraints are often converted to soft constraints with a penalty cost that is sufficiently high but not as high as the Value of Lost Load (VOLL), causing the solver to prioritize the use of hydro resources and inflows in hours of scarcity. This avoids the triggering of adequacy indicators. Details on the optimization can be found in chapter 2.5.

All of the above information can be provided for each climate year, while the information on storage size, turbine and pump power is generally available and applies to every climate year. In the PEMMDB 3.0 database format, this information is also recorded for each power plant, while storage sizes are aggregated per storage type. The resolution at the level of individual power plants is not used in MAF and ERAA modeling, but is used in this work, where a hydropower plant cascade is discussed for adequacy simulations (see chapter 4.5).

### 3.1.3 Thermal

The resolution of thermal generation units as part of the data collection with the new database format has been significantly improved. Thermal plants are recorded on unit-by-unit resolution with detailed geographical information that includes net generation capacity, fuel type, commissioning and decommissioning date, operating status and additional technical constraints such as start-up and shutdown information. If available from the TSO, also cost information on start-up, fixed and variable costs as well as $CO_2$ emission rates and outage information for the supplied thermal units are also recorded. The TSO can also provide capacity derating, must run ratios or inelastic profiles in hourly resolution. By default standard thermal parameters such as efficiency range, $CO_2$ emission factor, variable costs, etc. are centrally defined for all thermal generation types and matched with TYNDP studies. The standard thermal characteristics can be downloaded from the ERAA website [12].

Within the optimization, thermal units are dispatched prior to their decommissioning date following their marginal fuel price including costs for $CO_2$ emissions (not for biofuel units). Start-up costs are considered when units need to be started.
Units with must-run constraints are supposed to generate at least as much as the constraint requires.
Derating constraints can be made available by the TSO in hourly time series, which means that the entire installed capacity of a block is not always available and is therefore offered on the market. Only the reduced quantity is taken into account in the economic dispatching. Reasons for a capacity reduction may be that generators provide a system reserve or use inferior fuels, or that their output is limited by transmission and cooling constraints.

### 3.1.4 Reserves

Ancillary services are of crucial importance for a TSO as a control area operator. In order to stabilize or restore the frequency within a control area after a major disturbance (e.g. tripping of blocks) the following categories of reserves are available: Frequency Containment (FCR) and Frequency Restoration (FRR) reserves are used for the very short-term operation (< 1 hour). From ERAA 2021, both FCR and FRR reserve types will be used as part of adequacy processes with two different approaches: reducing thermal production – this is achieved by adding the reserves to the electric load, while for countries that provide reserves as part of the hydropower generation, these reserves are deducted from the maximum hydropower generation per generation type [12]. For Austria, 32 MW are added to the load and 513 MW deducted from hydro maximum capacity, according to the formula below:

$$P_{\mathrm{max,ERAA}} = P_{\mathrm{max,instTSO}} - P_{\mathrm{reserve,hydro}}$$

where

| | |
|---|---|
| $P_{\mathrm{max,ERAA}}$ | total maximum generation capacity input to the model |
| $P_{\mathrm{max,instTSO}}$ | total installed capacity within the country node |
| $P_{\mathrm{reserve,hydro}}$ | total reserve defined as reduction from hydro production |

### 3.1.5 Demand Side Response (DSR)

In addition to the types of generation described in sections 3.1.1 to 3.1.3, which bid either at zero cost or marginal price, there is a degree of price-elastic demand side response (DSR) in the system.

Price elasticity in this case means that when a certain threshold is reached, a customer (e.g. industry) is able to reduce its demand in that hour as soon as the activation price is reached. For Austria, in the target year 2025 of the ERAA 2021 process, 200 MW of explicit DSR are placed in the system for the target year 2030, which start to react at an activation price of 500 €/MWh. An additional constraint is the number of hours in which this reduction can be performed, and this value for Austria is 24 hours per day for the ERAA 2021 process. According to the first results of the ERAA 2021 output, the available DSR of 24 hours per day seems to be too optimistic (meaning that the demand reduction most likely cannot be applied for every hour of the day if it is an industrial process). The number of hours per day in which explicit DSR can be activated is reduced in later processes.

In future, the reaction of end consumers to price signals must be taken into account in the system. In addition to the explicit DSR quantity - mostly industries – an additional representation must be created to reflect the flexible behavior of demand components like heat pumps (HPs) or electric vehicles (EVs). These units can shift their demand according to price signals, also referred to below as implicit DSR (iDSR). This shifting possibility is elaborated via the approach for short cycle storage described in chapter 4.3. The theoretical description of a possible development path for EVs and HPs in the demand sector was elaborated together with the Austrian Institute of Technology and is described in chapter 3.2. The implication of the modeling approach is discussed in chapter 6.5. This thesis describes a first attempt at possible modeling approaches, which should serve as a starting point for future investigations. The amount of shift able demand provided by the TSOs as part of the data collection stayed at a very low level. Austria stated a flexible share of 5 %, which increased to up to 50 % in the context of this work. 50 % served as an academic assumption in combination with the cautious opinion of a 100 % penetration of the flexible share of heat pumps and EVs in the Austrian system.

### 3.1.6 Austrian generation fleet

The provision of input data by the TSOs is one of the most important workflows necessary for the start of the modeling activities at ENTSO-E. For reasons of transparency, Table 3.2 provides an overview of the input data for Austria for all MAF and ERAA processes carried out between 2017 and 2022 and targeting the year 2025. Only publicly available data is shown. The modeling in this work includes test models based on the MAF 2019, ERAA 2021 and ERAA 2022 data. Publicly accessible information on energy storage and the detailed breakdown of storage were introduced in the ERAA 2022.

The separation of run of river and swell capacity is available in the MAF 2018 input data, while this separation disappeared from MAF 2019 onwards and was only available in aggregated format. It took three editions of MAF and ERAA publications before the separation of run of river and swell was successfully implemented again. This improvement in data collection is based on the findings that were carried out as part of this work [50] accompanied by a bachelor thesis [51].

On the thermal side of the Austrian generation mix, the decommissioning of thermal plants can also be tracked over time. With each data collection, the available installed gas capacities are re-discussed based on the available contracts for the Austrian grid reserve. The MAF 2019 process shows the lowest assumption with regard to the availability of thermal units.
The high installed capacity from hydropower in the MAF 2018 compared to the subsequent processes is due to the fact that the hydropower plants of the “Kraftwerksgruppe Obere Ill Lünersee” were still allocated to the Austrian control area in this process, while they switched to the German control area in 2017 and account for around 1,7 GW. This shift has been taken into account since the MAF 2019 and is included in the Winter Outlook Report 2017/2018 [52].

It should be noted that the information below is the best information available within APG at the time of data collection. The data collection is based on sources from Oesterreichs Energie, E-Control and projects listed on the basis of grid access applications within APG. This means that construction-related project delays are reflected differently each year in the individual processes.

Demand Side Response was delivered and implemented for the first time as part of the ERAA 2021 process, electrolyzers and batteries for the first time as part of the ERAA 2022 process.

**Table 3.2:** Installed turbine and pump power and storage capacities in MAF and ERAA processes provided for target year 2025

| National Estimates 2025 - AT | MAF 2018 | MAF 2019 | MAF 2020 | ERAA 2021 | ERAA 2022 |
|---|---|---|---|---|---|
| **Generation power in MW** | | | | | |
| **Thermal** | | | | | |
| Nuclear | 0 | 0 | 0 | 0 | 0 |
| Lignite | 0 | 0 | 0 | 0 | 0 |
| Hard Coal | 0 | 0 | 0 | 0 | 0 |
| Gas | 4863 | 3416 | 3416 | 3982 | 4146 |
| Oil | 178 | 168 | 168 | 164 | 120 |
| Others non-renewable - includes combined heat and power (CHP), waste and any type of non-dispatchable thermal generation | 956 | 955 | 953 | 957 | 845 |
| **Hydro** | | | | | |
| Swell (turbine) | 1345 | 6130 | 6130 | 6072 | 1147 |
| Run of River (turbine) | 4702 | | | | 4825 |
| Traditional Reservoir (turbine) | | 2430 | | 2489 | 2756 |
| OL PSP (turbine) | 8888 | 4188 | 6617 | 3943 | 3774 |
| CL PSP (turbine) | | 0 | | 300 | 0 |
| PSP OL (pump) | -5385 | -3160 | not | -3146 | -3283 |
| PSP CL (pump) | | 0 | published | -300 | 0 |
| **Renewables** | | | | | |
| Wind Onshore | 4400 | 5500 | 5500 | 5500 | 5000 |
| Solar (photovoltaic) | 3200 | 5002 | 5000 | 5000 | 5000 |
| Others renewable | 595 | 609 | 601 | 586 | 644 |
| Biofuel | 0 | 0 | 0 | 0 | 0 |
| **Other** | | | | | |
| Electrolyser | 0 | 0 | | 0 | 15 |
| Demand Side Response | 0 | 0 | | 200 | 200 |
| Batteries (discharge) | 0 | 0 | | 0 | 33 |
| Batteries (charge) | 0 | 0 | | 0 | -33 |
| Batteries (storage) | 0 | 0 | | 0 | 0,05 |
| **Hydro energy storage in GWh** | | | | | |
| Swell | | | | 5,59 | 5,31 |
| Traditional Reservoir | | | | 2491 | 769 |
| Pump Storage Open Loop | | | | | 1739 |
| Pump Storage Closed Loop | | | | | 0 |
| **total installed power and storage capacity** | | | | | |
| turbine power in MW | 29127 | 28398 | 28385 | 29193 | 30985 |
| pump power in MW | -5385 | -3160 | 0 | -3146 | -3283 |
| storage capacity in GWh | | | | 2497 | 2514 |
| total annual demand in TWh | 76 | 77 | 76 | 73 | 76 |
| maximum peak load GW | 13 | 13 | 13 | 13 | 14 |

## 3.2 Electricity Demand

As the demand for electricity fluctuates greatly depending on the different climatic conditions, very cold winter days, for example, lead to high peak values due to the increased demand for heating (e.g. in France and Belgium, many households simply use electric heaters). In modern households throughout Europe, heat pump systems are coming onto the market that also exhibit special behavior below a threshold of around -5°C. At this so-called point of bivalence, the heat pumps switch their behavior to full electric heating. The temperature dependency on the demand side must therefore be given special attention in the context of the adequacy assessment.

Between 2017 and 2022, ENTSO-E used a temperature regression and load forecasting tool called TRAPUNTA [53] to create hourly demand time series for the respective target years with uncertainty analysis under different climate conditions. With this approach, it is possible to forecast electricity demand based on the analysis of historical time series.

As information is available on the timing of electricity generation projects in Austria and the NECP provides clear development streams for these generation units, there are a number of reasonable sources of information for annual growth on the generation side. For the demand side, however, several assumptions must be made and the growth rates of the various demand components must be carefully estimated.

The specifications of future additional load components are discussed in the following chapters. Since these technologies mainly affect the consumer side, which is very often also connected to its own PV system, the interaction between these technologies within a household is much more complex to predict than for traditional household loads. The theoretical background of the individual components is discussed in this chapter, while the practical implementation in the modeling approach is discussed in chapter 5. The investigations in this thesis serve as a starting point for the evaluation of an initial approach for flexible consumer behavior. Electricity prices were still at a very low level during the period under investigation of this thesis (2018 - 2021). The drastic increase in electricity spot prices, but also the increase in fuel prices at the end of 2021, may already lead to a motivation on the consumer side to invest in these new technologies.

### 3.2.1 Heat Pumps

In line with the European Commission's carbon neutrality targets [54], it is not only the electricity generation sector that is affected by a system change. On the consumer side, new-build households are also opting for heat pumps as an efficient heating system due to their energy-efficient building fabric. In addition, existing oil and gas fired heating systems are being replaced with heat pump systems.

In their basic function heat pumps absorb heat from the environment (air, water, ground) and use a built-in compressor with inverter technology to raise the temperature inside the building to a comfortable level [55]. In order to run the thermal cycle, the heat pump uses a compressor which acts as an electrical load. It is supplied with electricity from the grid or, in certain cases from the building's own PV system. As a rule, heat pumps are used for underfloor heating and also for domestic hot water supply. A boiler can act as a thermal storage in the household and thus conserve a certain amount of PV surplus which is available for hot water use at a later time. Heat pumps are also often used as part of a hybrid energy system that combines several thermal and electrical technologies [56]. The future goal of households using a combined system of PV, heat pump and storage, is to:

- minimize energy consumption from the grid
- minimize or avoid dependency on fossil fuel consumption (if available)
- maximize the use of self-generated energy from the PV system

The number of installed units and their expected development over the next decade is important for use in adequacy studies. The results of the study conducted together with AIT are summarized below [57].

Based on the historic data of the Austrian "Technologie-Roadmap für Wärmepumpen", and development streams elaborated in the yearly report of "Energie und Umweltforschung über innovative Energietechnologien in Österreich" [58] , an estimate on the development until 2030 is presented in Figure 3.1:

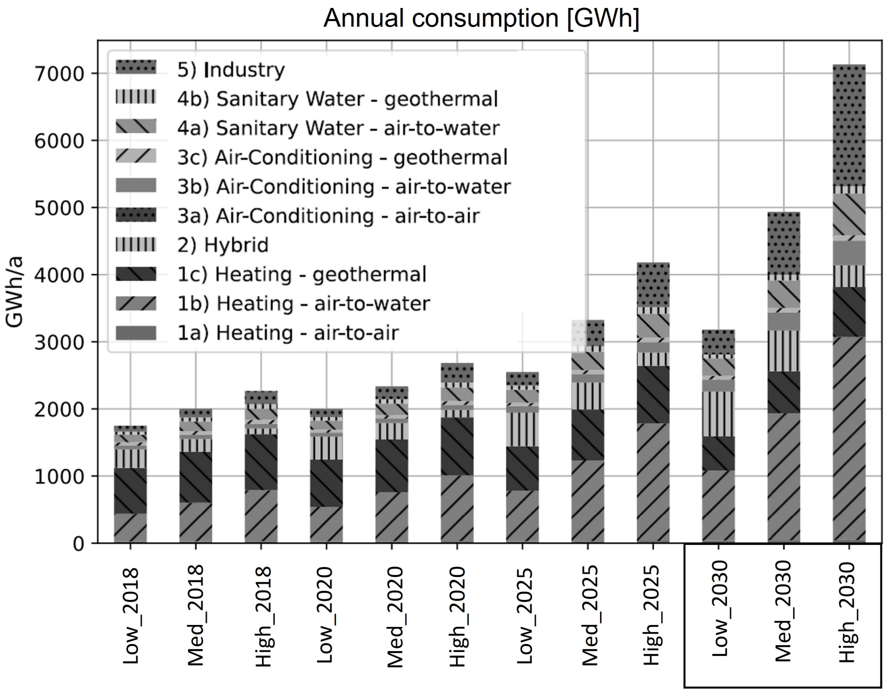


**Figure 3.1:** Expected yearly energy consumption for the different heat pump categories for 2018, 2020, 2025, 2030 [57]

The values for 2020 are taken from the publicly available installed systems of the Austrian heat pump association, which at the time of publication only contained historical values up to 2015, which is why the years 2018 and 2020 are also presented as scenarios. The breakdown of the different heat pump types (classification) is based on the categories of the different heat pump types required in the ENTSO-E PEMMDB 3.0 data collection guideline.

For the different penetration rates, which depend on different external factors (e.g. electricity & fuel prices, subsidies), scenarios for low, medium and high penetration rates are assumed. Air-to-water heat pumps appear to be the most commonly used variant. This can be explained by the lower installation effort compared to heat pumps that use primary energy from the ground or from geothermal energy, and thus by the lower installation costs [55].

The values in this diagram are given in GWh per year, i.e. the average annual consumption per heat pump category is shown. For the year 2030, the estimates show an annual average consumption of slightly more than 7 TWh for the high scenario, which corresponds to 7.7 % of the total projected demand of 90.76 TWh in 2030, while the low scenario assumes slightly more than 3 TWh, which would account for 3.3 % of the total projected demand of 90.76 TWh in 2030. Weather scenarios from the meteonorm software version 7.3 [59] were used as the climatic basis for the development of the energy values listed.

The total yearly energy amount provides a first indication of additions to the load, whereby the winter months and especially winter days with very low temperature are of peculiar interest for adequacy calculations. Depending on the manufacturer settings of the heat pump, the point of bivalence at which the heat pump begins to use additional electric heating elements is around -5°C. For the present work, -5°C is assumed as the bivalence point.

An estimate on the maximum electrical power output in MW of the scenarios described above (low, medium, high) is shown in Figure 3.2 assuming an outside temperature of -8°C.

At an outside temperature of -8°C, the scenario for a high market penetration of installed heat pump capacities assumes an additional peak load of almost 4000 MW, while the low scenario for 2030 assumes values of just over 1500 MW.

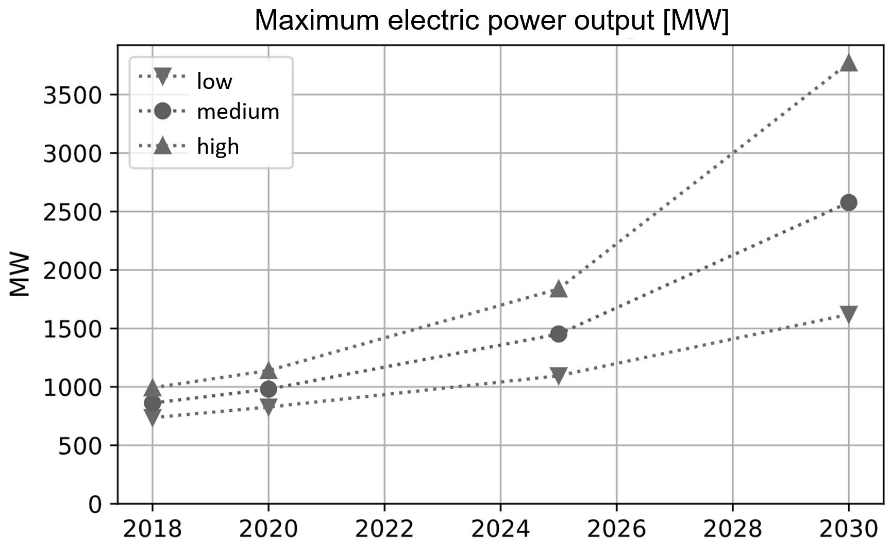


**Figure 3.2:** Historical and forecast maximum capacity of heat pumps in MW - taking into account the additional electrical heating at − 8°C outside temperature [57]

On winter days with temperatures below - 5 °C (specific value depending on the manufacturer), heat pumps switch on additional direct heating, which must be taken into account when creating the load profiles. In Figure 3.2, this proportion of direct heating is already included at an outside temperature of - 8 °C, which accounts for around 15 % to 20 % of the maximum heat pump output shown in the graph. At an outside temperature of - 12 °C instead of - 8 °C, the purely electrical heating component would already account for 30 % of the maximum heat pump output.

Since the dependence of heat pump behavior on the ambient temperature strongly influences the calculations on the adequacy of resources, so that very cold winter days are very likely to lead to a shortage, heat pump behavior must be adequately taken into account when creating time series for electricity demand.

Figure 3.3 shows the temperature dependence of the electrical output of heat pumps installed in Austria for the year 2020. In this case, historical weather data (meteonorm 7.2, measured historical values) [59] is used for the medium penetration scenario.

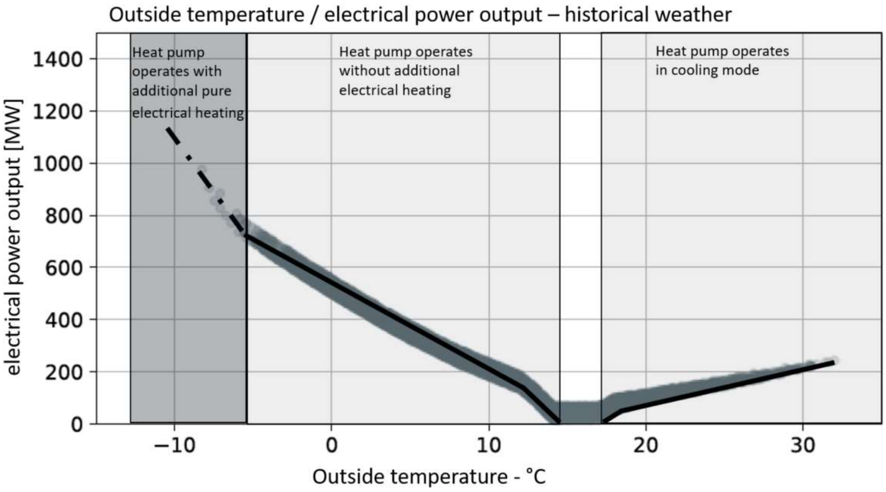


**Figure 3.3:** Power output of heat pumps as a function of the outside temperature

Heat pumps normally operate in heating mode as soon as the outside temperature is below 15°C. Between -5°C and 15°C outside temperature, heat pumps operate close to their optimum coefficient of performance (COP), which is defined as the ratio between the output power generated by the heat pump and the electrical input power required to supply the compressor. At temperatures below -5°C, the heating output cannot solely be provided by normal operation of the air to water heat pump system, thus an additional electrical heater with a conversion factor of 1 is required to cover the heating demand. This can be seen in the diagram shown in Figure 3.3, in which the linear behavior changes at -5°C. This temperature point depends on the manufacturer of the heat pump system, but is generally in the range of -5°C.

Temperature values are available from 35 measurement locations in Austria, distributed at the NUTS 3 geographical level. In a second step, these 35 measured values are averaged for the Austrian country node. The NUTS levels are usually used for the geographical division of a country. The NUTS 3 level shows the division of Austria between district and federal state level [60]. Figure 3.4 displays the NUTS3 division of Austria.

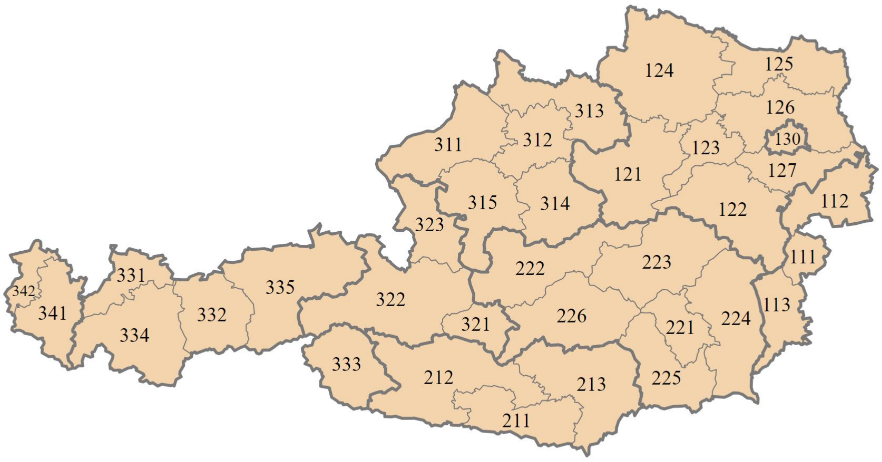


**Figure 3.4:** Map of Austria divided in NUTS3 regions

A certain proportion of heat pumps are also used for cooling in summer, although the impact on the adequacy of resources is not yet discussed at this stage. At the time of publication of this paper, load shortfalls occur mainly in the winter months. It cannot be excluded that the effects on the summer months will also need to be investigated in the future.

An additional feature of heat pumps that affects the adequacy modeling is the fact that heat pumps can shift their electricity consumption to a different number of hours under the right circumstances (introduction of smart meters, availability of a variable hourly tariff structure, available grid components). In 2021, this behavior is not yet state of the art in Austria, as the prerequisites such as the introduction of smart meters and a variable hourly tariff structure are not yet very well developed. For the future, it is difficult to predict if only the heat pump owner is interested in shifting the operating time of the heat pump or whether grid operators could also be interested in a centralized approach to controlling heat pump operation in private households. At the time of the research, only a few electricity suppliers, including two heat pump suppliers, offered the option of price-reactive control of heat pump consumption [61][62][63].

While the previous implementation of the shift able electricity consumption for heat pumps remains a negligible variable, the estimated potential for the flexible electricity consumption of heat pumps for the average penetration rate is estimated as follows: Figures 3.5 and 3.6 illustrate the shift able electricity consumption for the year 2020, which has a maximum positive flexible behavior of 700 MW for three hours at a temperature of -5°C, while the maximum negative flexible consumption at -5°C is about 200 MW for five hours. Considering warmer outdoor temperatures, e.g. 10°C for the year 2020 (Figure 3.5), 200 MW can be shifted in a positive direction in a time frame of 15 hours, while 750 MW can be shifted in a negative direction for two hours and 400 MW for the time frame of three to four hours (Figure 3.6).

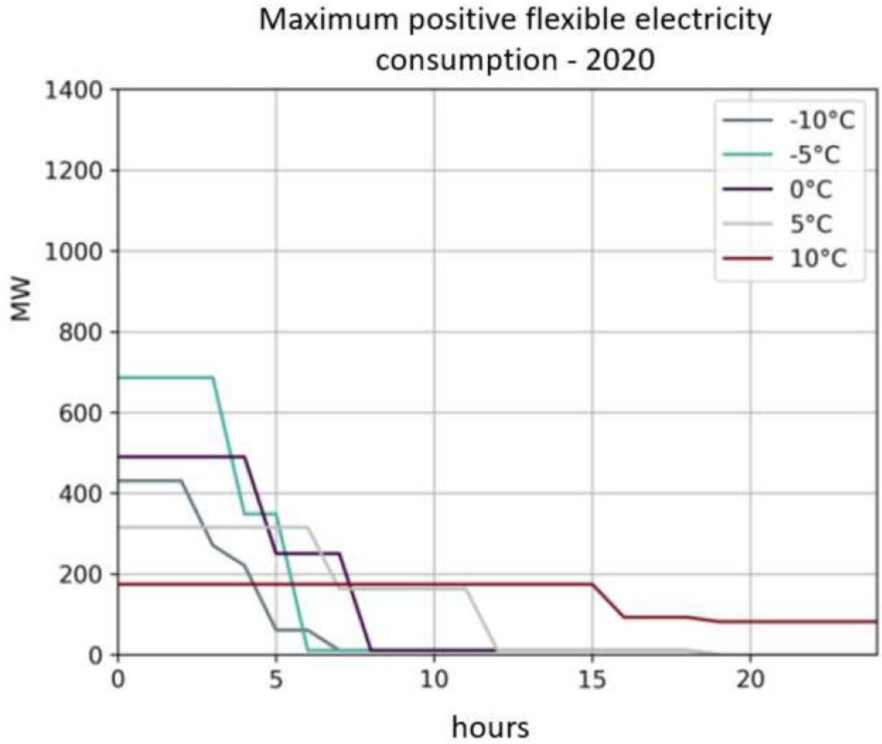


**Figure 3.5:** Maximum positive flexible electricity consumption for the year 2020 (medium HP penetration scenario)

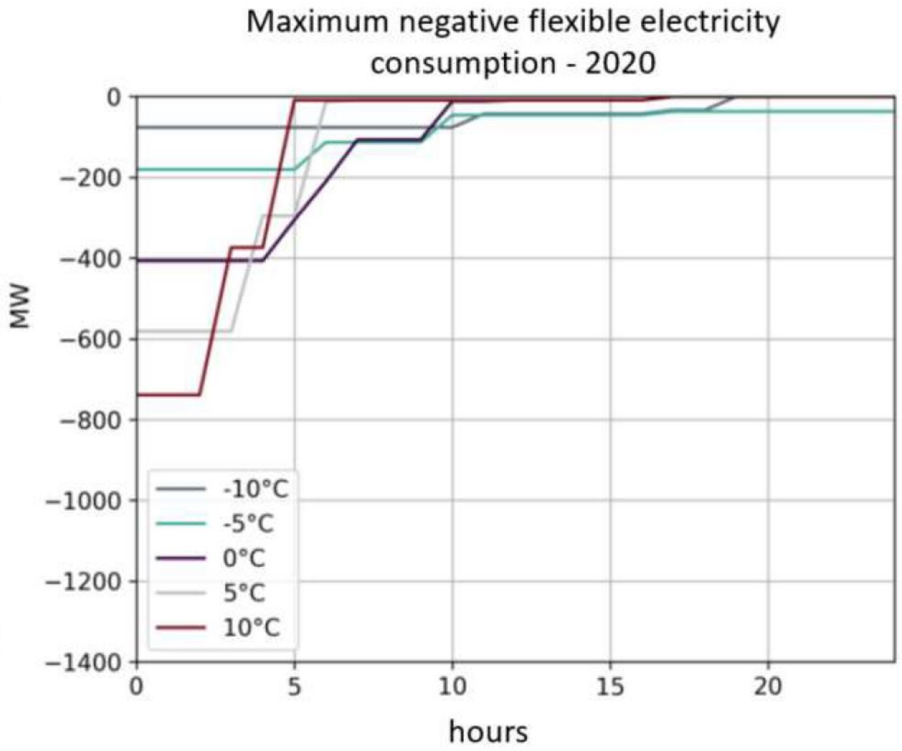


**Figure 3.6:** Maximum negative flexible electricity consumption for the year 2020 (medium HP penetration scenario)

Of interest for the adequacy calculations is the maximum positive flexible power consumption, which leads to the instantaneous electrical power in the hours of scarcity being shifted to the neighboring hours. For ERAA 2022, a modeling approach of 6 hours of shift able power with a total of 5 % of the total installed power was assumed for the model building (assumptions in consultation with the APG management based on the figure 3.5).

While the theoretically usable potential for flexible load shifting of heat pumps is presented in this section, the use in adequacy assessments is explained in chapter **??**, results are presented in chapter 6.5.

### 3.2.2 Electric Vehicles

As with heat pumps, an estimate of future electric vehicle penetration for Austria is being prepared in close cooperation with the AIT [64]. The load profiles for the Austrian electric vehicle fleet for the target years 2020, 2025, 2030 and 2040 are created with the help of the load profile generator developed by AIT. The load profiles are created on the basis of the 35 historical climate years (1982 - 2016) for the respective target years. The input data required to create the load profiles are described below.

First, two different user types of electric vehicles are defined and fed into the PEMMDB 3.0 together with their properties:

1. private electric vehicles
2. non-private (business) electric vehicles

Secondly, the types are also classified according to their charging behavior:

1. pure electrical charging (EVs)
2. mixed plug-in hybrid EVs (PHEV)
3. light commercial vehicles (LCV)[1]

As a starting point for EV development, historical data from Statistics Austria is used and the following future scenarios are assumed: 2025 and 2030 are based on the IEA Sustainable Development Scenario (SDS) [65], while the development for 2040 is to be based on a 100 % carbon-neutral scenario, therefore EV targets from the ONE100 study are used [66]. This distinction applies for the reason that the data up to 2030 is used for resource adequacy assessments guided by the development of the NECP, while the data for 2040 is used for transmission adequacy studies where the scenario assumes that the 100 % carbon neutrality target is achieved in 2040.

Based on the development scenarios described above, a breakdown between private and commercial EVs and PHEVs, their share of the total fleet and the market entry of e-LCVs is assumed and shown in the table 3.2.2.

**Table 3.3:** EV, PHEV and e-LCV market share and future penetration

| Year | $\frac{EV}{EV+PHEV}$ | $\frac{PHEV}{EV+PHEV}$ | total market EV share | total market e-LCV share |
|---|---|---|---|---|
| 2020 | 75 % | 25 % | 1 % | 0 % |
| 2025 | 77 % | 23 % | 7 % | 7 % |
| 2030 | 79 % | 21 % | 21 % | 33 % |
| 2040 | 100 % | 0 % | 70 % | 73 % |

If the above table is transferred to a graphical overview of the percentage shares of private and commercial EVs in the total fleet in the forecast target year, the following picture emerges (Figure 3.7):

[1] Not available in the 2020 statistical data, but taken into account for the target years from 2025 - classified as type “Truck N1” in Austria Total weight < 3.5 t

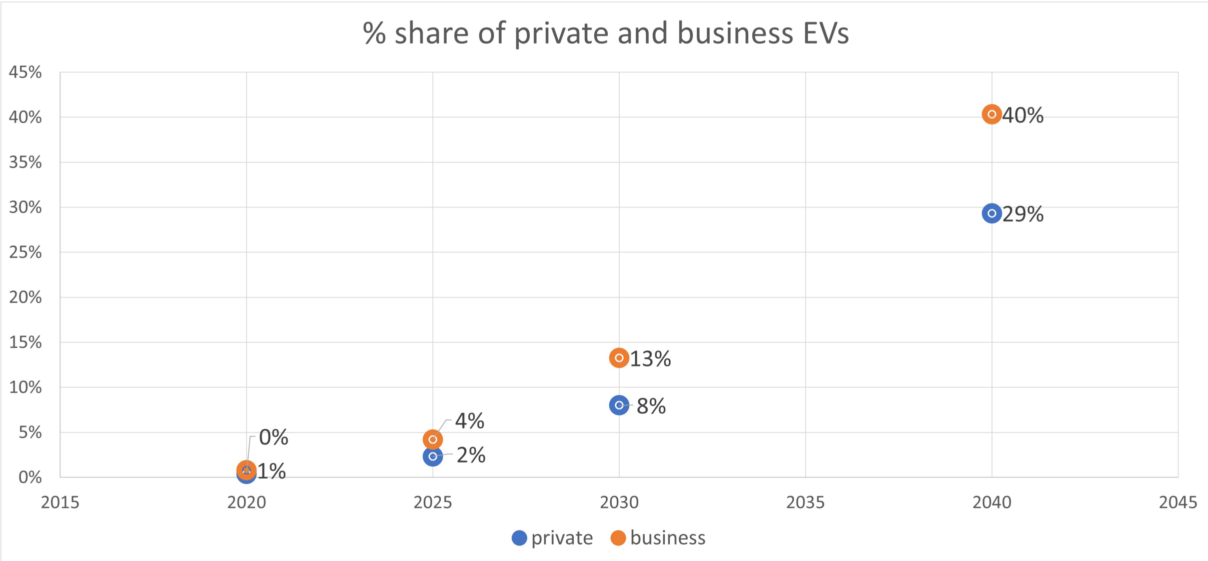


**Figure 3.7:** Percentual share of private and business EVs on the total fleet

For the years in between, a logistic growth rate is assumed, which is shown in Figure 3.8 and illustrates the total number of EVs in the system up to 2040. The blue line shows the development of private EVs, while the orange line shows the development of commercial EVs.

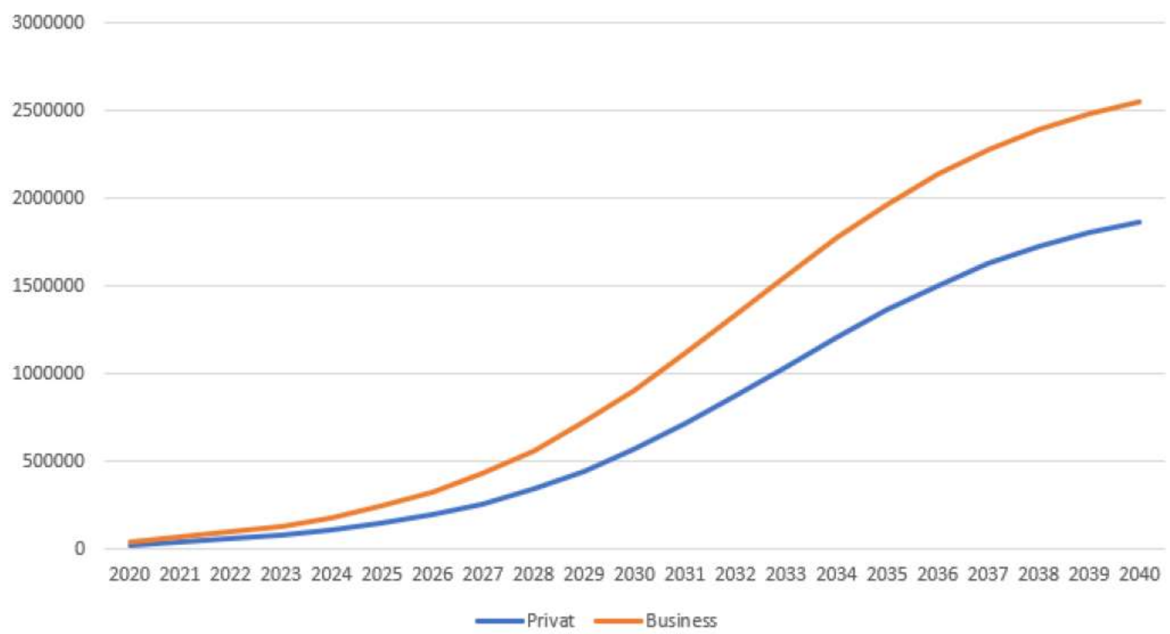


**Figure 3.8:** Estimated development of total number of EVs in the Austrian mobility fleet until 2040

The modeling approach for the charging time series of EVs is based on a simulation model developed by AIT in-house, which maps the charging behavior of the EV types described above [67]. To create the load time series, parameters for the ten most frequently used EVs in Austria are taken from an online database called “EV-Database” [68].

The consumption of electric vehicles is dynamically dependent on the outside temperature. To map this temperature dependency, a factor is introduced that is multiplied by the EV-specific average consumption. The basis for this temperature-dependent factor comes from [69], and is shown graphically in Figure 3.9. The green individual points represent real-time observed values of the consumption of 500 EVs, which are approximated with first, second and third order polynomial functions.

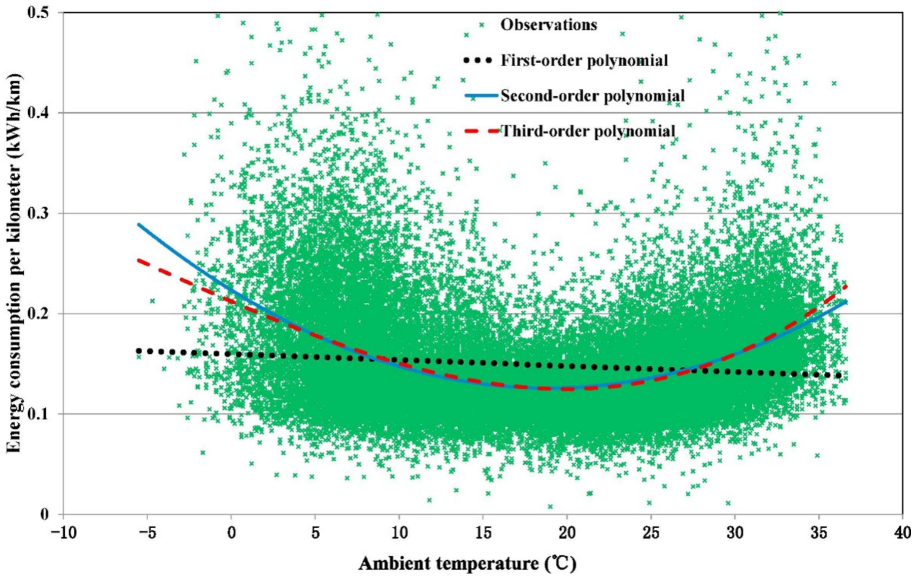


**Figure 3.9:** Temperature dependency of EVs in [69]

Additional input for the creation of EV load time series is the mobility behavior of the different EV user types. The study “Österreich unterwegs” serves as the basis for the evaluation of mobility behavior [70]. As this study was conducted in 2013 and 2014, it is assumed that mobility behavior in Austria will not change with the increasing spread of EVs.

The average daily distance traveled by the two different user types is determined on the basis of values from Statistik Austria [70] and is shown in Table 3.4.

**Table 3.4:** Daily average travel distance of private and business user types

| day type | Business (km/day) | Private (km/day) |
|---|---|---|
| working day | 53 | 36 |
| Saturday | 42 | 28 |
| Sunday | 0 | 26 |

Additional input for the EV demand time series are the commuter flows within Austria from one NUTS 3 area to another, which are separated according to the different EV usage categories “work”, “shopping” and “business”. Figure 3.4 displays the NUTS 3 division of Austria.

Commuter matrices which indicate the commuting behavior between each of the NUTS3 regions of Austria are created and serve as the basis for generating the EV load time series.

As an example Figure 3.10 provides an extract of the commuter matrix with the aim of private work travel. The matrix shows that 13.84 % of the cars from Mittelburgenland drive to Vienna for work reasons.

| | Mittelburgenland | Nordburgenland | Südburgenland | Mostviertel-Eisenw | Niederösterreich-Sü | St. Pölten | Waldviertel | Weinviertel | Wiener Umland-Nc | Wiener Umland-Sü | Wien |
|---|---|---|---|---|---|---|---|---|---|---|---|
| Mittelburgenland | 57.86% | 20.75% | 0.00% | 0.00% | 6.29% | 0.00% | 0.00% | 0.00% | 0.00% | 1.26% | 13.84% |
| Nordburgenland | 0.26% | 58.68% | 0.39% | 0.13% | 5.13% | 0.00% | 0.00% | 0.00% | 0.53% | 13.55% | 21.32% |
| Südburgenland | 0.52% | 1.31% | 67.62% | 0.00% | 0.52% | 0.00% | 0.00% | 0.00% | 0.00% | 0.52% | 3.66% |
| Mostviertel-Eisenwurzen | 0.00% | 0.00% | 0.00% | 79.82% | 0.00% | 5.90% | 1.36% | 0.00% | 0.23% | 0.00% | 3.17% |
| Niederösterreich-Süd | 1.20% | 1.81% | 1.20% | 0.00% | 62.05% | 6.63% | 0.00% | 0.00% | 0.00% | 9.64% | 15.06% |
| St. Pölten | 0.00% | 0.00% | 0.00% | 2.97% | 3.96% | 80.20% | 1.98% | 0.00% | 1.98% | 1.98% | 6.93% |
| Waldviertel | 0.00% | 0.16% | 0.00% | 1.44% | 0.16% | 6.74% | 84.11% | 0.32% | 1.61% | 0.80% | 3.69% |
| Weinviertel | 0.00% | 0.00% | 0.00% | 0.00% | 0.00% | 1.86% | 2.33% | 53.02% | 14.42% | 1.86% | 26.51% |
| Wiener Umland-Nordteil | 0.00% | 0.38% | 0.00% | 0.00% | 0.86% | 3.34% | 1.05% | 0.76% | 42.94% | 2.29% | 48.28% |
| Wiener Umland-Südteil | 0.00% | 1.77% | 0.00% | 0.11% | 2.32% | 0.55% | 0.00% | 0.00% | 0.66% | 50.22% | 44.15% |
| Wien | 0.00% | 0.52% | 0.00% | 0.34% | 0.52% | 0.43% | 0.34% | 0.09% | 6.45% | 9.38% | 81.58% |

**Figure 3.10:** Example of a commuter matrix

Commuters crossing the country are excluded from the time series of Austrian EV demand, as Austrian EVs also travel to neighboring countries and are initially charged in Austria.

There are three categories for the charging behavior of private EVs: “home charging”, “shop charging” and “work charging”, with the breakdown between the three categories shown in the

Figure 3.11. This classification agreed between AIT and APG experts is based on an approach that was developed for Germany in [67].

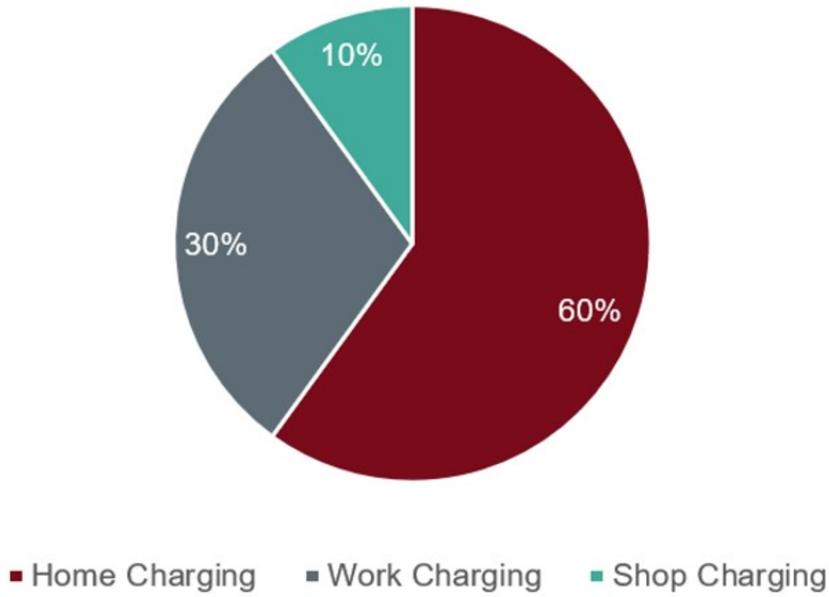


**Figure 3.11:** Different charging types of private EVs

The maximum charging power for the private charging types mentioned above and the charging type for commercial EVs is shown in Table 3.5. It should be noted that for most private charging, a power of 11 kW is used, which accounts for 60 % of the total charging types (see Figure 3.11). The maximum charging power increases when charging at work or in stores, where a share of 10 % to 20 % is also supplied by maximum charging powers of 22 kW and 50 kW, while when charging in companies, more than half of the charging processes are supplied with maximum charging powers greater than 22 kW. This distribution applies as an assumption for all target years of our analysis and has been agreed between AIT and APG experts on the basis of the research work carried out in [67].

**Table 3.5:** Maximum charging power output distribution of different charging types

| maximum charging power output | home charging | work charging | shop charging | business charging |
|---|---|---|---|---|
| 11 kW | 95 % | 80 % | 70 % | 45 % |
| 22 kW | 5 % | 20 % | 10 % | 40 % |
| 50 kW | | | 20 % | 10 % |
| 150 kW | | | | 5 % |

Figure 3.12 shows the arrival times of the different types of charging according to the study

”‘Österreich Unterwegs”’ [70] - red lines stand for working days, green lines for Saturdays and blue lines for Sundays.

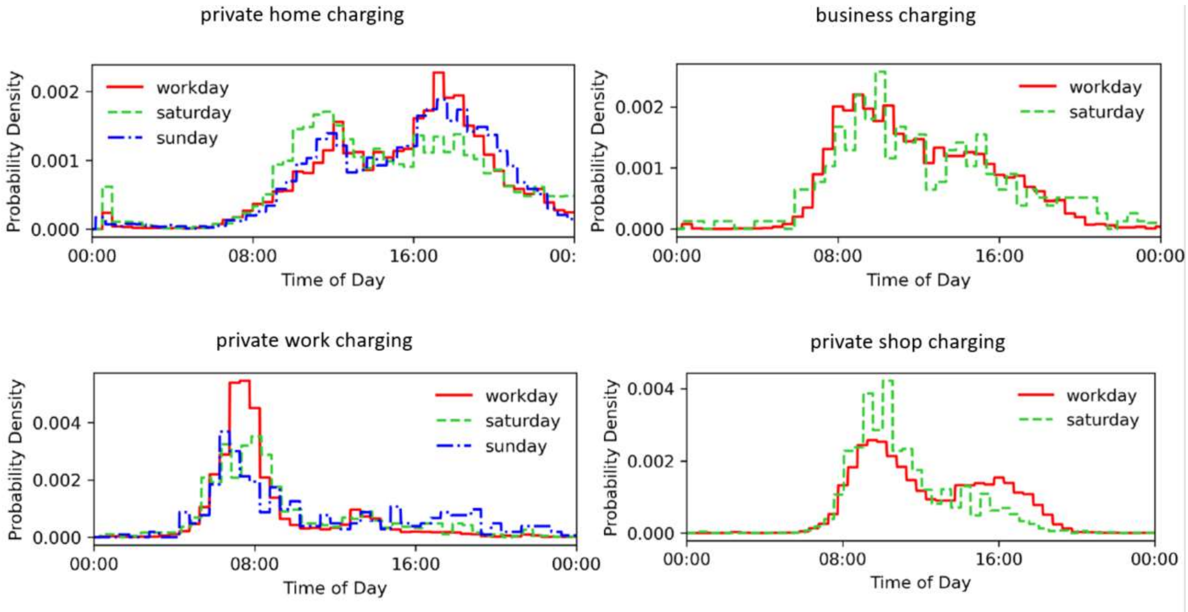


**Figure 3.12:** Distribution of arrival times of the different charging types [64]

For the final EV load profile generation for the target years 2020, 2030 and 2040, the same meteorological data is used as for the heat pump load profile generation (software meteonorm version 7.3 scenario IPCC AR4 A1B [59]), while for the target year 2025 the two meteonorm datasets for 2020 and 2030 are used to approximate the target year 2025.

Based on Meteonorm climate projections, annual EV charging profiles are created for the user type “Private” by first taking the daily charging profiles (Figure 3.12) for the respective use case and applying their weighting according to Figure 3.11. In a second step, the daily charging profiles shown in Figure 3.12 are combined into annual profiles that take into account the charging cycles that start before midnight and end the next day (these are added manually to the next day). For the three private user types, an aggregated profile is created from all three types. This leads to the final creation of an annual load profile for residential user types. The same approach is also used for commercial users, where no weighting needs to be applied as there is no separation between charging at home, business or work, as is the case for private EVs.

Looking at the annual development figures up to the year 2040, the following forecasts for annual electricity consumption and peak consumption result (using Meteonorm climate data):

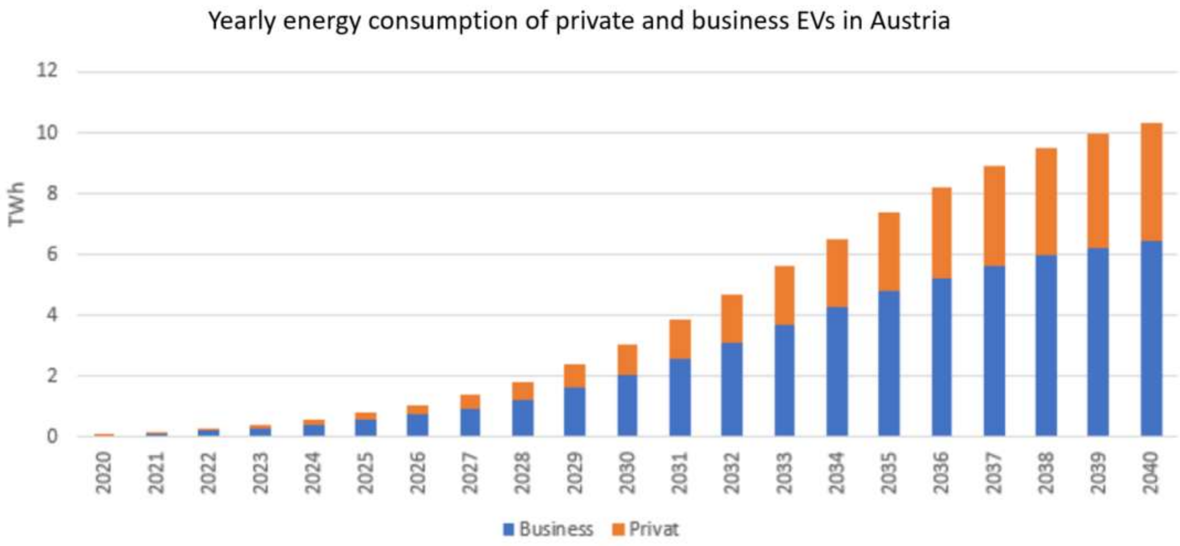


**Figure 3.13:** Yearly energy consumption of private and business EVs in Austria in TWh

Figure 3.13 shows the annual energy consumption of private and business EVs until 2040. For the year 2030, the annual EV demand is slightly above 3 TWh, which is needed for electric commuting in Austria. These 3 TWh, which were determined by using Meteonorm climate data, are in the same range as the average over all 35 PECD climate years, which are used as input data for the creation of the climate year-dependent demand time series for EVs. Averaging these 35 individual demand time series results in 3.26 TWh average annual electricity demand for EVs, which corresponds to 3.6 % of the total annual electricity demand for Austria projected in the ERAA 2022 process to be 90.76 TWh for the target year 2030.

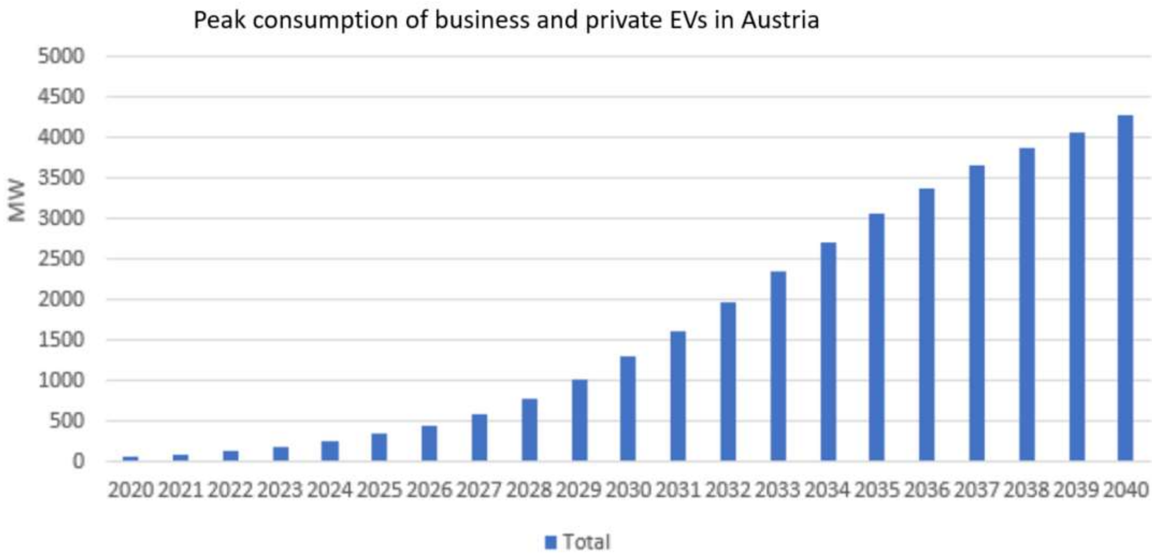


**Figure 3.14:** Peak consumption of business and private EVs in Austria in MW

Figure 3.14 illustrates the peak consumption of electric vehicles for the future target years. In 2030, the peak charging power of all EVs is below 1.5 GW. This figure does not take into account the flexible behavior of EVs. Both figures are based on future weather forecasts from the meteorological data used by AIT and may therefore differ from the PECD climate data used for the adequacy calculations.

### 3.2.3 Battery Storage

In addition to the significant development and installation of renewable energy generation in Europe and around the world, the need for battery storage is also part of the discussion.

Firstly, there is the use case of battery home storage systems (BHS). The private installation of PV systems goes hand in hand with production during the day, when private household owners are generally not at home and cannot use their self-generated energy. To optimize their self-consumption, private PV owners install battery storage systems next to their PV system to minimize their grid consumption by storing self-generated energy during the day, which is then available for household energy consumption at night. The development of BHS installation is price-dependent: One argument in favor of installing a BHS were the high electricity prices in 2020 and 2021, but also subsidies that provide an incentive for private PV system owners to expand their system with a BHS. Figure 3.15 shows the development of private BHS systems from 2014 to 2022 [71], whereby 90 % of private BHS systems were subsidized by the Austrian government (red bars). In 2022, a total of 230 MWh were built, resulting in a total installed BHS capacity of 481 MWh in Austria in 2022. The black line shows the development of the cumulative amount of installed BHS systems in Austria.

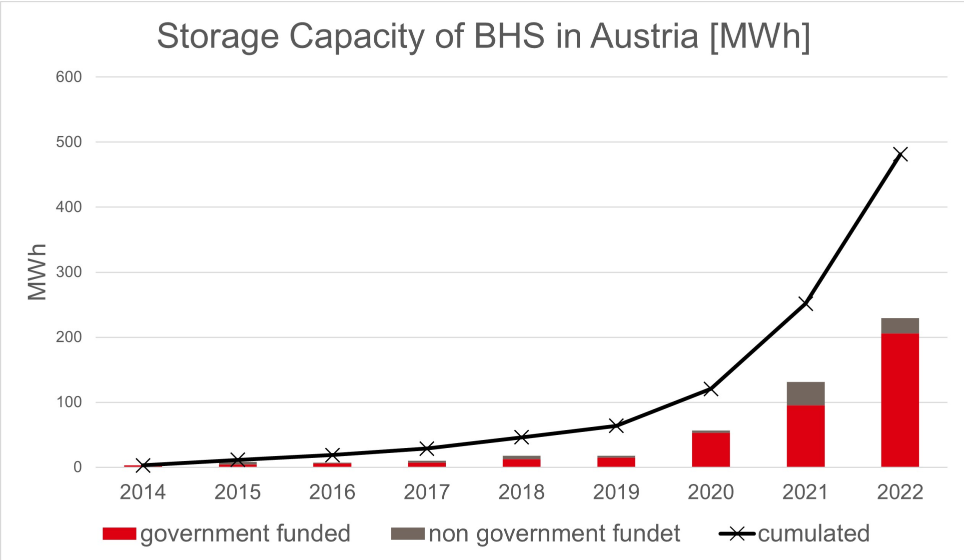


**Figure 3.15:** Annually installed and cumulative BHS storage in Austria [71]

The development in recent years shows a doubling of the number of installed BHS systems in Austria. BHS systems are not modeled in the 2021 ERAA process. As of ERAA 2022, an initial estimate is included in the input data set, although the actual modeling approach cannot be carried out correctly with either the TRAPUNTA tool or its successor, the ENTSO-E Demand Forecasting Tool (DFT). The development work for the correct modeling of BHS systems with the demand forecasting tool has not yet been completed, which is why battery storage systems in the household sector are not included in this work.

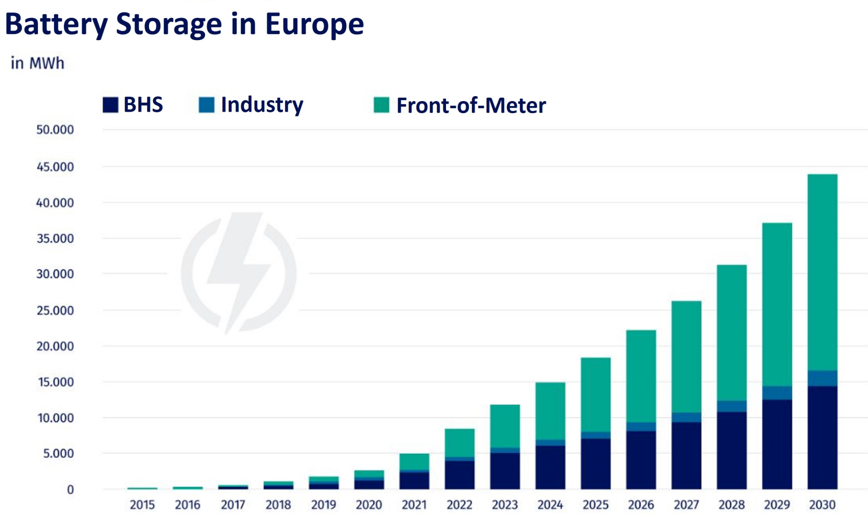


**Figure 3.16:** Annual development of various battery storage systems in Europe [72]

Secondly, one use case in various countries is the installation of larger storage units that are used as fast-response technologies such as primary control reserves or even faster, or in some cases also operate on the energy-only market. Figure 3.16 shows the European development of three different storage categories for battery storage: batteries behind the meter (dark blue), referred to as battery home storage (BHS), industry (light blue), which has the smallest share, while batteries in front of the meter, i.e. technologies participating in the market and are also fast-response, are shown in green. In 2030, BHS systems will account for 15 GWh, leaving 30 GWh for industrial and front-of-meter applications. Looking at the development in Europe in 2030, one third of the installed battery storage systems will be residential (BHS), while two thirds will continue to be installed front-of-meter.

Table 3.6 lists some Austrian projects for front-of-meter batteries:

**Table 3.6:** Installed market participating front-of-meter batteries in Austria in 2023

| name | location | installed capacity | storage size | commissioning date |
|---|---|---|---|---|
| Blue Battery | Wallsee - Mitterkirchen | 8 MW | 14.2 MW h | 2020 |
| NGEN | Arnoldstein | 10.3 MW | 20.6 MW h | 2023 |

Looking at Table 3.6, 18.3 MW of installed batteries with a storage capacity of 34.8 MW h of front-of-meter storage systems is available in Austria in 2023. The development up to 2030 can be estimated in different ways, a simple approach, which was carried out in 2020, is based on an orientation towards the German market. This approach was used to estimate the installed capacity of front-of-meter storage systems for Austria in the ERAA process in 2022 and 2023. The estimate was carried out in 2020 together with the AIT:

In 2020, 450 MW of market-participating batteries were installed in Germany, which act as a frequency containment reserve (FCR) [73]. In addition to these 450 MW, a further 450 MW are to be installed in 2022 to serve as an alternative to grid reinforcement. 1200 MW are assumed for 2025 and 2000 MW for 2030 [74], while 3800 MW of market-participating battery units are expected to be available in the German transmission grid in 2040 [75]. According to [75], larger storage facilities are expected to have a significant use case in the FCR market and thus the need for FCR should be reduced by the availability of large storage facilities. According to an AIT estimate based on a differentiation into the four sectors of FCR, direct marketing of renewable energy, energy supply and various other components (transmission and distribution use) [76], a possible development stream for Germany could look as follows (Figure 3.17). A constant amount of 600 MW for the FCR should be reached in 2022 and remain constant until 2040, while the other use cases start to develop from 2022, with the dominant use case of direct marketing of renewables starting to grow significantly from 2026.

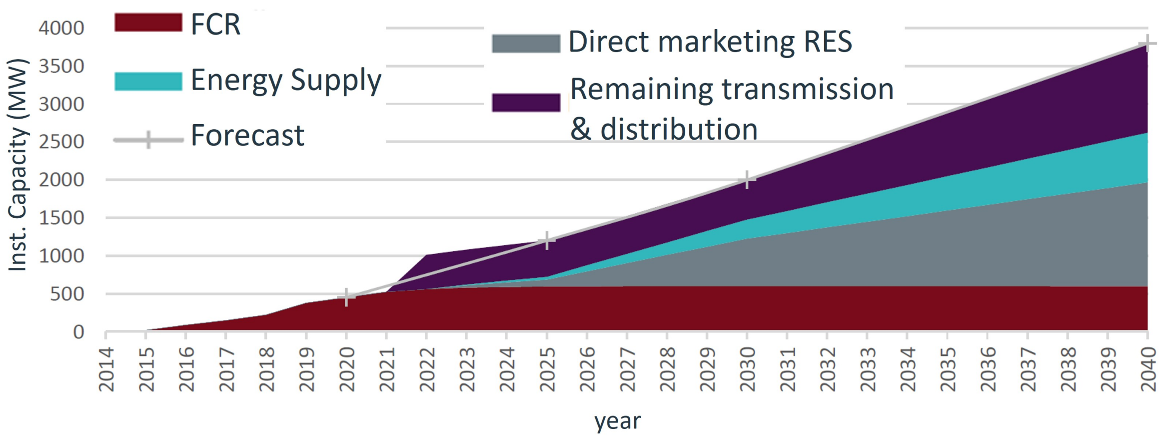


**Figure 3.17:** Development of bulk storage by use case in Germany until 2040 (source: AIT)

Taking the developments in Germany as basis and assuming the following:

- FCR in 2020 in Austria is around 70 MW
- one front-of-meter battery storage project of 8 MW in 2020
- assuming a delay of implementation of five years compared to the German market

the development stream for Austria could look like as follows, excluding the remaining category for the use of transmission and distribution batteries (see Figure 3.18): Assuming a growth in FCR in 2022, front-of-meter batteries could reach an amount of around 68 MW with a storage size of 102 MW h in 2030, leading to a possible estimate of around 250 MW of installed capacity with a storage size of slightly over 350 MW h in 2040.

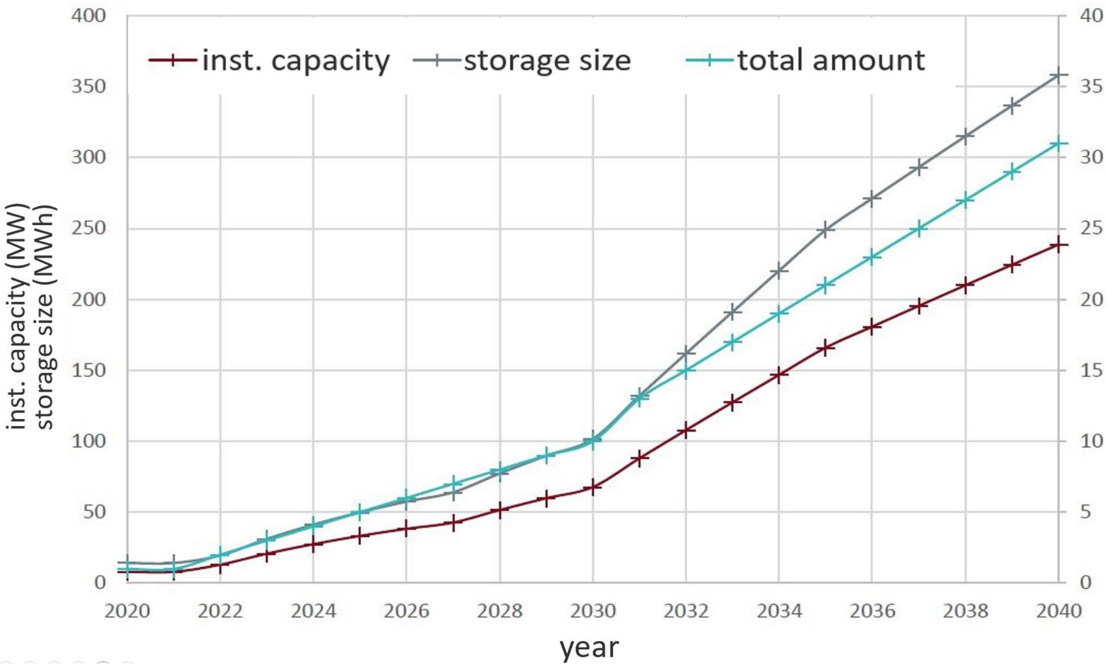


**Figure 3.18:** Development of bulk storage by use case in Austria until 2040 (source: AIT)

The approach described above for the estimating front-of-meter battery development was the best available approach for APG in 2020 for estimating front-of-meter battery development, which was also used in the 2022 and 2023 editions of ERAA.

In 2023, the Federal Ministry for Climate Action, Environment, Energy, Mobility, Innovation and Technology published the Austrian Integrated Development Plan for Grid Infrastructure (ÖNIP) for consultation [2]. This report estimates the development for front-of-meter battery storage in 2030 at 1284 MW and 2568 MWh in 2030 and 5782 MW and 11 564 MWh in 2040. The figures based on the ÖNIP estimate result in a 20-fold increase for front-of-meter battery storage in 2030 and a 46-fold increase in 2040 compared to the AIT estimate. This development can also be confirmed for Germany, which has a total installed capacity of 4.82 GW and 7.16 GWh of battery storage in April 2023, with the majority also acting as FCR [77]. Three years after the assumptions made for Germany in 2020 (450 MW), the assumptions for 2023 are already 10 times higher than those for 2020.

Based on the differences in the development trajectories of the battery storage systems on the market that have been identified for Austria and confirmed by the German developments, the value of 33 MW with 50 MWh storage size for the target year 2025 provided for the ERAA process 2022 and 2023 is used as the starting point in this work. This value is gradually increased until the values published in [2] are reached.

The investigations carried out are discussed in chapter 6.5. The focus of this work is on the representation of batteries participating in the market, as the behavior of BHS systems must be taken into account when creating the demand time series. The feedback from the research on market-participating batteries conducted as part of this work is incorporated into the BHS development stream in the ENTSO-E Demand Forecasting Tool.

### 3.2.4 Austrian Demand Figures

Demand figures (annual demand in TWh and annual maximum peak demand in GW) are shown below for processes carried out during the period of this thesis. Detailed figures for EVs and HPs are available based on a sound methodology that was introduced from ERAA 2022:

**Table 3.7:** Demand figures used in the MAF and ERAA process for the target year 2025

| | MAF 2018 | MAF 2019 | MAF 2020 | ERAA 2021 | ERAA 2022 |
|---|---|---|---|---|---|
| total annual demand | 75.53 TWh | 77.48 TWh | 76.24 TWh | 73.03 TWh | 75.62 TWh |
| max peak | 12.75 GW | 13.21 GW | 13.49 GW | 13.18 GW | 14.02 GW |
| EV annual demand | | | | | 0.85 TWh (1.1 %) |
| EV max peak | | | | | 0.45 GW (3.2 %) |
| HP annual demand | | | | | 3.91 TWh (5.2 %) |
| HP max peak | | | | | 3.99 GW (28.5 %) |

## 3.3 Network Representation

From the ERAA 2022 edition, the transmission system infrastructure is represented in the resource adequacy assessment by net transfer capacities (NTCs) in combination with a simplified flow-based representation for the CORE region[2]. From the MAF 2017 to the ERAA 2021, the NTC representation is used for all countries connected within the model region. In this work, all calculations are performed on an NTC model. Since ERAA 2022, the flow-based approach is used. Each country is represented by a country node, although for larger countries such as Norway, Sweden or Italy, the countries are divided into several bidding zones. A line connects two country nodes and contains a time series for the NTC values per direction in hourly resolution.

In Austria, all borders, with the exception of the border with the Slovak Republic, are connected via 220 kV or 380 kV AC lines. Figure 3.3 shows the Austrian transmission grid at 220 kV and 380 kV voltage level.

[2]Definition CORE bidding zones: Austria, Belgium, Croatia, the Czech Republic, France, Germany, Hungary, Luxemburg, the Netherlands, Poland, Romania, Slovakia and Slovenia

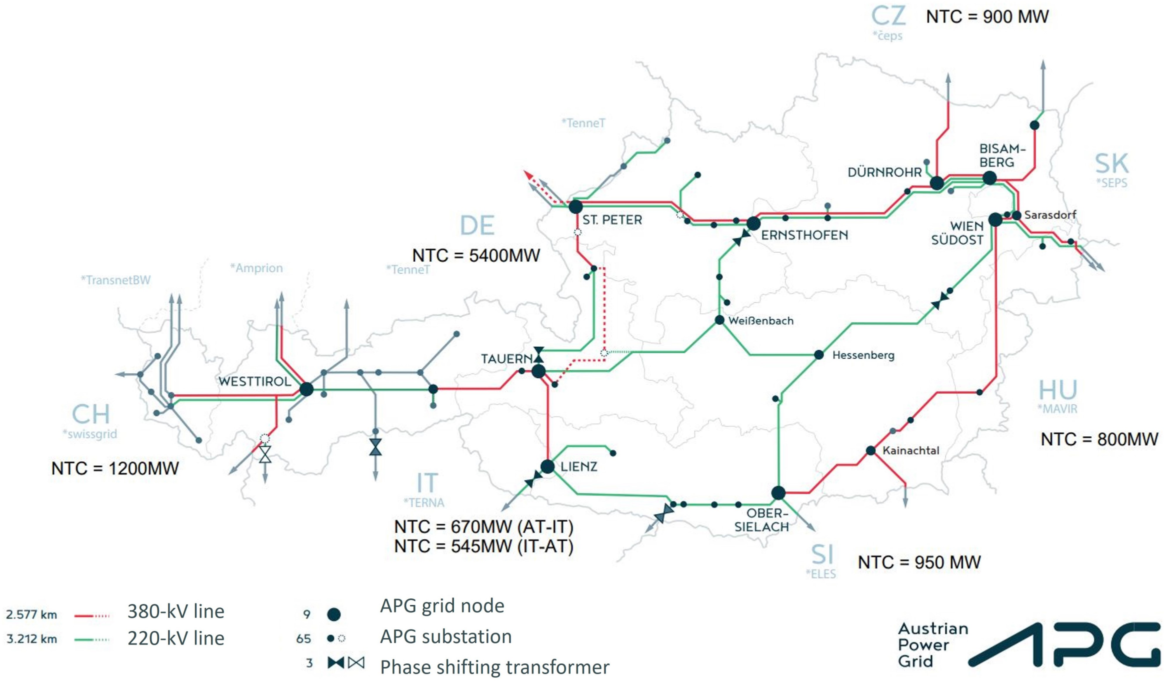


**Figure 3.19:** Transmission grid 220 and 380 kV APG (Source: APG 2022)

For the NTC representation, the maximum capacities of the individual AC lines are aggregated for each border and a time series is created between two country nodes. The grid expansion is shown for the respective target year, including the projects that will be put into operation by this year. The NTC values are given in hourly resolution so that a seasonal pattern can be taken into account. Table 3.8 provides an overview of the NTC values used for the target year 2025 (values on January $1^{st}$) as they were used in the various processes. The hourly time series are available in the public download area of the ERAA process on the ENTSO-E website [78].

**Table 3.8:** NTC values in MW used in MAF and ERAA processes for the Target Year 2025

| border | MAF 2018 | MAF 2019 | MAF 2020 | ERAA 2021 | ERAA 2022 |
|---|---|---|---|---|---|
| AT00-CH00 | 1700 | 1200 | 1200 | 1200 | 1200 |
| CH00-AT00 | 1700 | 1200 | 1200 | 1200 | 1200 |
| AT00-CZ00 | 900 | 900 | 900 | 900 | 900 |
| CZ00-AT00 | 800 | 900 | 900 | 900 | 900 |
| AT00-DE00 | 7500 | 5400 | 5400 | 5400 | 5400 |
| DE00-AT00 | 7500 | 5400 | 5400 | 5400 | 5400 |
| AT00-HU00 | 800 | 800 | 800 | 800 | 800 |
| HU00-AT00 | 800 | 800 | 800 | 800 | 800 |
| AT00-ITN1 | 710 | 680 | 660 | 660 | 670 |
| ITN1-AT00 | 490 | 500 | 490 | 490 | 545 |
| AT00-SI00 | 950 | 950 | 950 | 950 | 950 |
| SI00-AT00 | 950 | 950 | 950 | 950 | 950 |

In the context of the present work, flow-based modeling is excluded in the assessment of resource adequacy; the methodology applied can be found in the description of the ERAA 2023 methodology [79].

# 4 New Concepts on Hydro Storage Representation within Antares

This chapter explains the developments in the representation of hydropower plants for resource adequacy modeling using the Antares tool [80]. Antares is a tool developed by the French transmission system operator RTE [17]. RTE has introduced this tool as a system adequacy modeling tool capable of performing several hundred Monte Carlo simulations in a reasonable computing time, taking into account the stochasticity resulting from the volatile behavior of renewable energies. In order to achieve these reasonable computing times, the tool must accept a certain degree of modeling reductions compared to full economic calculations. The model simplifications in the representation of hydropower are discussed in this chapter. Based on the results of the work carried out as part of a master's thesis [22], this chapter discusses investigations into new modeling approaches for the representation of swell power and further developments for the representation of hydropower pumped storage.

- the hydropower representation as used after the introduction of a new database format (PEMMDB 3.0), is described in chapter 4.1
- an alternative hydropower pre-optimization approach following a water value calculation for each filling level of a hydro reservoir is elaborated in chapter 4.2
- a representation for short cycle storage (closed loop pump storage units) is elaborated in chapter 4.3
- an enhanced representation for swell generation is elaborated in chapter 4.4
- a representation for an Austrian hydropower cascade (Kaprun) is described in chapter 4.5

In the course of this work, tool developments also led to new possibilities for the representation of hydropower (e.g. use of internal pumping function as well as a different approach to pre-optimize hydropower using water values). All of these developments contributed to improving the representation of hydropower generation and are explained individually in this chapter. The indices H, D and W are used to distinguish between the inputs provided in hourly, daily or weekly resolution.

## 4.1 Hydropower representation following the new database format PEMMDB 3.0

In 2019, a new database format PEMMDB 3.0 was introduced for the collection of TSO input data. This new database follows a different method for collecting input data for hydropower plant data. A new classification is used for the various hydropower plant categories:

- run of river and swell (ROR & swell)
- traditional reservoir (TR)
- pump storage open loop (PSP OL)
- pump storage closed loop (PSP CL)

This chapter explains the representation of hydropower generation according to the PEMMDB 3.0 database format. Figure 4.1 shows the representation in Antares with one main country node (dark blue), a supporting node to indicate the details of hydropower open loop pump storage (dark blue) as well as virtual nodes (light blue) used to represent the pumping behavior of PSP units. The information on run of river, swell and traditional reservoir generation is located in the main country node (dark blue), while the hydro open loop pump storage is specified in a separate node (dark blue), which is connected to the main country node with a bi-directional energy flow. The virtual pump and turbine nodes (light blue) allow the introduction of the pumping behavior of a pump storage unit. Since Antares version 6 does not provide internal pumping functionality for hydropower units that can be selected via a user interface, this chapter describes a solution for introducing the pumping functionality for open and closed loop pump storage hydropower plants.

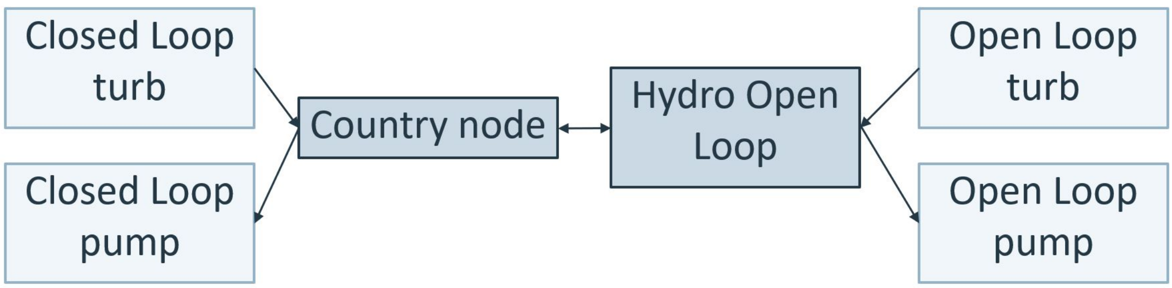


**Figure 4.1:** Hydropower representation with PEMMDB 3.0

where

1. country node
   - ROR & swell inflow time series in hourly resolution
   - traditional reservoir - all details (inflow time series, minimum and maximum reservoir levels, reservoir size, turbine power)
   - PV & wind time series
   - thermal power plant information
   - load time series
   - miscellaneous generation
2. hydro open loop node - contains all details of the PSP OL (inflow time series, minimum and maximum reservoir levels, size of the reservoir, maximum turbine and pump power)
3. closed loop turbine node (virtual) - contains one thermal unit with 100 000 MW operating at zero cost
4. closed loop pump node (virtual) - contains one load of 100 000 MW and one thermal cluster with 100 000 MW operating at zero cost
5. open loop turbine node (virtual) - contains one thermal unit with 100 000 MW operating at zero cost
6. open loop pump node (virtual) - contains one load of 100 000 MW and one thermal cluster with 100 000 MW operating at zero cost

The links between the virtual turbine and pump nodes with the country node (hydro open loop node respectively), contain the maximum turbine and pump power in hourly resolution.

**Run of river and swell (ROR and swell):**

The main country node contains the ROR and swell time series in hourly resolution. Run of river time series that follow the PEMMDB 3.0 format also contain the additional amount of inflows from swell production. Since the inflow values in the new database are provided on a daily basis, the calculation of hourly ROR production is based on the following formula:

$$\mathrm{E}_{\mathrm{ROR(Antares),H}} = \frac{\mathrm{Inf}_{\mathrm{ROR,D}}}{24\ \mathrm{h}} + \mathrm{E}_{\mathrm{min,TR,H}} + \mathrm{E}_{\mathrm{min,OL,H}}$$

where

$E_{ROR(Antares),H}$ energy available for hourly run of river output supplied to Antares, $E_{ROR(Antares),H}$, $[E_{ROR(Antares),H}] = MWh$

$Inf_{ROR,D}$ inflow in daily resolution for run of river and swell hydro production, $Inf_{ROR,D}$,$[Inf_{ROR,D}] = MWh$

$E_{min,TR,H}$ minimum generation of hydro traditional reservoir, $E_{min,TR,H}$,$[E_{min,TR,H}] =$ MWh, calculated from the provided minimum power, $P_{min,TR,H}$, $[P_{min,TR,H}] =$ MW multiplied with 1 h

$E_{min,OL,H}$ minimum generation of hydro open loop, $E_{min,OL,H}$, $[E_{min,OL,H}] = MWh$, calculated from the provided minimum power, $P_{min,OL,H}$, $[P_{min,OL,H}] = MW$ multiplied with 1 h

As Antares cannot process the minimum power output of the storage units directly in the tool, the sum of all minimum power outputs from hydro storage units is converted into a minimum generation by multiplying the minimum power in MW by 1 hour. This minimum generation in MWh is added to the ROR and swell inflow time series and immediately dispatched. Since the new database provides 35 climate-dependent inflow time series for each hydropower plant type, a matrix with a size of 35 x 8760 inflow time series for ROR and swell production is entered directly to Antares.

According to the formula described above for the ROR and swell power generation, both inflows are combined in a single time series, which leads to an immediate dispatch of both categories. This suggests that the system loses short-term flexibility, which results in particular from the daily storage potential of swell power plants. In Austria, the input data for swell power plants in the MAF 2018 process accounted for 22 % of the total turbine power of ROR and swell power plants. Swell power plants follow a daily storage behavior, which is lost in the representation according to the new database format. More detailed investigations on the representation of swell power plants and further developments of the representation of swell power plants in future processes are described in chapter 4.4.

**Traditional Reservoir (TR):**

The database format PEMMDB 3.0 enables the provision of trajectories for the minimum and maximum reservoir level of a bidding zone. This enables Antares to apply an internal heuristic to divide the annually available energy lots into monthly lots. For this purpose, the TSOs provide time series of hydro inflows (from PEMMDB 3.0 in weekly resolution), which are aggregated by Antares into an annual inflow. The heuristic then distributes this annual inflow to monthly and daily energy lots proportional to the net load of each bidding zone (details are given in chapter 2.6.1).

If no trajectories for the minimum and maximum reservoir levels are provided, the input data is provided in a deterministic way, which means that historically measured weekly reservoir levels for each climate year are used in the calculation (see Figure 2.8). The approach to calculate monthly energy targets based on weekly inflows and weekly reservoir levels per climate year is applied:

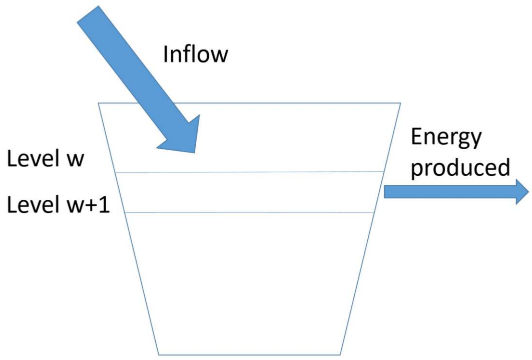


**Figure 4.2:** Storage level of two consecutive weeks (w, w+1)

$$E_{TR(Antares),M} = \sum_{Month} Inf_{TR,W} + \Delta S_{TR,W} - E_{min,TR,W}$$

with

$$\Delta S_{TR} = S_{TR}(w+1) - S_{TR}(w)$$

and

$$E_{min,TR,W} = P_{min,TR} \cdot 168 \text{ h}$$

where

| | |
|---|---|
| $E_{TR(Antares),M}$ | energy available for traditional reservoir generation as input for Antares on a monthly basis, $E_{TR(Antares),M}$, $[E_{TR(Antares),M}]$ = MWh |
| $Inf_{TR,W}$ | inflow for traditional reservoir generation delivered in weekly resolution, $Inf_{TR,W}$, $[Inf_{TR,W}]$ = MWh |
| $P_{min,TR}$ | minimum power for traditional reservoirs of a bidding zone in weekly resolution, $P_{min,TR}$, $[P_{min,TR}]$ = MW |
| $E_{min,TR,W}$ | minimum generation during a week, $E_{min,TR,W}$, $[E_{min,TR,W}]$ = MWh, calculated from the provided minimum power, $P_{min,TR}$, $[P_{min,TR}]$ in MW multiplied with 168 h |

Since the minimum power of the traditional reservoir category is already added to the inflow time series of ROR and swell in order to be dispatched immediately, the minimum power must be subtracted from the maximum power of the traditional reservoir power plants.

$$P_{max,TR(Antares)} = P_{max,TR} - P_{min,TR}$$

A disadvantage of the described method, which does not use the Antares reservoir management functionality, is the fact that the monthly energy lots must be used within the respective month and cannot be carried over to a later month. If the user specifies minimum and maximum reservoir levels and uses the reservoir management functionality, the sum of all hydro inflows to the reservoir over the year is aggregated and passed to the Antares heuristic, which divides the annual energy from hydropower to monthly energy lots according to the heuristic described in chapter 2.6.1. The annual energy for traditional reservoir is then aggregated according to the following formula:

$$E_{TR(Antares),Y} = \sum_{Year} Inf_{TR,W} - E_{min,TR,W}$$

The use of the Antares heuristic, which divides the annual inflow proportionally to the net load of a bidding zone into monthly energy lots, has been available since the data collection with the new database format PEMMDB 3.0 and offers a redistribution of energy from hydropower throughout the year. However, the approach of distributing the monthly hydropower energy lots proportionally to the net load within a bidding zone is questionable. For this reason, an approach for allocating water values to the reservoir filling levels is described in chapter 4.2.

**Closed Loop Pump Storage Plant:**

As Antares version 6 does not provide an integrated pumping function for hydropower plants, the pumping behavior for closed loop pump storage power plants is represented by two virtual nodes connected to the main country node. The *Closed Loop Turb* node has unlimited generation, while the *Closed Loop Pump* node has unlimited demand. The maximum constraints for $P_{max,turb}$ and $P_{max,pump}$ are taken from the PEMMDB 3.0 database, as the total installed CL turbine power and total installed CL pump power, respectively. The maximum hourly turbine and pump time series are placed as energy flows to the link between the turbine and pump node and the country node as unidirectional flows. The round-trip efficiency of the CL PSP cycle is assumed to be 75 % for all European PSP hydropower plants and is set as a linear binding constraint between the country node and the virtual turbine and pump nodes:

$$0,75 \cdot \sum_{D,W} [E_{CL,pump} \rightarrow \text{ country node}] = \sum_{D,W} [E_{CL,turb} \rightarrow \text{country node}]$$

where

| | |
|---|---|
| $[\mathrm{E_{CL,pump}} \rightarrow$ country node$]$ | energy flow from the CL pump node to the country node (negative by convention) during daily or weekly optimization |
| $[\mathrm{E_{CL,turb}} \rightarrow$ country node$]$ | energy flow from the CL turbine node to the country node (positive by convention) during daily or weekly optimization |

Since the total cycles can be limited by a daily or weekly constraint, a time constant $\tau_{CL}$ is estimated representing the cycle of the reservoir as a daily ($\leq 24$ *hours*) or weekly ($> 24$ *hours*) according to the following formula:

$$\tau_{CL}[h] = \min\left(\frac{\Sigma_{CL}}{\mathrm{P_{max,turb,CL}}}, \frac{\Sigma_{CL}}{\mathrm{P_{max,pump,CL}}}\right); \left\{\begin{array}{c} \tau_{CL} > 24\,\mathrm{h} \rightarrow T = \mathrm{week} \\ \tau_{CL} \leq 24\,\mathrm{h} \rightarrow T = \mathrm{day} \end{array}\right\}$$

where

| | |
|---|---|
| $\tau_{CL}$ | time constant of the closed loop plant fleet |
| $\Sigma_{CL}$ | total installed reservoir capacity of the closed loop power plant fleet, $\Sigma_{CL}$, $[\Sigma_{CL}] = \mathrm{MWh}$ |
| $\mathrm{P_{max,turb,CL}}$ | maximum turbine power of the closed loop power plant fleet, $\mathrm{P_{max,turb,CL}}$, $[\mathrm{P_{max,turb,CL}}] = \mathrm{MW}$ |
| $\mathrm{P_{max,pump,CL}}$ | maximum pumping power of the closed loop power plant fleet, $\mathrm{P_{max,pump,CL}}$, $[\mathrm{P_{max,pump,CL}}] = \mathrm{MW}$ |

The total reservoir capacity is divided by the total installed pump power and by the total installed turbine power. The lower value of the two results is taken and evaluated if:

- it is smaller or equal 24 hours, then a daily binding constraint is applied, or
- it is greater than 24 hours, then a weekly binding constraint is applied.

The obtained dimension of $\tau$ is entered into the model via a user interface that specifies a daily or weekly binding constraint.

This first applied approach to consider the use of pumped storage results from the first models created by RTE under the PEMMDB 2.0 representation in MAF. This first attempt for PSP representation was also applied to the ERAA model using the PEMMDB 3.0 database. Unfortunately, this representation, which uses virtual nodes to mimic the pumping behavior of PSPs, does not allow tracking the size of the reservoir and accounting for its boundaries. As a first solution to overcome this limitation, an approach to apply the pumping behavior of CL PSPs considering the minimum and maximum reservoir levels is developed in chapter 4.3.

**Open Loop Pump Storage Plant (OL PSP):**

Based on the above description of traditional reservoir and closed loop pump storage hydropower plants, the following procedure applies to the description of OL PSPs.

An additional virtual external *hydro open loop* node is connected to the *country node*, which receives the same input parameters for the hydro reservoir connected to the open loop PSP units and is characterized by the following equations:

$$\mathrm{E_{OL(Antares),M}} = \sum_{\mathrm{Month}} \mathrm{Inf_{OL,W}} \; + \; \Delta \mathrm{S_{OL,W}} \; - \; \mathrm{E_{min,OL,W}}$$

with

$$\Delta \mathrm{S_{OL}} = \mathrm{S_{OL}(w+1) - S_{OL}(w)}$$

$$\mathrm{E_{min,OL}} = \mathrm{P_{min,OL}} \cdot 168 \text{ h}$$

where

$\mathrm{E_{OL(Antares),M}}$ energy available for open loop pump storage generation as input to Antares on a monthly basis, $\mathrm{E_{OL(Antares),M}}$, $[\mathrm{E_{OL(Antares),M}}] = \mathrm{MWh}$

$\mathrm{Inf_{OL,W}}$ inflow for open loop pump storage generation delivered in weekly resolution, $\mathrm{Inf_{OL,W}}$, $[\mathrm{Inf_{OL,W}}]$ in MWh

$\mathrm{P_{min,OL}}$ minimum power output for open loop pump storage of a bidding zone in weekly resolution, $\mathrm{P_{min,OL}}$, $[\mathrm{P_{min,OL}}] = \mathrm{MWh}$

$\mathrm{E_{min,OL,W}}$ minimum generation for open loop pump storage, $\mathrm{E_{min,OL,W}}$, $[\mathrm{E_{min,OL,W}}] =$ MWh calculated from the provided minimum power $\mathrm{P_{min,OL}}$, $[\mathrm{P_{min,OL}}]$ multiplied with 168 h

Since the minimum power of the OL pump storage category is already added to the inflow time series of ROR and swell in order to be dispatched immediately, the minimum power must be subtracted from the maximum power of the OL power plants.

$$\mathrm{P_{max,OL(Antares)}} = \mathrm{P_{max,OL}} - \mathrm{P_{min,OL}}$$

$\mathrm{P_{max,OL(Antares)}}$ is defined as the maximum hourly energy flow on the link between the virtual *hydro open loop* node and the *country node* in both directions.

As with the pre-optimization of hydro storage using the Antares heuristic, when a TSO provides trajectories for minimum and maximum reservoir levels, the inflows from OL PSPs are aggregated to an annual energy that is transferred to the tool for the allocation of the monthly energy lots according to the Antares heuristic:

$$\mathrm{E}_{\mathrm{OL(Antares),M}} = \sum_{\mathrm{Year}} \mathrm{Inf}_{\mathrm{OL,W}} \; - \; \mathrm{E}_{\mathrm{min,OL,W}}$$

To account for pumping of open loop pump storage units, two virtual nodes are connected to the hydro open loop node in the same way as for the main country node to which the closed loop turbine and pump virtual nodes are connected. The values for the maximum pump and turbine power are taken from the database and expressed as hourly energy flows on the links between the virtual *OL turb* and *OL pump* nodes and the *hydro open loop* node, taking into account the maximum installed open loop pump power. As with CL pump storage, the round-trip efficiency is assumed with 75 % and is set as a linear binding constraint between the country node and the virtual turbine and pump nodes:

$$0,75 \cdot \sum_{\mathrm{D,W}} [\mathrm{E}_{\mathrm{OL,pump}} \rightarrow \; \text{Hydro OL node}] = \sum_{\mathrm{D,W}} [\mathrm{E}_{\mathrm{OL,turb}} \rightarrow \text{Hydro OL node}]$$

where

| | |
|---|---|
| $[\mathrm{E}_{\mathrm{OL,pump}} \rightarrow$ Hydro OL node] | energy flow from the pump node to the Hydro OL node (negative by convention) during daily or weekly optimization |
| $[\mathrm{E}_{\mathrm{OL,turb}} \rightarrow$ Hydro OL node] | energy flow from the turbine node to the Hydro OL node (positive by convention) during daily or weekly optimization |

The duration of the cycle is estimated using the time constant $\tau_{OL}$, which can be evaluated as follows:

$$\tau_{OL}[h] = \frac{\Sigma_{OL}}{\mathrm{P}_{\mathrm{max,turb,OL}}}; \left\{ \begin{matrix} \tau_{OL} > 24\,\mathrm{h} \rightarrow T = \mathrm{week} \\ \tau_{OL} \leq 24\,\mathrm{h} \rightarrow T = \mathrm{day} \end{matrix} \right\}$$

where

| | |
|---|---|
| $\tau_{OL}$ | time constant of the open loop power plant fleet |
| $\Sigma_{OL}$ | total storage capacity of the open loop power plant fleet, $\Sigma_{OL}$, $[\Sigma_{OL}]$ in MWh |
| $\mathrm{P}_{\mathrm{max,turb,OL}}$ | maximum turbine power of the closed loop power plant fleet, $\mathrm{P}_{\mathrm{max,turb,OL}}$, $[\mathrm{P}_{\mathrm{max,turb,OL}}]$ in MW |

The storage capacity of the open loop power plant fleet is divided by the total installed turbine power and evaluated if:

- it is smaller or equal 24 hours, then a daily binding constraint is applied, or
- it is greater than 24 hours, then a weekly binding constraint is applied.

The obtained dimension of $\tau$ is entered into the model via a user interface that specifies a daily or weekly binding constraint.

## 4.2 Enhanced approach for Traditional Reservoir and Open Loop representation by introducing Water Values

Hydro pre-optimization, which follows a load-proportional heuristic using the climate year dependent reservoir levels provided by the user (see Figure 2.8) and explained in chapter 4.1, was offered to Antares users during the MAF processes between 2017 and 2019. The old database format (predecessor PEMMDB 2.0), which was still in use at that time, did not satisfactorily support using the reservoir management functionality of Antares in combination with minimum and maximum reservoir levels (Figure 2.7).
With the new database format PEMMDB 3.0, data can be provided to use the reservoir management functionality of Antares together with the provision of minimum and maximum reservoir levels by the user. This allows to develop further possibilities for a better pre-optimization of hydropower.

As the interest of various TSOs in the Antares tool increased after the introduction of the new database format, the development led to the introduction of water values as input for the Antares optimization. The interface was completed with Antares version 7. The calculation of the water values as input parameters per node remains a task for the user.

To take the water values into account in the main optimization of Antares, the tool expects a matrix with the size of 365 x 100 to be filled for each day of the year, which provides a water value ($\omega$) for each reservoir filling level (between 0 % to 100 %). The values can be entered manually via the graphical user interface or they are fed to the tool after the calculation, e.g. according to the algorithm described in chapter 2.6.2.

The use of the water value functionality is described in various approaches in this thesis, e.g. enhanced swell representation (see chapter 4.4.3) or an approach developed for short cycle storage (see chapter 4.3.2). In this chapter two attempts for the traditional reservoir pre-optimization are elaborated:

- estimation of water values based on a marginal costs of a previous calculation (chapter 4.2.1)
- calculation of water values based on Bellman's principle of optimality (chapter 4.2.2)

### 4.2.1 Discretization of the reservoir on the basis of marginal costs

When using water values in the main optimization of Antares ($C_{\mathrm{Hydro}}$ as described in chapter 2.6.3), a matrix must be filled in that provides a shadow price (so called water value $\omega$) for each percentage filling level of the reservoir and each day of the year. As an alternative to the

Bellman optimality principle (as described in chapter 2.6.2) to calculate water values, which is also very time consuming, a simplified approach is elaborated in this chapter.

For bidding zones that already provide trajectories for minimum and maximum reservoir levels (see figure 2.7), a simplified approach for using the water value matrix can be applied by dividing the reservoir into two sections between the minimum and maximum reservoir level rule curves:

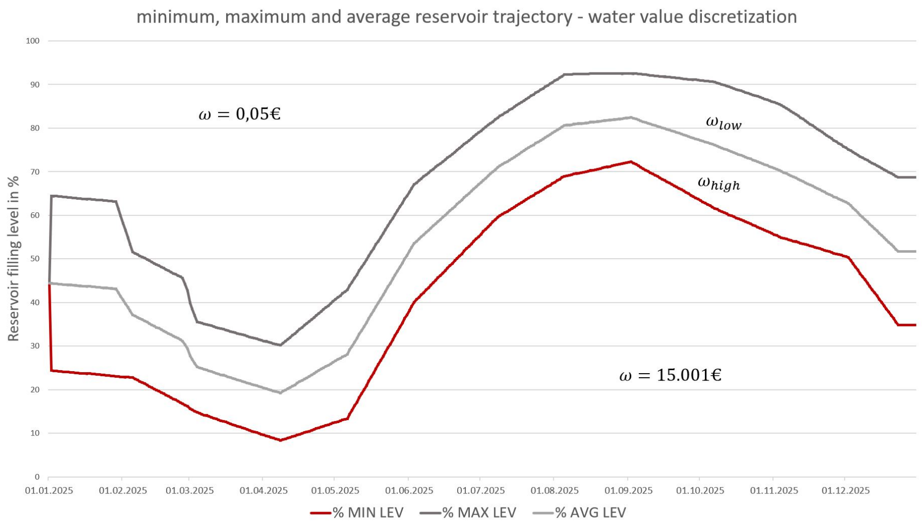


**Figure 4.3:** Water values using marginal cost approach

- the section below the average rule curve receives a higher water value ($\omega_{\text{high}} = \overline{\text{C}_{\text{total}}} + \text{X} \cdot \text{STD}$)
- the section above the average rule curve receives a lower water value ($\omega_{\text{low}} = \overline{\text{C}_{\text{total}}} - \text{X} \cdot \text{STD}$)

where

| | |
|---|---|
| $\omega_{\text{low}}$ | water value *low* is applied for the area above the average curve and below the maximum rule curve |
| $\omega_{\text{high}}$ | water value *high* is applied for the area below the average curve and above the minimum rule curve |
| $\overline{\text{C}_{\text{total}}}$ | average marginal costs of all annual time series resulting from a previous calculation using the Antares heuristic |
| STD | standard deviation of the average marginal costs determined during the run using the Antares heuristic |
| X | value to be defined by the user |

The average marginal costs ($\overline{\text{C}_{\text{total}}}$) used to approximate the lower and higher water value sections are taken from the calculation of a previous run using the Antares heuristic. The marginal costs used to calculate the lower and higher water values are an average of all Monte Carlo simulations. The standard deviation of the average marginal cost ($\overline{\mathrm{C}_{\mathrm{total}}}$) is also extracted from the Antares run using the heuristic (see chapter 2.6.1), where $X$ can be arbitrarily chosen by the user. The value X = 3 was used for the investigations carried out within this thesis as an assumption.

Setting the values outside the rule curves is a necessary step: if the values below the lower rule curve remain too low, the reservoir could be completely emptied within a very short time. The functionality of considering the rule curves as hard limits leads to infeasibility. It was therefore decided to set the values 15 001 € and 0.05 €. Details of the results of this approach are discussed in chapter 6.1.

The approach described above defines two different water value sections that lie between the minimum and maximum rule curves of a reservoir. Since the rule curves for the reservoir are treated as soft constraints in the optimization, they can be violated with very high penalty costs. A manual approach to force the model to comply with these soft constraints leads to a very high value for the area below the minimum curve, which exceeds the Value of Lost Load (VOLL = 15 000 €), while the values above the maximum rule curve are set to zero. As Antares regularly has problems with zero entries, the value 0.05 € is selected for the values above the upper rule curve.

### 4.2.2 Application of Bellman's optimality principle to calculate water values

The idea of optimizing the hydro reservoir levels by the means of dynamic programming has already been presented in chapter 2.6.2. The Bellman optimality principle is applied, which starts from the final reservoir level of a year and gradually moves towards the beginning of the year, whereby the values for each day of a year are determined by introducing a series of sub-problems that are solved step by step.
To retrieve the solution for each reservoir level for each day of the year, the algorithm was built into an R-based app as part of a master's thesis conducted at RTE in 2021 [38]. This app is available on github and therefore free to use. During the period of the work at RTE, there was an intensive exchange between the modeling department of RTE and APG. APG contributed with its knowledge of the limitations in hydropower modeling identified in previous years and adapted the script for internal use. Following the investigations as part of this thesis, the calculation of the water values was carried out according to Bellman's optimality principle, first for the ERAA 2022 model.

First, a complete European model is created in the same way as when applying the Antares heuristic (2.6.1). The country node and the reservoir for which the water values are to be calculated is selected. The user must specify for how many climate years the algorithm is carried out. Depending on the selected algorithm (either "average of grids", "grids of means" or "grids of quantiles" - see chapter 2.6.2), a value is calculated for each day of the year and for each of the 100 levels of the reservoir. Following a minimal approach, 35 climate years are sufficient to cover the methodology of the ERAA model.

The water values determined by the algorithm can be displayed, whereby in a first step the values below the minimum reservoir level rule curve and above the maximum reservoir level rule curve are not taken into account. Figure 4.4 shows the values determined by the algorithm for Austria (yellow colored areas show a high water value and blue colored areas a rather low water value).

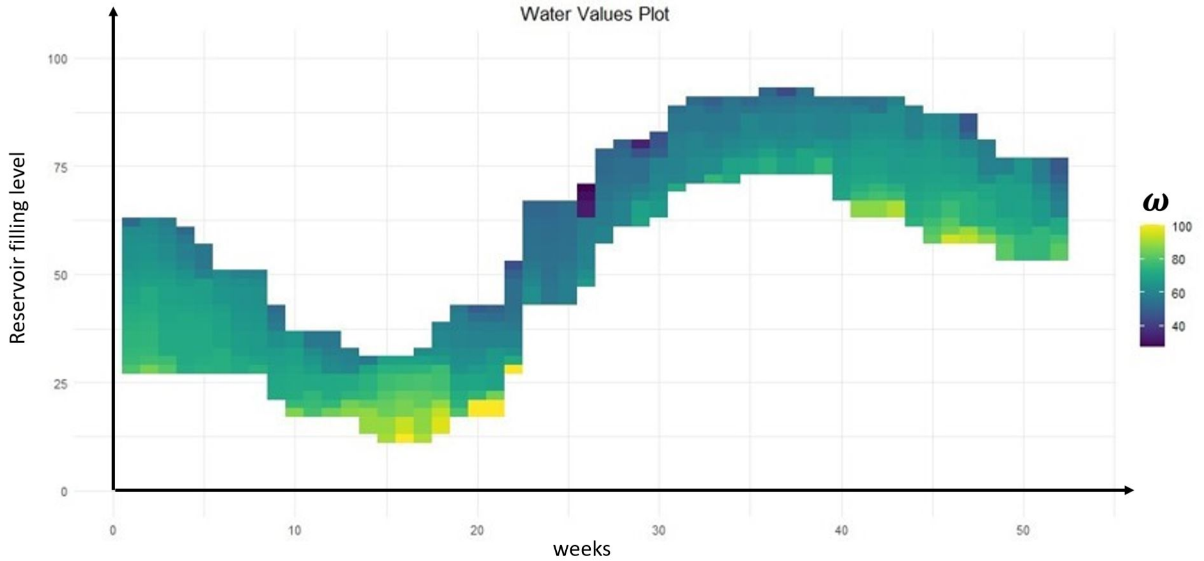


**Figure 4.4:** Water values determined by applying Bellman's optimality principle

In a second step, post-processing is triggered in order to assign values to the reservoir levels below the minimum and above the maximum reservoir level rule cure. The same assumption applies here as in chapter 4.2.1, values below the minimum reservoir level rule curve are assigned a value of 15 001 € and values above the maximum reservoir level rule curve are assigned a value of 0.05 €.

In a third and final step, the values are written directly into the Antares study.

Depending on the performance of the calculation engine, the calculation time for a complete ERAA study for a reservoir of a bidding zone can last up to 30 hours (server machine with two processors Intel(R) Xeon(R) Gold 6144CPU @ 3,5 GHz and 128 GB RAM). Depending on the structure of a bidding zone's hydropower plant park, one calculation must be performed for the traditional reservoir and one for the hydro open loop category.

Both methods described above for placing water values for traditional reservoirs or open loop reservoirs serve to overtake the reservoir management functionality of Antares applying a net-load proportional heuristic. A comparison of the representation using the Antares heuristic and the two water value methods described in this chapter is discussed in chapter 6.1.

## 4.3 Enhanced approach for Closed Loop representation

In the original representation for closed loop pump storage units - as described in chapter 4.1 - there is a significant disadvantage in that the size of the reservoir cannot be transferred to Antares as an input and is therefore not taken into account by the tool.
For this reason, two further attempts to represent CL PSPs are presented and described below.

### 4.3.1 Enhanced approach for Closed Loop representation using thermal clusters and binding constraints

Investigating some training material provided with the Antares tool and some insights from RTE R&D, an approach was developed where two additional virtual nodes in combination with binding constraints are introduced to control the use of the reservoir and define the maximum storage size of a PSP unit.

The idea of the described approach is to place the hydro reservoir information inside the virtual nodes as thermal units which are forced to not generate and constrain the provided time-series inside these thermal units (thermal clusters) with the help of binding constraints. The thermal clusters specify the reservoir in a way that the reservoir filling level is forced to reach 50 % of its maximum reservoir size by the end of a cycle (e.g. week, day). Figure 4.5 shows two weeks of the storage level of a CL PSP using a weekly cycle, where the reservoir is forced to reach 50 % of its filling level at the end of each week.

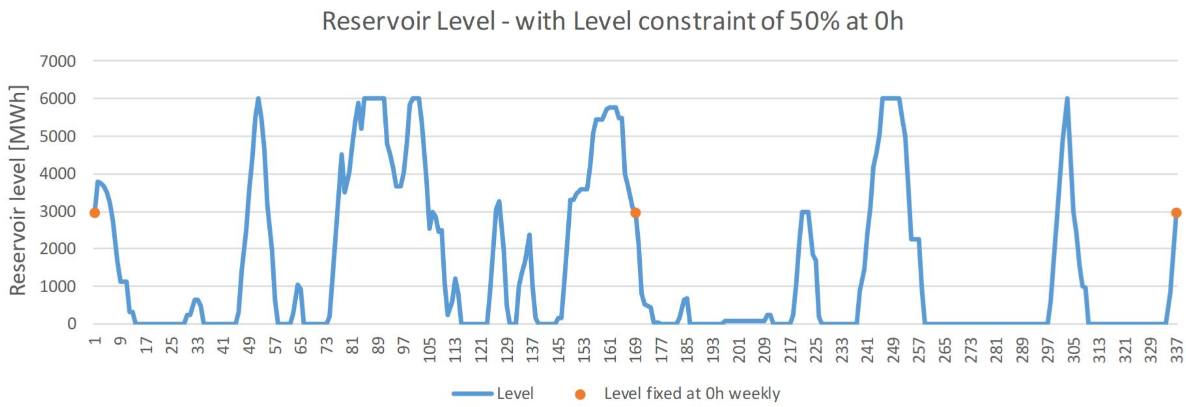


**Figure 4.5:** Reservoir filling level of a CL PSP forcing the reservoir to reach 50 % of its filling level by the end of a week (source: RTE)

The following information is required to define the CL PSP:

- $\mathbf{P_{max}}$ - maximum turbine and pump power for CL PSP units in MW

- **$\mathbf{Cap_{max}}$** - maximum reservoir capacity in MWh
- **fixed values of the storage levels** for specific hours, which are forced to be reached at the end of a cycle

Since binding constraints in Antares can be applied to either links or thermal units, thermal units inside the two virtual nodes are used to characterize the CL PSP reservoir.

The following representation is used and explained below:

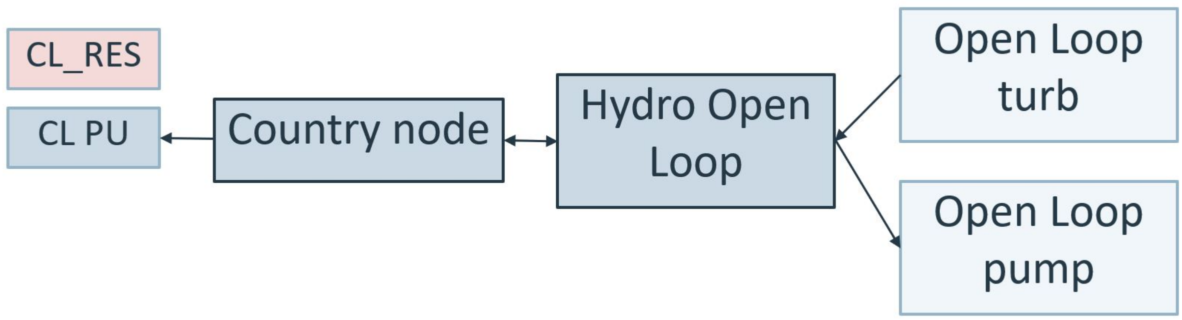


**Figure 4.6:** Antares representation using thermal clusters to constrain the PSP reservoir

The following list provides an overview of the input parameters used and how they can be integrated into the model to represent closed loop pump storage units via thermal units to specify the properties of the PSP unit:

1. country node: the maximum turbine power of the CL PSP is placed within the country node as a thermal unit (Turb_CL) whose maximum power corresponds to the maximum turbine power of the CL PSP. This thermal unit operates at zero cost and receives 35 time series in hourly resolution containing the maximum turbine power in each hour.

2. CL_PU: the blue virtual node which is connected to the country node via a link, supports the characterization of the maximum pumping power of the CL PSP. The maximum pumping power is placed as an hourly time series on the link between the country node and the virtual pump node ([CL_PU → country node]). The virtual node receives a time series with a high load (100 000 MW).

3. CL_RES: the red virtual node, which is not connected to the country node, is used to specify the reservoir characteristics of the CL PSP. Within this virtual node, two thermal units are created that specify the reservoir and a forced to not generate:

   - CL_RES_L1 - a thermal cluster within the CL_RES virtual node containing one thermal unit characterized by 35 time series containing the maximum size of the reservoir; to bring the reservoir to 50 % of its filling level at the end of the weekly cycle, the value is manually set to half the reservoir size every Monday at 00:00.

- CL_RES_L2 - a thermal cluster within the CL_RES virtual node containing one thermal unit, characterized by 35 time series containing the maximum size of the reservoir; to bring the reservoir to 50 % of its filling level at the end of the weekly cycle, the value is manually set to half the reservoir size every Monday at 00:00.

The two thermal units within the virtual node CL_RES are used to imply a time offset via a binding constraint.

Two binding constraints are implied on the thermal clusters CL_RES_L1 and CL_RES_L2. For the constraint of the maximum pumping power the constraint remains on the link, which is set in brackets [*] below:

- BC 1: CL_RES_L2(t + 1) = CL_RES_L1(t) + eff · [CL_PU → country node] − Turb_CL - The storage level at time $(t + 1)$ is equal to the storage level at time $t$ plus the energy pumped into the storage, multiplied by the efficiency, minus the turbined energy.

- BC 2: CL_RES_L1 = CL_RES_L2 - used to introduce the time offset between L1 and L2

Attention needs to be given to the sign convention, which specifies the direction of the flow used for the pumping in BC 1. Antares follows the alphabetical order while processing the input data inside the nodes. Therefore, each binding constraint must be created taking into account the naming to imply the correct link directions from node A to node B.

The major advantage of this approach is that for the entire European model, for all countries that have CL PSPs in their power plant fleet, the information that specifies the pumping behavior and the size of the reservoir can be placed in two virtual nodes for the entire perimeter. Two thermal units per bidding zone are then placed in the virtual node that specifies the reservoir (CL_RES). The maximum pumping power is placed on the link between the CL pump node (CL_PU) and the respective bidding zone.

This approach helps to reduce the total number of virtual nodes to two for the whole perimeter to represent a CL PSP.

### 4.3.2 Enhanced approach for Closed Loop representation using water values and internal pumping functionality

With Antares version 7, a function for pumping has been introduced on the condition that either the reservoir management functionality or the water value approach is used. To use this new functionality for the CL PSP representation, a *Hydro Closed Loop* supportive node is created

and connected to the country node in the same way as the supportive node for *Hydro Open Loop*.
Figure 4.7 shows the setup for the hydro representation after the introduction of the water value functionality and that of the internal pump function.

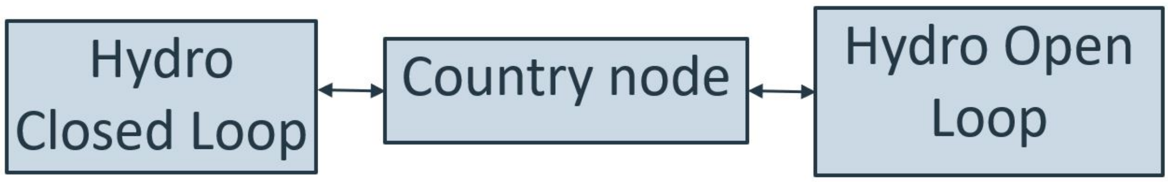


**Figure 4.7:** Antares representation using water values and internal pumping for CL PSPs

where

1. country node
   - ROR & swell inflow time series in hourly resolution
   - traditional reservoir - all details (inflow time series, minimum and maximum reservoir levels, reservoir size, turbine power)
   - PV & wind time series
   - thermal power plant information
   - load time series
   - miscellaneous generation
2. hydro open loop node - contains all the details of the OL PSP (inflow time series, minimum and maximum reservoir levels, reservoir size, maximum turbine and pump power) and the round-trip efficiency
3. hydro closed loop node - contains all the details of the reservoir of the CL PSP (size of the reservoir, maximum turbine and pump power), the round-trip efficiency and the water value matrix. The hydro closed loop node uses the water value functionality, where all values within the water value matrix are manually set to zero.

The values on the links between the country node and the supportive hydro nodes receive the minimum and maximum turbine and pumping power.

This approach is developed to respect the limits of the reservoir size and to test the internal pumping function of Antares. A first feedback of this function introduced with Antares version 7 in combination with the use of the water value functionality, is that pumping is underutilized when the storage size is relatively small compared to the total installed turbine and pump capacity. This limitation is also visible in the results of the calculations performed on the trilateral test model and discussed in chapter 6.2 in this thesis and is investigated at RTE R&D.

## 4.4 Enhanced approach for swell representation

Results of the investigations carried out as part of a master's thesis to describe the differences in hydropower modeling approaches between the MAF 2018 and 2019 [22], the introduction of the new database format PEMMDB 3.0 revealed limitations in the representation of generation from swell units. In MAF 2018 (and earlier), the swell inflows were provided by the TSOs as a single category. In the initial hydro representation in Antares, the delivered swell inflows were merged with the only existing reservoir in the country node. When the new database PEMMDB 3.0 was introduced and used for the first time in MAF 2019, the problem arose that the inflows from run of river and swell units were aggregated in a joint time series and dispatched immediately. The assumption was that a certain flexibility potential was missing due to the lack of daily storage behavior of swell units. Various approaches are therefore being investigated in order to obtain an improved representation of run of river and swell split.

This chapter describes three approaches that help to separate the inflows from run of river and swell, which are treated by the model as follows: inflows from run of river are dispatched immediately, while inflows from swell can be stored inside the swell reservoir and discharged when the market requires it.

- Since the initial swell investigations are related to MAF modeling, the first approach described in chapter 4.4.1 was developed within Antares version 6 and uses additional virtual nodes and binding constraints to allow for a storage behavior of swell generation.
- A second representation, which can also be used with Antares version 6, is described in chapter 4.4.2. This approach uses the same modeling attempt as described in chapter 4.3.1, where a virtual node is introduced to define the properties of the swell reservoir following the representation for short cycle storage of CL PSP units.
- A third approach has been available since the introduction of Antares version 7 and is described in chapter 4.4.3. This approach uses the water value functionality to represent the properties of the swell generation including their daily storage behavior.

In all the approaches described below, the initial starting condition is a separation of the time series of run of river and swell inflow. This is achieved by introducing the following equations:

$$\mathrm{Inf}_{\mathrm{ROR}} = \mathrm{Inf}_{\mathrm{ROR+Swell}} \cdot \frac{\mathrm{P}_{\mathrm{max,ROR}}}{\mathrm{P}_{(\mathrm{max,ROR+Swell})}}$$
$$\mathrm{Inf}_{\mathrm{Swell}} = \mathrm{Inf}_{\mathrm{ROR+Swell}} \cdot \frac{\mathrm{P}_{\mathrm{max,Swell}}}{\mathrm{P}_{(\mathrm{max,ROR+Swell})}}$$

where

| | |
|---|---|
| $\mathrm{Inf}_{\mathrm{ROR}}$ | share of ROR inflow |
| $\mathrm{Inf}_{\mathrm{Swell}}$ | share of swell inflow |
| $\mathrm{Inf}_{(\mathrm{ROR+Swell})}$ | provided merged time series for ROR and swell inflows |
| $\mathrm{P}_{\mathrm{max,(ROR+Swell)}}$ | installed power from ROR and swell units |
| $\mathrm{P}_{\mathrm{max,ROR}}$ | installed power from ROR units |
| $\mathrm{P}_{\mathrm{max,Swell}}$ | installed power from swell units |

### 4.4.1 Separate node constraining daily energies

This approach was developed during MAF 2019 after the new database format PEMMDB 3.0 was introduced. The PEMMDB 3.0 database contains only one time series for hydro inflows of ROR and swell units. As a starting point, the summarized hydro inflow time series are divided according to their installed turbine power.

A virtual node (Swell) is connected to the main country node, which is used together with a supporting node (Hydro_Help) to characterize the swell reservoir. The setup is shown in Figure 4.8

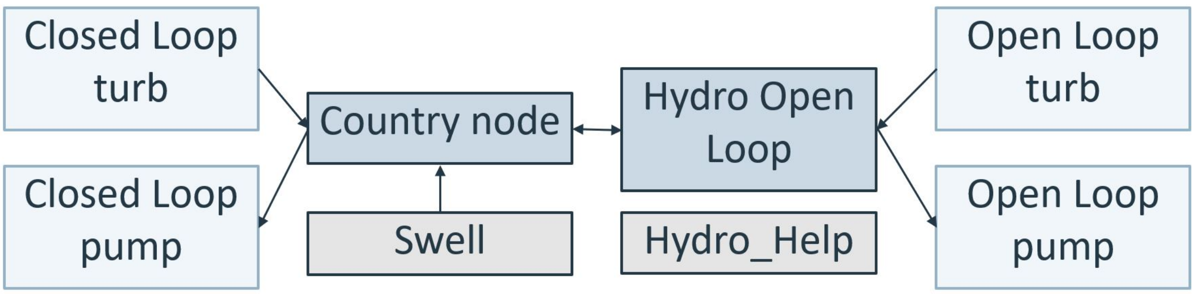


**Figure 4.8:** Hydro swell representation using one additional node connected to the country node, and one supportive hydro node

where

1. Country node (AT):

    - time series for pure ROR generation

- traditional reservoir - all details (inflow time series, minimum and maximum reservoir levels, reservoir size, turbine power)
- PV & wind time series
- thermal power plant information
- load time series
- miscellaneous generation

2. Swell node - receives the 35 time series of the maximum turbine power of swell units $P_{\mathrm{max,turb,Swell}}$ as a thermal cluster operating at zero cost
3. Link [$\mathrm{AT}_{\mathrm{Swell}} \rightarrow \mathrm{AT}$] - obtains the maximum turbine power of all swell units $P_{\mathrm{max,turb,Swell}}$ as hourly time series on the link between the swell node and the country node
4. Hydro support node (Hydro_Help):

   a) obtains the 35 hourly time series of swell Inflows $\mathrm{Inf}_{\mathrm{Swell}}$ in MWh as a thermal cluster operating at zero cost

   b) obtains the 35 hourly time series for the maximum energy to be generated from swell units ($E_{\mathrm{max,Swell}} = P_{\mathrm{max,Swell}} \cdot 1$ h) in MWh as a thermal cluster operating at zero cost

5. binding constraints (values in [*] represent links between nodes):

   a) daily binding constraint (equal): the maximum daily energy to be generated within the swell node and thus measured on the link between the country node and the swell node equals the inflow from swell generation ($\mathrm{Inf}_{\mathrm{Swell}}$)
   $\mathrm{BC1} : [\mathrm{AT} \rightarrow \mathrm{AT}_{\mathrm{Swell}}] = \mathrm{Inf}_{\mathrm{Swell}}$

   b) hourly binding constraint (above): the hourly value on the link between the swell and the country node needs stay lower than the specified maximum total energy resulting from of maximum output of the swell turbine in this hour ($E_{\mathrm{max,Swell}}$):
   $\mathrm{BC2} : [\mathrm{AT} \rightarrow \mathrm{AT}_{\mathrm{Swell}}] < E_{\mathrm{max,Swell}}$

Figure 4.9 displays the above described time series:

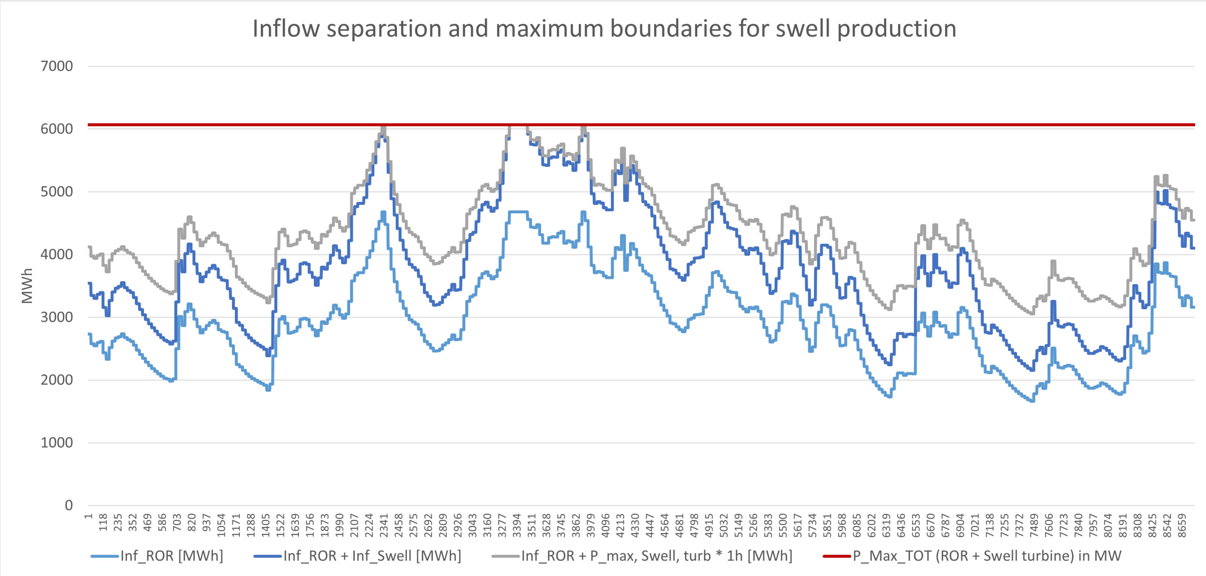


**Figure 4.9:** Hourly inflows of run of river and swell in Austria as used in the ERAA 2021 process

- light blue line - time series of the ROR inflow in MWh that must be dispatched immediately
- dark blue line - ROR and swell inflow time series in MWh
- grey line - run of river inflow time series plus the maximum turbine power of all swell units
- red constant line - maximum installed run of river and swell power

### 4.4.2 Applying the approach for short cycle storage

An alternative approach for the swell representation can be achieved by applying the methodology for short cycle storage generation as described in chapter 4.3.1. This representation is also used for CL PSPs, batteries or implicit DSR: it forces a reservoir at the end of a period (X hourly, daily or weekly) to reach the same reservoir filling level as at the beginning of the period (50 % filling level in the case of this thesis). In the representation for swell generation, the cycle period is set to one week.

Figure 4.10 displays the technical implementation in the model:

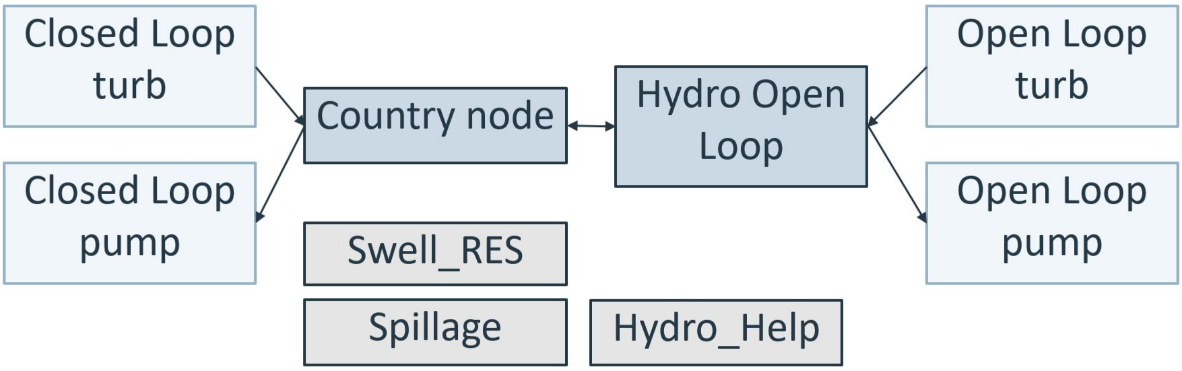


**Figure 4.10:** Approach for short cycle storage used to represent swell production

1. External swell node (Swell_RES) - not connected to the country node receives two thermal clusters (Swell_RES_L1 and Swell_RES_L2) that operate at zero cost and whose size corresponds to the size of the entire reservoir. This unit receives 35 time series in hourly resolution with the maximum reservoir size for each hour. Each Monday at 00:00, the size of the reservoir is reduced to half of its size. This is achieved by dividing the time series for this hour by a factor of 2 every Monday 00:00.

2. Country Node - receives one additional thermal cluster - a unit with the turbine power of the total installed swell units ($\mathrm{P}_{\mathrm{max,Swell}}$). This cluster contains 35 time series in hourly resolution with $\mathrm{E}_{\mathrm{turb,Swell}} = \mathrm{P}_{\mathrm{max,Swell}} * 1\mathrm{h}$ for each hour.

3. Supportive hydro node (Hydro_Help) - the swell inflow time series ($\mathrm{Inf}_{\mathrm{Swell}}$) are placed in the supportive hydro node as a thermal cluster, which operates at zero cost and contains 35 time series with the 35 climate-dependent inflow time series in hourly resolution.

4. Spillage node: This node is introduced with a thermal cluster that is operated at zero cost and has a total installed capacity of 100.000 MW. This thermal cluster is used to absorb hydro energy when the inflows exceed the possible maximum turbine power of the swell units.

5. Binding constraints:

   a) BC 1: Swell_RES_L1 = Swell_RES_L2 - The reservoirs placed in the external swell node as thermal clusters are set equal (hourly). This is necessary to introduce the time offset in BC 2.

   b) BC 2: $\mathrm{Swell\_RES\_L2(t+1)} = \mathrm{Swell\_RES\_L1(t)} + \mathrm{Inf}_{\mathrm{Swell}} - \mathrm{E}_{\mathrm{turb,Swell}} - \mathrm{Spillage}$ - The reservoir level at the time $(t+1)$ is defined as the reservoir level at time $t$ plus the swell inflows minus the turbined energy minus spillage

### 4.4.3 Separate node using water values

This representation uses idea of the additional swell node introduced in chapter 4.4.1 in combination with the ability of Antares to use water values for hydro reservoirs as described in 4.3.2 (a functionality available since Antares version 7). This approach, where the additional swell node is used to define the properties of the swell reservoir of a bidding zone, a water value matrix is introduced for the different reservoir filling levels of swell production for the whole year, as shown in figure 4.11:

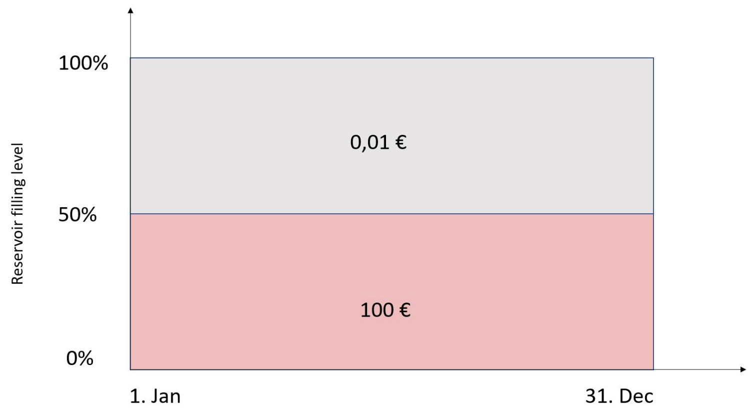


**Figure 4.11:** Water values used to represent swell production

Values below 50 % of the reservoir filling level receive a relatively high value within the matrix (100 €), values above 50 % of the reservoir filling level receive a rather low value (0.01 €). The values were selected after various test calculations were carried out for the higher value and the results showed hardly any deviations.

Figure 4.12 displays the representation of the approach using one additional node to specify the swell reservoir using the above water values matrix:

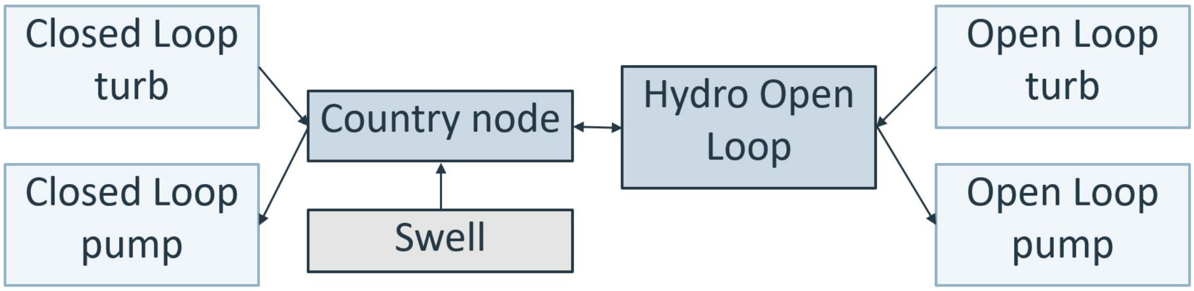


**Figure 4.12:** Swell representation using an additional node that is connected to the country node and contains the swell reservoir information and a water value matrix

1. Country node
   - time series for pure ROR generation resulting from inflow time series portion of the ROR inflow ($\mathrm{Inf}_{ROR}$), which should also be turbined at zero cost as a must-run generation
   - traditional reservoir - all details (inflow time series, minimum and maximum reservoir levels, reservoir size, turbine power)
   - PV & wind time series
   - thermal power plant information
   - load time series
   - miscellaneous generation
2. Swell node
   - contains the time series of swell inflows ($\mathrm{Inf}_{Swell}$) as inflows to a reservoir with a defined reservoir size
   - place the water value matrix as displayed in figure 4.11
   - water value functionality activated for the swell reservoir
3. Link [$Swell \rightarrow AT$] - receives the hourly values of the energy flow on the link as the maximum turbine power of all swell units

The three investigations described above on swell representation are elaborated in a tri-lateral test model and the hourly results were compared in a bachelor thesis in summer 2021 [51]. As a result and due to similarities with many of the newly emerging short cycle storage approaches, the approach that is also used for CL PSPs was chosen for further calculations (from ERAA 2023 onwards). The difference between the results of the various approaches are discussed in chapter 6.3.

## 4.5 Enhanced approach for Traditional Reservoir and Open Loop representation - Introducing Hydro Cascades

Austria has a considerable number of installed pumped storage units in the western part of the country, which are distributed across the entire mountainous region of the Austrian Alps. The question arises as to whether aggregating all storage units in a common large reservoir is sufficient for Austria. The power plant cascades in the west of the country, which extend over larger mountain ranges, are a specific feature of the Austrian power plant park. In the simplest case, a power plant cascade consists of an upper and a lower reservoir connected to some turbine and pump units. A graphical explanation is shown in Figure 4.13.

As a final study to improve the representation of hydropower plants in Austria in resource adequacy calculations, one power plant cascade is therefore elaborated and separated from the Austrian reservoir. This chapter describes the separation of the Kaprun power plant group in the province of Salzburg and its implementation in the modeling of resource adequacy within the framework of Antares.

The Kaprun power plant group consists of two hydro reservoirs: The Mooserboden with a size of 84,9 million $m^3$ as the upper reservoir at 2036 m above sea level and the Wasserfallboden with a size of 81,2 million $m^3$ as the lower reservoir at 1672 m above sea level. Both reservoirs are connected by Kaprun Oberstufe with a total installed turbine power of 112 MW and pumping power of 130 MW and Limberg 2, which was commissioned in 2011 with a total installed turbine and pumping power of 480 MW. Construction of the Kaprun Limberg 3 power plant has been underway since 2021, with commissioning planned beyond 2025. Kaprun 3 will also have a total turbine and pump power of 480 MW. The Kaprun Hauptstufe power plant with a turbine power of 280 MW is connected to the lower reservoir Wasserfallboden [81]. Figure 4.13 shows the structure of the power plant group as it is in operation and is used for the calculations carried out in this thesis. Smaller generation or pumping units are excluded for an initial representation in the context of resource adequacy.

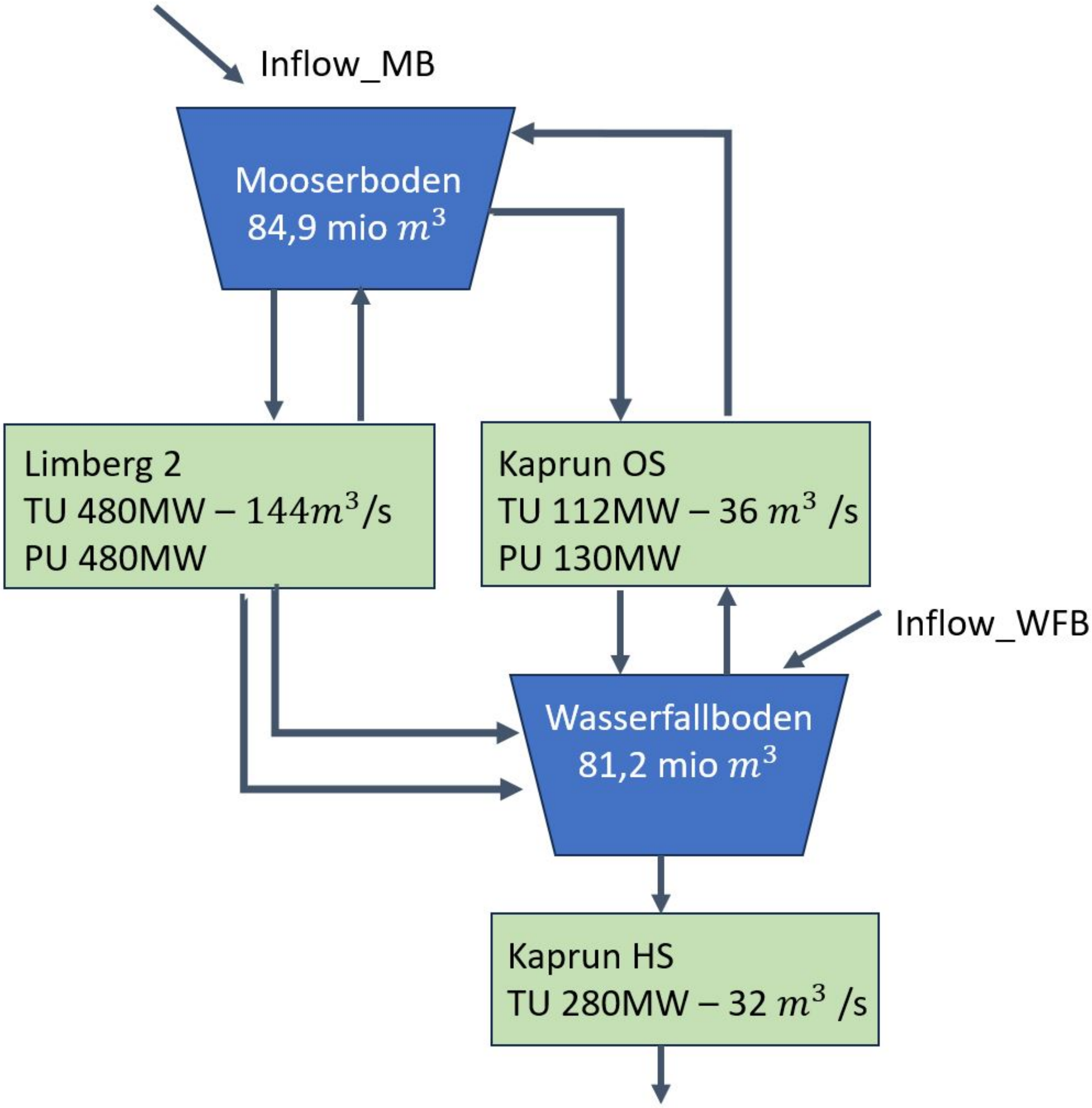


**Figure 4.13:** Kaprun power plant representation in 2024

First, the inflows into the Mooserboden and Wasserfallboden reservoirs are divided proportionally to the reservoir size:

$\mathrm{Inf}_{\mathrm{MB}} = \frac{\Sigma_{\mathrm{MB}}}{\Sigma_{\mathrm{OL}}} \cdot \mathrm{Inf}_{\mathrm{OL}}$
$\mathrm{Inf}_{\mathrm{WFB}} = \frac{\Sigma_{\mathrm{WFB}}}{\Sigma_{\mathrm{OL}}} \cdot \mathrm{Inf}_{\mathrm{TR}}$

where

| | |
|---|---|
| $\text{Inf}_{\text{MB}}$ | hydro inflow to reservoir Mooserboden |
| $\text{Inf}_{\text{WFB}}$ | hydro inflow to reservoir Wasserfallboden |
| $\text{Inf}_{\text{OL}}$ | hydro inflow to Open Loop reservoir |
| $\text{Inf}_{\text{TR}}$ | hydro inflow to traditional reservoir |
| $\Sigma_{\text{OL}}$ | total storage capacity of the open loop power plant fleet |
| $\Sigma_{\text{TR}}$ | total storage capacity of the traditional reservoir power plant fleet |
| $\Sigma_{\text{MB}}$ | total storage capacity of the upper reservoir Mooserboden |
| $\Sigma_{\text{WFB}}$ | total storage capacity of the lower reservoir Wasserfallboden |

Secondly, the total installed reservoir capacity of open loop reservoir and traditional reservoir are reduced by the installed reservoir capacities of Mooserboden and Wasserfallboden. The capacity of the upper reservoir is deducted from the open loop reservoir and the capacity of the lower reservoir is deducted from the traditional reservoir.

$$\Sigma_{\text{OL,NEW}} = \Sigma_{\text{OL}} - \Sigma_{\text{MB}}$$
$$\Sigma_{\text{TR,NEW}} = \Sigma_{\text{TR}} - \Sigma_{\text{WFB}}$$

Third, the maximum turbine and pump power is also deducted from the open loop and traditional reservoir total aggregated power:

$$\text{P}_{\text{max,turb,OL,NEW}} = \text{P}_{\text{max,turb,OL}} - \text{P}_{\text{max,turb,Kaprun,OS}} - \text{P}_{\text{max,turb,Li2}}$$
$$\text{P}_{\text{max,pump,OL,NEW}} = \text{P}_{\text{max,pump,OL}} - \text{P}_{\text{max,pump,Kaprun,OS}} - \text{P}_{\text{max,pump,Li2}}$$
$$\text{P}_{\text{max,turb,TR,NEW}} = \text{P}_{\text{max,turb,TR}} - \text{P}_{\text{max,turb,Kaprun,HS}}$$

where

| | |
|---|---|
| $\text{P}_{\text{max,turb,OL,NEW}}$ | maximum turbine power for the Open Loop PSP aggregated cluster after deduction of Kaprun power plants |
| $\text{P}_{\text{max,turb,Kaprun,OS}}$ | maximum turbine power of power plant Kaprun Oberstufe |
| $\text{P}_{\text{max,turb,Li2}}$ | maximum turbine power of power plant Limberg 2 |
| $\text{P}_{\text{max,pump,OL,NEW}}$ | maximum pump power for the Open Loop PSP aggregated cluster after deduction of Kaprun power plants |
| $\text{P}_{\text{max,pump,Kaprun,OS}}$ | maximum pump power of power plant Kaprun Oberstufe |
| $\text{P}_{\text{max,pump,Li2}}$ | maximum pump power of power plant Limberg 2 |
| $\text{P}_{\text{max,turb,TR,NEW}}$ | maximum turbine power for the traditional reservoir aggregated cluster after deduction of Kaprun power plants |
| $\text{P}_{\text{max,turb,Kaprun,HS}}$ | maximum turbine power of power plant Kaprun Hauptstufe |

As a fourth and final step in the preparation of input for the cascade representation, a coefficient called *upper to lower discharge coefficient* $\epsilon$ is introduced, which indicates how much energy of 1 MW turbined energy in the upper power plant is brought to the lower lower power plant and can be turbined there.

$$\epsilon_{\text{Kaprun}} = \frac{\text{P}_{\text{max,turb,low}} \cdot \text{FR}_{\text{up}}}{\text{P}_{\text{max,turb,up}} \cdot \text{FR}_{\text{low}}}$$

where

| | |
|---|---|
| $P_{max,turb,up}$ | maximum turbine power connected to the upper reservoir, $P_{max,turb,up}$, $[P_{max,turb,up}]$ in MW |
| $P_{max,turb,low}$ | maximum turbine power connected to the lower reservoir, $P_{max,turb,low}$, $[P_{max,turb,low}]$ in MW |
| $FR_{up}$ | flow rate of the turbine units connected to the upper reservoir, $FR_{up}$, $[FR_{up}] = m^3/s$ |
| $FR_{low}$ | flow rate of the turbine units connected to the lower reservoir, $FR_{low}$, $[FR_{low}]$ in $m^3/s$ |

For Kaprun Oberstufe and Limberg 2 this coefficient is calculated as follows using the nominal turbine power and the flow rates of the upper and lower power plant:

$$\epsilon_{OS+Li2} = \frac{280\,\text{MW}\cdot(144+36)m^3/s}{(480\,\text{MW}+112\,\text{MW})\cdot 32m^3/s} = 2,66$$

As an example it can be said that 1 MWh turbined from the upper reservoir brings 2.66 MWh to the lower reservoir.

Once all the proportional inflows, the adjusted reservoir sizes, the maximum turbine and pumping power and the upper to lower discharge coefficient have been defined, the representation in Antares looks as follows: Two nodes are used to define the reservoirs Mooserboden and Wasserfallboden with all the details specifying the reservoir and defining the connected turbine units. A supporting node is used to represent the pumping behavior (see Figure 4.14. For the cascade representation, the pumping functionality of Antares as delivered with Antares version 7 cannot be used for the power plants connected to the upper reservoir. A solution to implement the pumping behavior is described below.

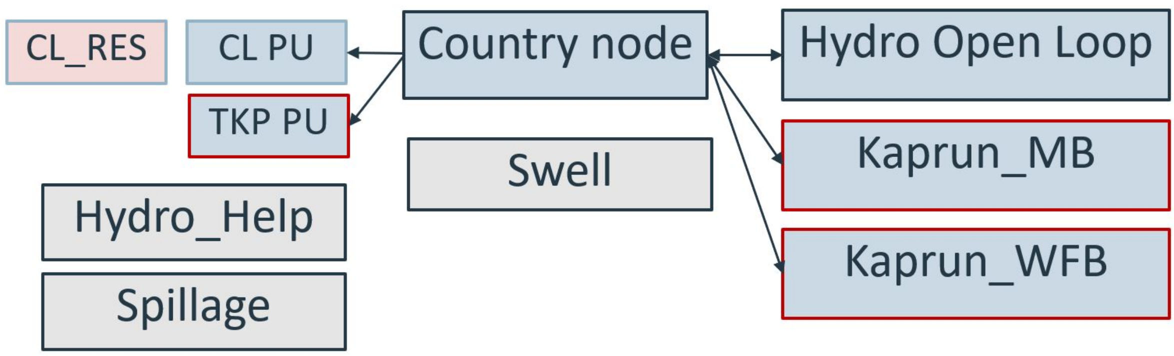


**Figure 4.14:** Kaprun power plant representation in Antares

1. Country node

    - time series for pure ROR generation resulting from inflow time series portion of the ROR inflow ($Inf_{ROR}$) that is turbined as must-run generation at zero cost

- traditional reservoir properties
  - inflow time series deducted by the inflows to the reservoir of Wasserfallboden
  - reservoir size deducted by the reservoir size of the reservoir of Wasserfallboden
  - maximum turbine power deducted by the turbine power of Kaprun Hauptstufe power plant
  - minimum and maximum reservoir levels
- PV & wind time series
- thermal power plant information
- load time series
- miscellaneous generation

2. Open Loop Hydro node
   - inflow time series deducted by the inflows to the reservoir of Mooserboden
   - reservoir size deducted by the reservoir size of the reservoir Mooserboden
   - maximum turbine and pump power deducted by the turbine and pump power of Kaprun Oberstufe and Limberg 2 power plant
   - minimum and maximum reservoir levels

3. Kaprun_MB

   This node is used to specify the upper hydro reservoir (Mooserboden) as well as the turbine power of Kaprun Oberstufe and Limberg 2

   - inflow time series of Mooserboden (Inf_MB)
   - reservoir size of the reservoir Mooserboden
   - maximum turbine power of power plants Kaprun Oberstufe and Limberg 2
   - minimum and maximum reservoir levels as used for Hydro Open Loop
   - enable the water value functionality using a water value matrix based on the calculation of the simplified approach using the marginal price of a previous calculation

- disable the pumping functionality

4. Kaprun_WFB

   This node is used to specify the lower hydro reservoir (Wasserfallboden) as well as the turbine power of Kaprun Hauptstufe power plant

   - inflow time series of Wasserfallboden (Inf_WFB)
   - reservoir size of the reservoir Wasserfallboden
   - maximum turbine power of power plant Kaprun Hauptstufe
   - minimum and maximum reservoir levels as used for Traditional Reservoir
   - enable the water value functionality using a water value matrix based on the calculation of the simplified approach using the marginal price of a previous calculation
   - enable the pumping functionality with an infinite (100 000 MW) pumping power and an efficiency of 1
   - supportive thermal unit (Fake_WFB_turb) operating at zero cost with infinite (100 000 MW) nominal power used to imply the binding constraint for the cascade

5. Kaprun_PU - this node receives a very high load (100 000 MW) and a thermal cluster with a very high nominal power (100 000 MW) operating at zero cost.
6. Link [Kaprun_PU → country node] - receives a uni-directional energy flow (hourly time series) with the maximum pumping power of Kaprun Oberstufe and Limberg 2
7. Link [Hydro Open loop → country node] - receives a bi-directional energy flow (hourly time series) with the reduced turbine and pump max power of the Open Loop power plant cluster
8. Link [Kaprun_MB → country node] - receives a uni-directional energy flow of the maximum turbine power of Kaprun Oberstufe and Limberg 2 (turbine direction)
9. Link [Kaprun_WFB → country node] - receives a uni-directional energy flow of the maximum turbine power of Kaprun Hauptstufe (turbine direction)
10. Binding Constraint BC 1: PU_efficiency · [Kaprun_PU → country node] = [Kaprun_MB → Country node]

    This binding constraint is used in a similar way as described in chapter 4.1, where the total round-trip cycle efficiency of the pump storage power plant is implied on the link between the pump node and the country node (or the Open Loop node respectively) using a weekly cycle.

11. Binding Constraint BC 2: (Fake_WFB_turb) = $\epsilon_{\text{Kaprun}} \cdot$ [Kaprun_MB → Country node] - [Kaprun_PU → country node]

    This binding constraint is used to define the additional energy in the lower reservoir that is available through the turbines of Kaprun Oberstufe and Limberg 2, minus the pumped energy returned to the upper reservoir.

The main feature of a hydropower plant cascade is the dependency between the lower reservoir and the upper reservoir, which are connected via the turbine and pumps between the two reservoirs. To account for the inflow to the lower reservoir resulting from the Kaprun Oberstufe and Limberg 2 turbine units, a thermal unit with unlimited rated power is placed in the Kaprun_WFB node. This thermal unit is used to imply the second binding constraint where the *upper to lower discharge coefficient* $\epsilon_{\text{Kaprun}}$ is multiplied by the generation of the two turbine units Kaprun Oberstufe and Limberg 2 minus the pumped energy returned to the upper reservoir.

The approach described in this chapter is an initial starting point for a cascade representation in the context of Antares and can be expanded further.

To summarize the achievements of this representation:

- it is possible to specify per each power plant group individual efficiencies and characteristics
- reflect the dependency between the upper and lower reservoir

The additional effort for this representation, which leads to a higher level of detail in the presentation of hydropower, must be weighed against the benefit of the results and depends to a large extent on the available input data for the individual power plants. For a test case in academic work, this representation is interesting to investigate and could also be used in national analyses. A representation for the whole European area seems to be more challenging, as the input data for use by transmission system operators is difficult to obtain.

# 5 Investigations on additional storage and flexibility components

Accompanying the discussions on the high share of volatile renewable energy sources entering the European electricity market, the question of additional potential storage technologies arises at the same time. Austria is in the advantageous position of having installed hydropower storage units with a total turbine and pump power of 3.5 GW and a storage capacity of 1.7 TWh in 2023 [82]. In this chapter, the possibility of using various future storage components is developed. Based on the possibility of using the representation of short cycle storage described in chapter 4.3.1, an approach for the representation of market-participating batteries, as well as implicit demand side response (iDSR) by heat pumps (HPs) and electric vehicles (EVs) is developed. Based on the short cycle approach described in chapter 4.3.1 for the hydro Closed Loop representation, an implementation is developed, which allows EVs and HPs to act as demand flexible resources and respond to price signals.

Figure 5.1 shows the setup in Antares introducing all additional storage components (CL PSP, market-participating batteries, HP and EVs):

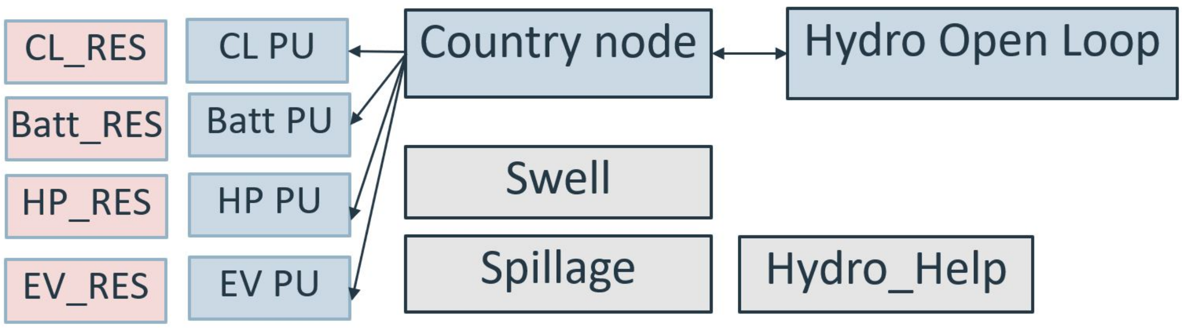


**Figure 5.1:** Antares modeling of additional flexible storage components

The modeling of the three components is explained below. Each of the virtual nodes contains information that can be duplicated and specified for any country using the same technology type within the same virtual node. This makes it possible to manage all four short cycle storage types with an acceptable number of eight virtual nodes for the entire perimeter.

## 5.1 Market participating batteries (front of meter)

This chapter describes batteries that participate in the day-ahead market and exhibit similar behavior to hydropower closed loop storage plants. They are described with storage size, charging and discharging capacity and efficiency and they can therefore follow exactly the same modeling as Closed Loop hydropower plants. The implementation in the Antares tool is described below, followed by the values used for Austria in the test cases of this work.

### 5.1.1 Implementation in the Antares tool

The representation of batteries participating in the day-ahead market follows the representation of CL PSPs very closely, with the difference being the cycle duration within which the storage facility is forced to reach its initial filling level at the end of a cycle. Figure 5.2 displays the battery storage level in % and the storage constraints forcing the storage level to reach 50 % by the end of a 24 hour cycle.

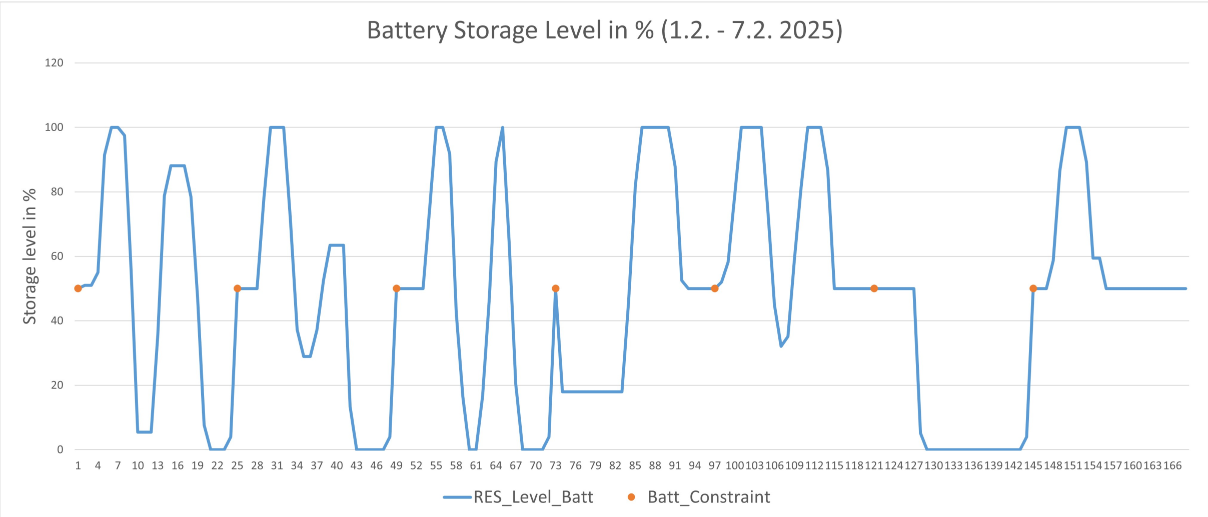


**Figure 5.2:** Battery storage level and its storage constraints of 24 hours

The following information is required to define the battery:

- $\mathbf{P}_{max}$- maximum charge and discharge power of the battery in MW
- $\mathbf{Cap}_{max}$ - maximum storage capacity of the battery in MWh
- **storage constraint** - defines the time window (number of hours) for the operation of the storage cycle - in the case of batteries 24 hours (see figure 5.2)

Figure 5.3 shows the modeling setup and the following list contains the required input data placed in the different nodes:

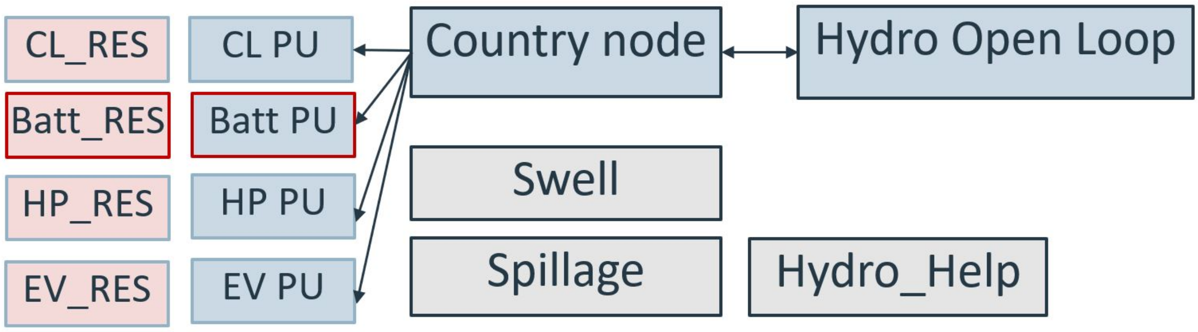


**Figure 5.3:** Virtual nodes used for the representation of batteries

1. country node - the discharge power of the battery is placed within the country node as a thermal unit operating with zero cost (AT_Turb_BATT) containing 35 time series with the maximum discharge power of the battery

2. Batt_RES (virtual) - this virtual node receives the information about the storage size of the battery in two thermal clusters:

    - BATT_RES_L1 - a thermal cluster within the virtual node BATT_RES containing one thermal unit with the maximum storage size of the battery. 35 hourly time series are used to force the storage at the end of the daily cycle to reach 50 % of its filling level - therefore every day at 00:00 the value is set to half of the storage size

    - BATT_RES_L2 - a thermal cluster within the virtual node BATT_RES containing one thermal unit with the maximum storage size of the battery. 35 hourly time series are used to force the storage at the end of the daily cycle to reach 50 % of its filling level - therefore every day at 00:00 the value is set to half of the storage size

    The two identically specified reservoirs L1 and L2 are required in order to imply the offset in the binding constraint used in BC 1.

3. BATT_PU node (virtual) - receives a time series with a high load (100 000 MW).

4. link [BATT_PU → Country Node] - the charging power of the battery is placed on the link between the virtual BATT_PU node and the country node as a time series with the maximum charging power in hourly resolution.

Two binding constraints are implied as follows:

- BC 1: BATT_RES_L2(t+1) = BATT_RES_L1(t) - BATT_eff · [BATT_PU → Coury

Node] - AT_Turb_BATT

- BC 2: BATT_RES_L1 = BATT_RES_L2

and follow exactly the same methodology as described for the CL PSP. The efficiency of the battery is set as a default value of 92 %. The second assumption is that battery operation is limited to daily cycles. This assumption is a starting point for further investigations.

### 5.1.2 Values retrieved for Austria

As described in chapter 3.2.3 estimates of future penetration rates for batteries vary depending on the source and approach chosen. Starting from a very rough estimate based on the German market development, newly published figures from the integrated Austrian grid infrastructure development plan [2] have led to a scenario estimate with penetration rates for front-of-meter batteries which reach up to a capacity of 1.3 GW and a storage size of 2.5 GWh:

**Table 5.1:** Demand capacities front of meter batteries used in ERAA 2022 process for the Target Year 2025 and 2030

| | 2025 | 2030 | 5 x 2030 target | 10 x 2030 target | 20 x 2030 target | ÖNIP targets |
|---|---|---|---|---|---|---|
| capacity (% of peak demand ERAA23) | 33 MW (0.2 %) | 68 MW (0.4 %) | 340 MW (2 %) | 680 MW (4 %) | 1360 MW (8 %) | 1284 MW (7.6 %) |
| storage size in MWh (% of annual demand ERAA23) | 50 MWh (0 %) | 102 MWh (0 %) | 510 MWh (0 %) | 1020 MWh (0 %) | 2040 MWh (0 %) | 2568 MWh (0 %) |
| total annual demand AT | 76 TWh | 90 TWh | | | | |
| peak demand in ERAA 2023 | 14.3 GW | 16.9 GW | | | | |

Looking at Table 5.1 and relating the battery size to the total Austrian demand, the values estimated by AIT are negligible, while the values estimated by ÖNIP result in a capacity of 8 % of the peak demand in 2030 with a relatively small storage size of 2.5 GWh. For comparison, the Austrian reservoir size for pump storage units in 2023 is 1.7 TWh.

## 5.2 Flexible demand components - heat pumps and electric vehicles

This section describes methods that help to describe the ability of flexible demand components such as heat pumps and electric vehicles to reduce or increase their demand in response to price signals. This flexibility component is achieved by combining the short cycle storage approach, as applied for CL PSPs, with additional storage constraints. In the representation for CL PSPs, a weekly cycle constraint is implied, while for battery storage a daily cycle constraint is applied. A different cycle duration is chosen for HPs and EVs: a time window of six hours is chosen, within which the storage is forced to reach its initial level again. Figure 5.4 illustrates the cycle duration of six hours for EVs:

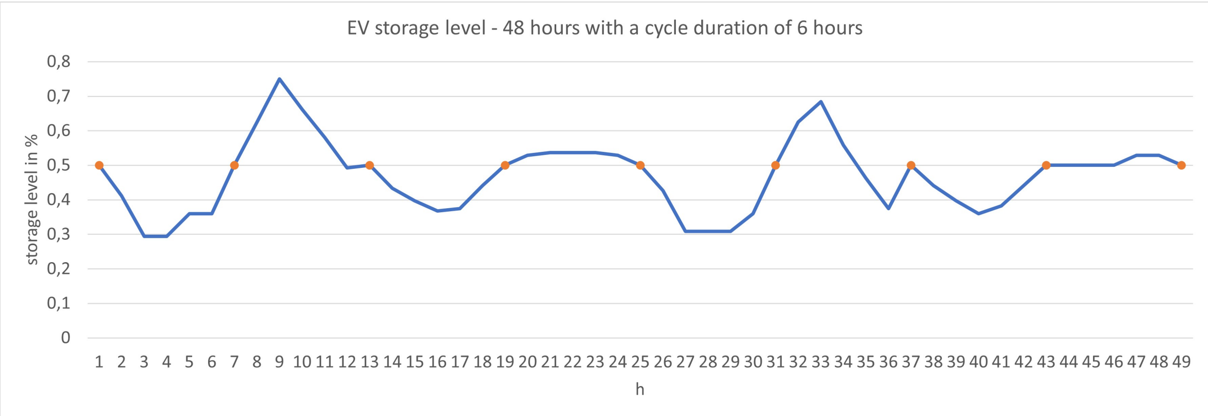


**Figure 5.4:** EV cycle duration of six hours - the storage constraints are displayed as orange dots

The methodology of the demand forecast for Austria uses an approach in which the base load is obtained from the ENTSO-E demand forecasting tool TRAPUNTA and the time series for heat pumps and electric vehicles come from a time series generator created by the Austrian Institute of Technology (see chapter 3.2). The individual 35 climate-dependent time series for HPs and EVs are analyzed and the necessary information to specify HP and EVs as flexible components is extracted as follows:

- **ratio of price-reactive share of EVs or HPs ($r_{HP}$ or $r_{EV}$)** - This ratio is determined by the TSOs that provide the input data to ENTSO-E. In the context of this work, it ranges between 5 % and 50 % as an academic exercise.
- **maximum installed (charge and discharge) power in MW** - is taken as the maximum over all hourly values of all 35 climate-dependent demand time series of EVs or HPs multiplied by the ratio defined as being price sensitive ($r_{HP}$ or $r_{EV}$).
- **hourly charging power in MW ($P_{char}$)** - hourly values of the HP or EV demand time series multiplied by the ratio being price sensitive ($r_{HP}$ or $r_{EV}$)

- **hourly discharging power ($\mathbf{P}_{disc}$)** - hourly values of the HP or EV demand time series multiplied by the ratio being price sensitive ($r_{HP}$ or $r_{EV}$)

- **starting level of the State of charge (SoC)** ($e^0$) - manually set to 50 % at the beginning of each cycle

- **storage constraint** - defines the time window (number of hours) for the operation of the storage cycle, meaning the number of hours until the storage level is forced to reach its starting level of 50 % (e.g. hour 0, 6, 12, 18 ... 8760; in case of a 6 hours interval - see figure 5.4)

- **maximum storage capacity ($Cap_{EV}$ or $Cap_{HP}$)** - is determined by the installed charging power multiplied by the number of hours of the time window specified for the cycle in which the HP or EV is operated (in the present approach six hours for EVs and HPs)

- **cycle efficiency** is 100 % in the theoretical case. In order to avoid simultaneous charging and discharging, the storage object achieves a cycle efficiency of 99 %.

The approach to extract the characteristics for the flexible share of EVs and HPs from its demand time series profile was developed by APG experts together with ENTSO-E TSOs active in the modeling task force of the ERAA process and published in [83].

### 5.2.1 Implementation in the Antares tool

Having the above-listed elements extracted from the hourly EV or HP demand time series, those can be implemented as follows. Figure 5.5 shows the transformation to Antares (the index HP used in the list below but can be applied for EV in the same manner):

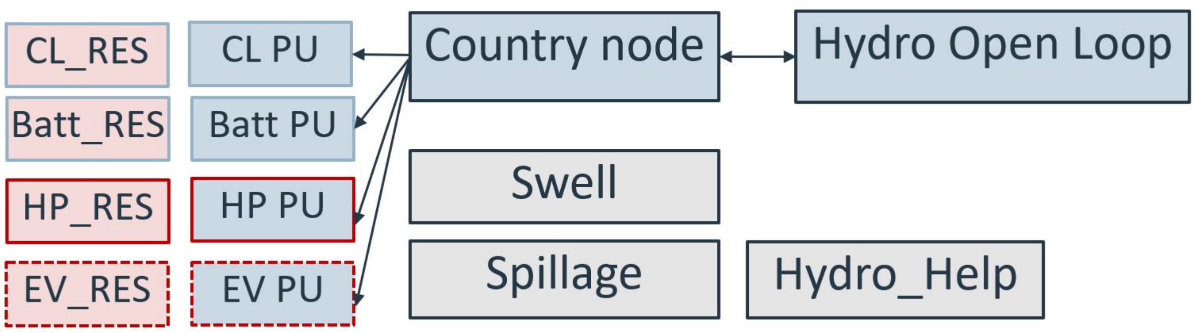


**Figure 5.5:** Virtual nodes for HP and EV representation

- country node - the discharging power of the HP is placed inside the country node as a thermal unit operating with zero cost (AT_Turb_HP) containing 35 time series with maximum discharging power of the HP

- HP_RES (virtual) - this virtual node receives the storage size information of the HP in two thermal clusters:
  - HP_RES_L1 - a thermal cluster inside the HP_RES virtual node containing one thermal unit with the maximum reservoir capacity $\mathrm{Cap_{EV}} or \mathrm{Cap_{HP}}$) operating at zero cost. 35 hourly time series with $\mathrm{Cap_{EV}}$ or $\mathrm{Cap_{HP}}$ are used to force the reservoir at the end of a cycle to reach 50 % of its filling level - therefore every day at 00:00, 06:00, 12:00, 18:00 the value is set to half of the reservoir size
  - HP_RES_L2 - a thermal cluster inside the HP_RES virtual node containing one thermal unit with the maximum reservoir capacity $\mathrm{Cap_{EV}} or \mathrm{Cap_{HP}}$) operating at zero cost. 35 hourly time series with $\mathrm{Cap_{EV}}$ or $\mathrm{Cap_{HP}}$ are used to force the reservoir at the end of a cycle to reach 50 % of its filling level - therefore every day at 00:00, 06:00, 12:00, 18:00 the value is set to half of the reservoir size

    The two identical reservoirs L1 and L2 are needed in order to imply the offset in the binding constraint which is used in BC 1.
- HP_PU node (virtual) - receives a time series with a high load (100 000 MW).
- link [HP_PU → AT] - the charging power of the HP is placed as a time series containing the maximum charging power in hourly resolution on the link between the virtual HP_PU node and the country node[1].

Two binding constraints are implied as follows:

- BC 1: HP_RES_L2(t+1) = HP_RES_L1(t) - HP_eff ·[HP_PU → Country Node] - AT_Turb_HP
- BC 2: HP_RES_L1 = HP_RES_L2

with an efficiency of 99 %.

[1] since Antares version 7 multiple time series can be placed on a link, therefore this approach can be applied for the 35 climate dependent HP and EV time series

### 5.2.2 Values retrieved for Austria

**Table 5.2:** EV & HP demand figures used as flexible iDSR in the test calculations for Target Year 2025

| | total | 5 % | 10 % | 20 % | 50 % |
|---|---|---|---|---|---|
| EV max peak | 451 MW | 23 MW | 45 MW | 90 MW | 226 MW |
| EV annual demand | 848 GWh | 42 GWh | 85 GWh | 170 GWh | 424 GWh |
| storage size 6 h | 5086 MWh | 135 MWh | 271 MWh | 542 MWh | 1354 MWh |
| HP max peak | 3986 MW | 199 MW | 399 MW | 797 MW | 1993 MW |
| HP annual demand | 3904 GWh | 195 GWh | 390 GWh | 781 GWh | 1952 GWh |
| storage size 6 h | 23 427 MWh | 1196 MWh | 2391 MWh | 4783 MWh | 11 957 MWh |

The results of the implementation of the various penetration rates for batteries and the percentage share of EVs and HPs are presented in chapter 6.5.

# 6 Modeling and Results

For the investigations executed in this thesis, three different models are used:

**Table 6.1:** Overview of Models used in this work

| Model | Description |
|---|---|
| Model 1 | An isolated model only representing the country node of Austria - no exchanges with neighboring countries exist |
| Model 2 | A geographically reduced model consisting of three bidding zones (Austria, Switzerland and Italy North) - connected via NTC cross border exchanges |
| Model 3 | A full European model consisting of all bidding zones as used in the ERAA process - this model is used to examine the hourly results of individual Monte Carlo years |

To compare adequacy indicators, a series of several hundred Monte Carlo simulations must be performed, resulting in calculation times of more than one day for the European perimeter if only annual values are exported and reported. In case of exporting hourly results, the calculation can take several days if all Monte Carlo Simulations are performed.

In order to quickly obtain results that can be compared with each other in terms of adequacy indicators, either the isolated model for Austria is used or a subset of three country nodes is selected that contains all information on generation fleet, demand and transmission capacities.

It must be noted that the geographical reduction (trilateral or AT isolated model) leads to an increased number of scarcity situations, as the majority of the European perimeter is excluded. This constant scarcity situation helps to investigate methodological developments and to assess whether an improved representation leads to better adequacy indicators for the bidding zone. It must be noted that the adequacy indicators used to compare modeling improvements from the geographically reduced model cannot directly be compared to the adequacy indicators determined through the official European process.

Even though the ERAA scenarios at the time of publication of this thesis follow a flow-based approach (at least for the CORE region[1]) and are subject to an economic viability assessment (EVA), the test models in this thesis are exclusively based on Net Transfer Capacities (NTCs) provided as fixed hourly time series for the interconnections between the bidding zones. The

[1] Definition CORE bidding zones: Austria, Belgium, Croatia, the Czech Republic, France, Germany, Hungary, Luxemburg, the Netherlands, Poland, Romania, Slovakia and Slovenia

introduction of flow-based domains for the CORE region leads to lower cross border exchanges for the Austrian bidding zone, which results from the way flow-based domains are calculated for the ERAA process (see chapter 4 of the ERAA 2023 Edition - Annex 2 Methodology [40]).

In the following, calculation results of the representations described in chapter 4, which focus on advanced methods for hydropower modeling, as well as calculation results of the representation described in chapter 5, which represent the behavior of additional storage components resulting from batteries, heat pumps and electric vehicles, are presented. The results of the individual calculations are shown in the chapters listed below.

| Chapter | Title |
|---|---|
| 6.1 | Results of an enhanced approach for Traditional Reservoir and Open Loop storage using water values |
| 6.2 | Results of an enhanced approach for Closed Loop representation |
| 6.3 | Results of an enhanced approach for swell representation |
| 6.4 | Results of an approach to introduce a cascade representation for the OL PSP Kaprun |
| 6.5 | Results of an approach for the representation of additional storage components |

## 6.1 Results of an enhanced approach for Traditional Reservoir and Open Loop storage using water values

In this chapter, the results of different approaches for modeling traditional reservoir and open loop pump storage are discussed. As explained in chapter 4.2, the hydro pre-optimization either follows the load-proportional heuristic of Antares or a cost value can be provided by a matrix for each level of a reservoir and each day of the year (either manually by the user or by means of a pre-calculation according to the Bellman principle of optimality), which is taken into account in the optimization.

Table 6.2 provides an overview of the scenarios discussed in this chapter, which are compared with historical values. The historical values are taken from the ENTSO-E transparency platform and the historical production of the year 2016 is scaled up to the installed turbine and pump values in 2025.

**Table 6.2:** Overview of scenarios used in the representation for traditional reservoir and open loop PSP representation

| Scenario | Description |
|---|---|
| A | In this scenario, the pre-optimization of hydropower follows the load-proportional heuristic of Antares, whereby the pumps for the hydro open loop are represented by two virtual nodes that are connected to the hydro open loop node. The representation of the hydropower follows the PEMMDB 3.0 representation, as explained in chapter 4.1. |
| B | In this scenario, the hydro pre-optimization of the load-proportional heuristics of Antares is used, whereby the Antares-internal pumping functionality has been available since Antares version 7 and is used in this scenario. |
| C | With the introduction of Antares version 7, the water value functionality is available. In this scenario, the water value functionality is used with the hydro pre-optimization according to Bellman's optimality principle, which is performed before the adequacy calculation. The description of the pre-optimization approach is elaborated in chapter 4.2.2. |
| D | In this scenario, the water value functionality is also used, but with a simplified water value matrix that the user defines according to the procedure described in chapter 4.2.1. |

First, a comparison is made of the annual energy generated and consumed for the model's turbine and pump output. For this comparison the whole European ERAA 2022 model is used to extract hourly results of one climate year (2016). The results of all four scenarios, which target the year 2025 and are based on the climate year 2016, are listed and compared with the historical production of 2016, rescaled to the installed power plant fleet in 2025. In 2016, the Austrian control area still included the Obere Ill / Lünersee power plant group. In 2017, this power plant group moved to the German control area and must therefore be excluded from the Austrian power plant fleet in the target year 2025. The reduction in the installed turbine and pump power of Obere Ill / Lünersee is therefore taken into account in the rescaling factor. As the classification into the categories of the traditional reservoir and open loop is not identical in the historical results of the transparency platform and the results of the adequacy modeling, the categories of traditional reservoir and open loop are aggregated for comparison. The turbine generation of the historical, rescaled measures is compared with the modeling results. The same applies to pump consumption, whereby the modeling results are compared with the historical, rescaled pump consumption.

Table 6.3 shows the annual results of the four scenarios for the target year 2025 and compares the annual energy production for turbine output and the pump consumption with historical measured values for 2016 (scaled up to 2025).

**Table 6.3:** Yearly energy produced and consumed by pump storage units - target year 2025 using Model 3 from Table 6.1

| TR & OL | Historic | A-3 | B-3 | C-3 | D-3 |
|---|---|---|---|---|---|
| Turbine | 8.65 TWh | 8.86 TWh | 8.47 TWh | 8.75 TWh | 8.65 TWh |
| (deviation) | | 2.40 % | −2.16 % | 1.05 % | −0.01 % |
| Pump | −2.32 TWh | −1.97 TWh | −1.54 TWh | −1.99 TWh | −2.00 TWh |
| (deviation) | | −14.91 % | −33.38 % | −14.08 % | −13.50 % |

Assuming a round-trip efficiency of the PSP units of 75 %, the turbined energy from OL reservoirs shows the highest deviation of the annual energy quantities of 2.40 % for the approach using the Antares heuristic with the pump representation by two virtual nodes (Scenario A). The lowest deviation for the turbined energy is shown when using the Antares water value functionality and providing the water value matrix by user-defined input via the marginal cost of a previous calculation (Scenario D). This approach also shows the lowest deviation for pump consumption (-13.50 %). The approach using the internal pump functionality of Antares in combination with the Antares heuristic shows the highest deviation (-33.38 %) for the pump consumption. This malfunctioning of the Antares internal pump functionality in combination with the Antares heuristic was also discussed with the RTE R&D and it is recommended to rather use the Antares water value functionality with the internal pump. Looking only at the annual results, it can be said that the initial representation as developed with the new PEMMDB 3.0 database for open loop PSPs was a sound approach at the time of the lack of an internal pumping function, accepting that no reservoir size tracking is possible with this approach. The introduction of water values also leads to acceptable results when using the internal pump functionality. From a practical point of view, deviations of up to 25 % can be considered acceptable. Deviations in turbine energy of only 1 % and pump deviations of up to 14 % can be considered acceptable if the water value functionality is used. Overall, there is less pumping in the Antares modeling than with historic measured values.

Figure 6.1 and 6.2 show the monthly turbine and pump volumes in TWh for the four different scenarios based on the ERAA 2022 model for target year 2025 extracted from climate year 2016 compared to historical production of the year 2016 (scaled up to 2025).

The green bars represent historical production, the red and orange bars show monthly results of the Antares heuristic, while the blue bars represent results following the Antares water values pre-optimization.

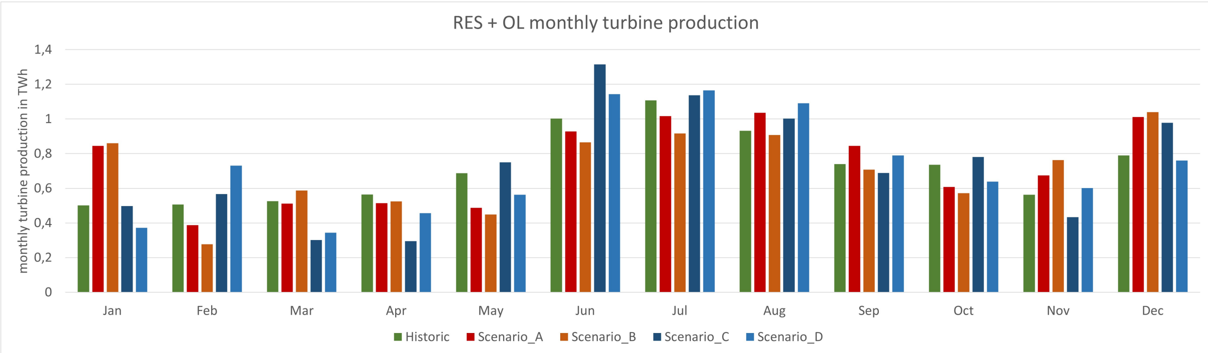


**Figure 6.1:** Monthly turbined energy in TWh from traditional reservoir and open loop turbines in the target year 2025 compared to historical production of 2016, scaled up to 2025

The turbine production of the Antares heuristic approach exceeds the historical production in November, December and January, with the model results in January being 86 % higher than the historical measured values. This could lead to the models assuming an over-availability of hydro energy in the most critical months for adequacy, when scarcity situations are most likely to occur due to low temperatures. The results of the water value approach exceed the historical production in the summer months, which could be less critical compared to the overestimation of hydropower production by the heuristic in the winter months. In the months of March and April, the Bellman water value approach (Scneario C) also shows a significantly lower hydropower production compared to historical measured values of up to -48 %.

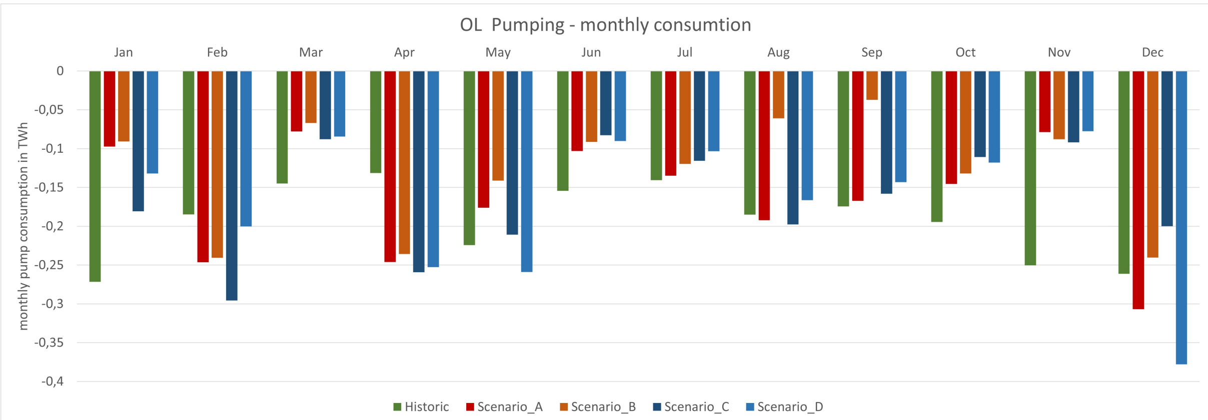


**Figure 6.2:** Monthly energy consumption for open loop pumps in TWh in the target year 2025 compared to historical pump consumption in 2016 scaled up to 2025

Figure 6.2 shows the monthly energy consumption by pump units, with the largest deviations in April, where all tool results exceed the historical pump consumption by up to 97 %. In January and November, the historical pump consumption is up to 70 % higher than the modeling results. The highest deviations are again measured for the approach using the Antares heuristic with internal pump functionality.

Next, the hourly results of the four scenarios are analyzed. A statistical comparison using the correlation index $r$ and the RMSE value is shown in Table 6.4, followed by a graphical comparison of the hourly dispatch for one week in July (Figure 6.3 and 6.4).

Definition of the correlation parameter $r$, where $-1 \leq r \leq 1$:

$$r = \frac{n(\sum xy)-(\sum x)(\sum y)}{\sqrt{[n\sum x^2-(\sum x)^2][n\sum y^2-(\sum y)^2]}}$$

where

| | |
|---|---|
| n | total amount of entries of the time series that are compared against each other |
| x | historical values |
| y | modeling output |

and the root mean square error (RMSE)

$$\text{RMSE} = \frac{\sqrt{(\sum (x-y)^2}}{n}$$

where

| | |
|---|---|
| n | total amount of entries of the time series that are compared against each other |
| x | historical values |
| y | modeling output |

The RMSE can also be normalized resulting in the nRMSE

$$\text{nRMSE} = \frac{\text{RMSE}}{y_{max}-y_{min}}$$

where

| | |
|---|---|
| RMSE | Root mean square error |
| $y_{max}$ | maximum value of the forecasted dataset |
| $y_{min}$ | minimum value of the forecasted dataset |

which can be used to facilitate the comparison between data sets or models with different scales.

The RMSE value is always positive, and a value of 0 would indicate a perfect data fit, while the correlation parameter of 1 would indicate a perfect correlation fit.

**Table 6.4:** Statistical measures for hourly results - target year 2025 using Model 3 from Table 6.1 and all Scenarios as described in Table 6.2

| OL and TR turbine | A-3 | B-3 | C-3 | D-3 |
|---|---|---|---|---|
| correlation | 0,33 | 0,34 | 0,37 | 0,38 |
| nRMSE | 1,48 | 1,39 | 1,41 | 1,35 |
| RMSE | 16,44 | 15,94 | 16,04 | 15,72 |

By definition, the correlation coefficient indicates a statistical relationship between two variables. The variables exist in two columns; in the case of this work, two time series are compared in hourly resolution. One time series contains the rescaled historical values for the production of open loop and traditional reservoir, the second time series contains the results of the four modeling attempts described above. A perfect correlation coefficient is defined by the value 1. In the case of the results of this comparison, the correlation coefficients determined are well below 1, which can be explained by the fact that the model produces time series with zero entries for up to 7400 hours in a year, while the historical time series contains PSP production from reservoirs and open loops, as well as parts of the swell power, which has a proportional constant daily cycle.

The correlation parameter shows very low results, which are very close for all four modeling attempts. The same observation applies to the statistical parameters RMSE and nRMSE. Looking at the hourly results, as shown in Figure 6.4, it is clear that Antares uses the traditional reservoir and the open loop in fewer hours in the year and up to the installed maximum turbine power. The hourly time series of the model outputs for the turbine from the traditional reservoir and the open loop show zero values for up to 7400 hours a year, making the comparison of the correlation parameters RMSE or nRMSE values for the determination of the modeling results unsuitable.

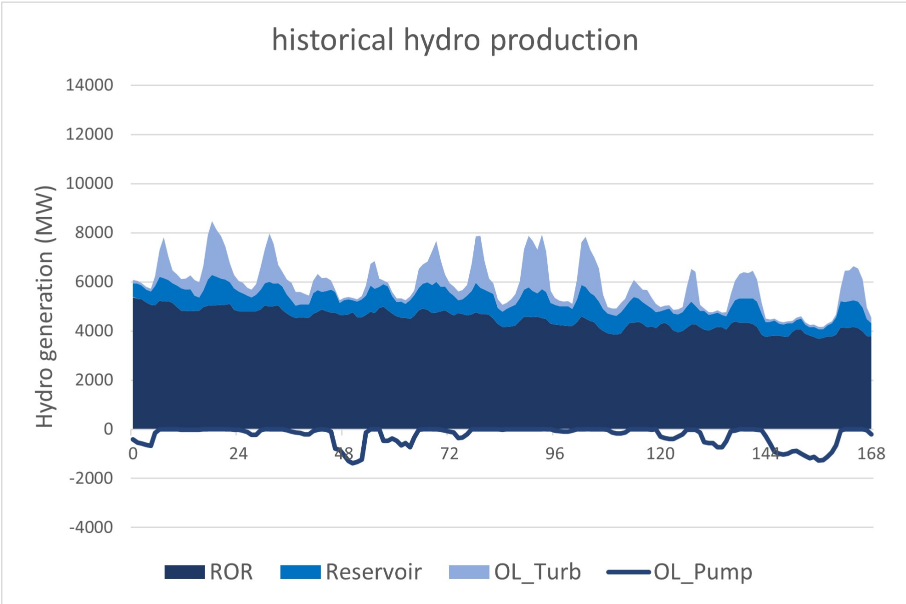


**Figure 6.3:** Historic hydro production July 5 to 11, 2016 scaled up to 2025

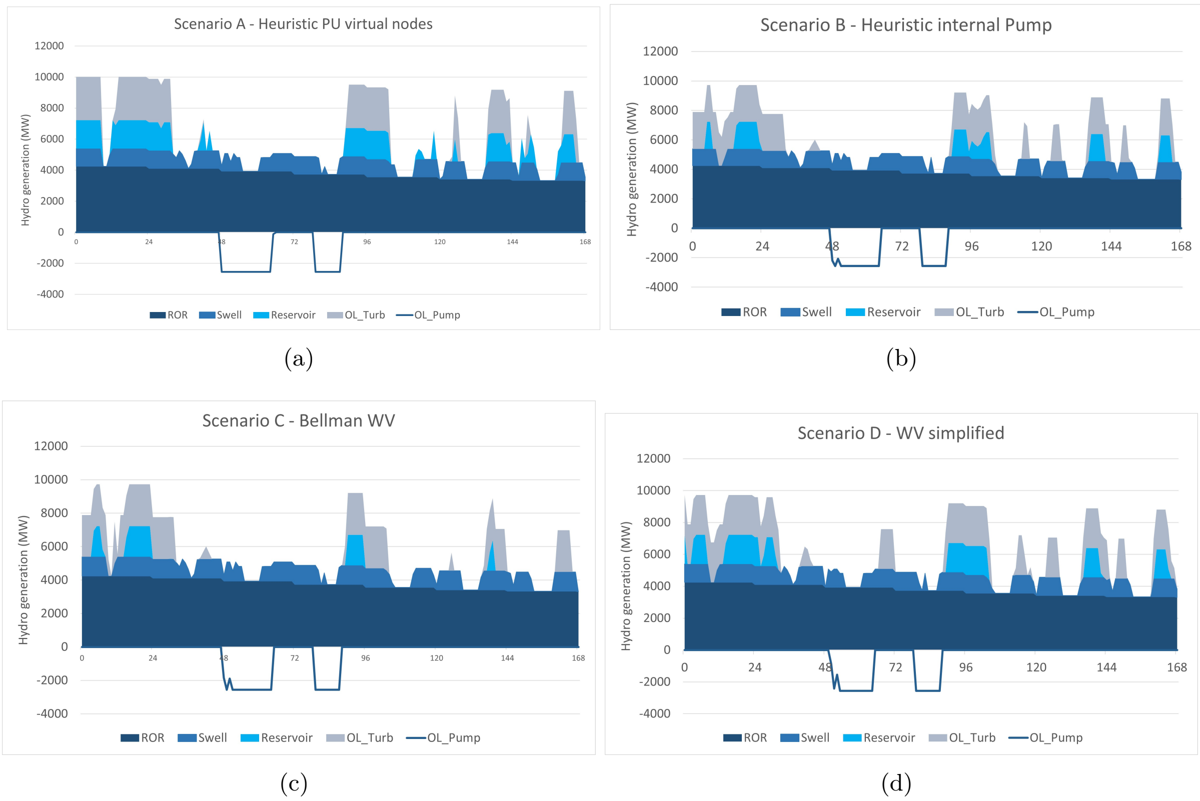


**Figure 6.4:** Hourly dispatch of one week in July (5 - 11 July) for the target year 2025 extracted from climate year 2016

Looking at the hourly results of the four different approaches (Figure 6.4) and comparing them with the historical production (Figure 6.3), the following can be noted:

- historical measured values show a more constant production during the day for all storage types
- historical values do not operate at maximum turbine or pump power
- historical values show a peak production of open loop turbines at least once a day
- historical pumping applies several times per week
- tool results show less often peak production, but if used with maximum turbine power
- tool results use the reservoir and open loop turbine for fewer hours per week
- tool results often operate at the maximum installed turbine and pump output

The historical pumping processes also take place more regularly during the week, with at least a few hours per night, while in the models there are only two pumping processes with maximum pumping power during the week under investigation. This behavior is model-specific and therefore no direct time-series comparison with historically measured values can be made. Comparing the maximum values during peak production, the historical values reach up to 8 GW, while the different results of the tool reach peak values up to 10 GW. This can be considered too optimistic, especially for the resource adequacy analysis, as the maximum peak production of all hydropower plants was not monitored in historic values. On the other hand, during real scarcity events, if climatic conditions allow, hydropower peaks can be expected, even if they have never been observed in the past.

One hypothesis regarding the constant production of various reservoirs in the historical measured time series is the fact that a different aggregation of hydrotypes could be applied and thus a certain proportion of the swell production is included in the reservoir curves of the historical values.

Finally, a comparison is made between the modeling attempts using the Antares Heuristic with internal pumping functionality and the Antares water value functionality with water values calculated according to the Bellman principle for the reservoir trajectories. The reservoir trajectories are shown for each climate year. Figure 6.5 shows the distribution of the 35 reservoir trajectories for each climate year using the Antares heuristic. The individual rule curves are very close to each other for most of the year and exceed the maximum reservoir level rule curve between calendar week 35 and 45. A greater spread of the 35 reservoir trajectories is achieved when the Antares water value functionality is used, as shown in Figure 6.6. When using water values, the maximum rule curve is also taken into account as a boundary condition during calendar weeks 35 and 45, which is not the case when using the Antares heuristic.

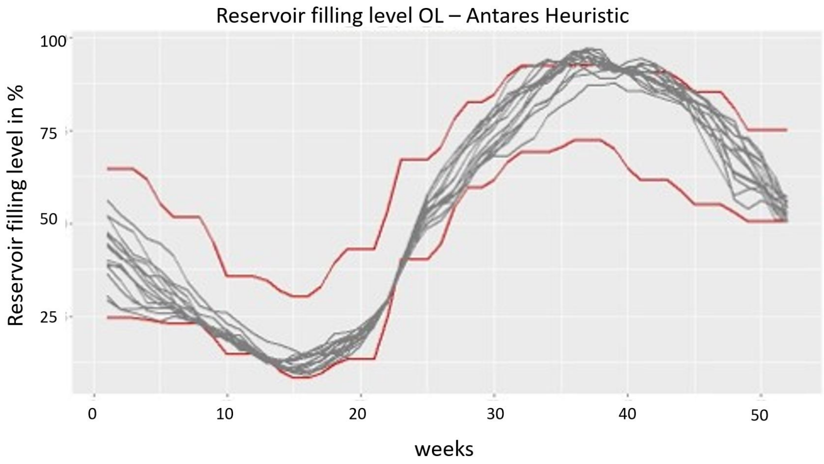


**Figure 6.5:** Reservoir level using Antares Heuristic

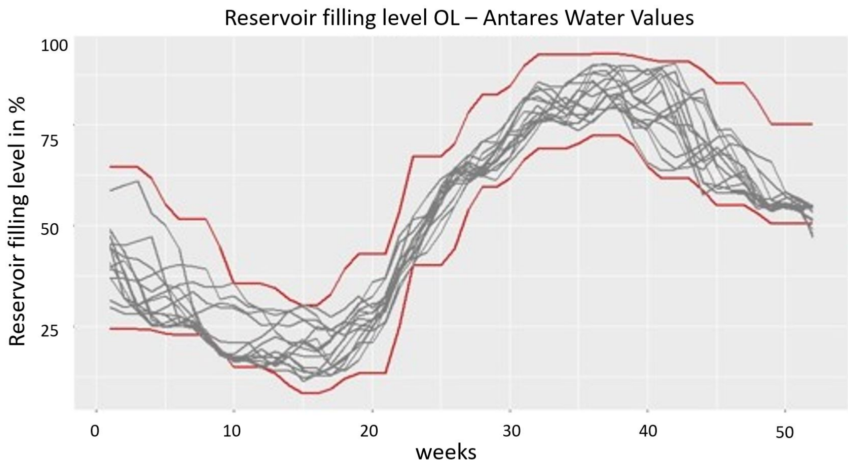


**Figure 6.6:** Reservoir level using Antares Water Values

The following list summarizes the findings of the approaches discussed in this chapter:

- The total pumping activity in the models is lower than the historical measured values with up to 15 % for Scenarios A, C and D. Scenario B shows the highest deviation in pump utilization with a difference of 33 %, which is due to a possible malfunction of Antares with the heuristics and the internal pump functionality. The results of scenario B with internal pumping and Antares heuristic are discussed with RTE R&D.

- The comparison of hourly dispatch results leads to many hours per year in which the traditional reservoir and open loop are not used (zero entries). Therefore, a statistical comparison with historical values using the correlation or nRMSE values does not provide sufficient judgment, it can only be used as an indicator in combination with other findings.

- Comparing the deviation of the monthly and annual energy quantities, it can be seen that using the Antares water value functionality either with the Bellman calculated water values or with the simplified approach using the marginal price of a previous calculation leads to acceptable results. The simplified approach to calculate the water values is also less time consuming and can therefore be proposed as preferable.

**Proposed approach:** Scenario D using a simplified water value matrix, due to the following findings of the analysis:

- simplified water value matrix based on marginal costs of a previous calculation is fast to determine
- lowest deviation of turbine and pump energy compared to historical values
- highest correlation and lowest statistical error (RMSE)

## 6.2 Results of an improved approach for the representation of Closed Loop PSPs

If the pumping functionality in Antares is applied using the approach of two virtual nodes connected to a country node for closed loop PSPs (as described in chapter 4.1 - pump storage units without natural inflows), a significant disadvantage of the methodology becomes clear: In this attempt to model the pumping behavior, it is not possible to comply with the physical limits of the reservoir (minimum and maximum reservoir levels), as the reservoir size cannot be defined in the Antares model. This limitation is evident when small storage reservoirs are operated with comparatively large connected turbine and pump units. In this chapter, the original representation with two virtual nodes to represent the pumping behavior (representation used in the calculation of MAF 2017 – 2019) in Scenario A is compared with two developed attempts to model closed loop PSPs (Scenario B and C):

**Table 6.5:** Overview of scenarios used in the representation for closed loop PSP representation based on the trilateral test model (Model 2 from Table 6.1)

| Scenario | Description |
|---|---|
| A | Original configuration as described in chapter 4.1: one virtual node introduced for the turbine and one virtual node for pumping, connected to the country node with a round-trip efficiency of 75 %, implied by a binding constraint |
| B | Application of a simplified water value approach as described in chapter 4.3.2: all reservoir levels on all days of the year are given as 0 € using the internal pumping functionality introduced with Antares version 7 |
| C | Application of the new representation for short cycle storage, as described in chapter 4.3.1, with the requirement that the reservoir must reach a filling level of 50 % at the end of a weekly cycle. |

To evaluate the three scenarios, the trilateral test model (Model 2 from Table 6.1) based on ERAA 2021 input data for the target year 2025 is used. The installed turbine and pump power for this category is 300 MW with a reservoir size of 1800 MWh. This is significantly less than the installed turbines of the traditional reservoir and open loop category in Austria.

Table 6.6 shows the yearly energy quantities of the turbine and pump usage of CL PSPs according to the three scenarios. In Scenario B, turbine energy is 17.6 % higher than in Scenario A, while in Scenario C, turbine production is 55 % higher than in Scenario A. The same range can be observed for pump consumption.

**Table 6.6:** Yearly energy turbined and pumped by CL PSPs following the three different representations

| | A-2 | B-2 | C-2 |
|---|---|---|---|
| turbine | 45.33 GWh | 53.30 GWh | 70.09 GWh |
| deviation | | 17.6 % | 54.6 % |
| pump | -60.44 GWh | -69.88 GWh | -93.45 GWh |
| deviation | | 15.6 % | 54.6 % |

A comparison of the monthly energy quantities for turbine and pump use is shown in Figure 6.7. The comparison of the monthly energy shows that only in January the two new approaches have lower generation, while in all the other months the energy volumes in Scenario B and C turbine and pump more than in Scenario A.

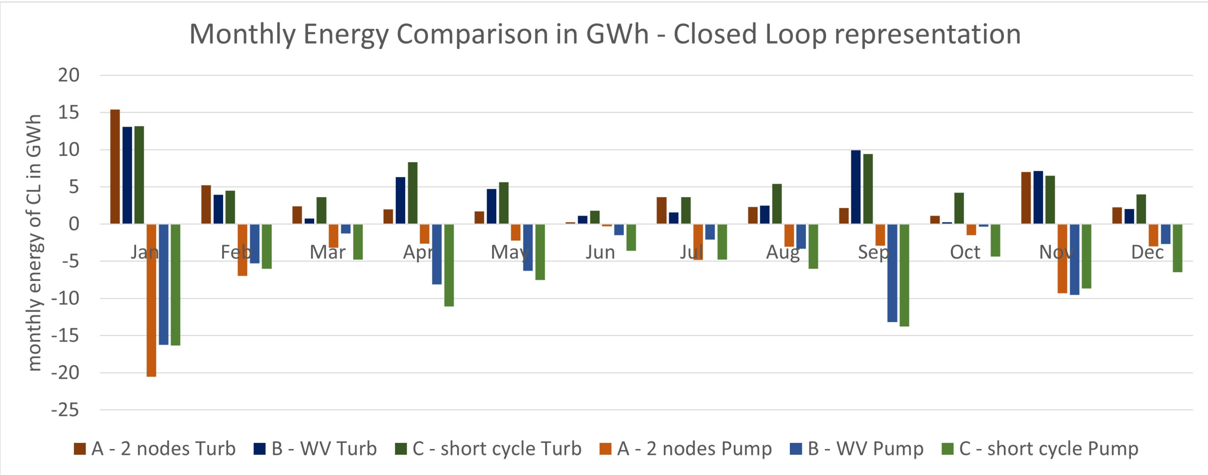


**Figure 6.7:** Monthly energy for closed loop turbine and pump utilization for target year 2025 in the trilateral model based on climate year 2016

Figure 6.8 shows the reservoir level of the CL representation using two virtual nodes to imply the pumping behavior for CL units, where no reservoir size can be passed to the Antares model. What is visible in this case is the fact that the upper and lower reservoir boundary is violated in both directions. This is an unacceptable behavior and can be avoided by introducing modeling attempts as described in Scenario B and C.

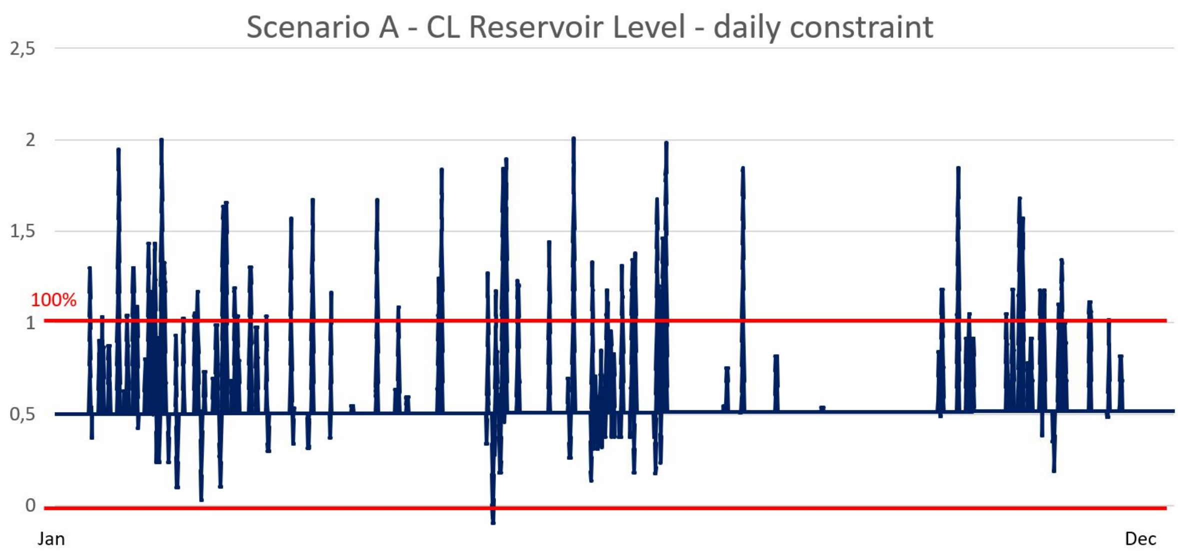


**Figure 6.8:** Reservoir level for Closed Loop representation following Scenario A - Target year 2025, CY 2016

Figure 6.9 shows the reservoir levels for the two developed scenarios B and C. For scenario B, which uses the water value functionality, and for scenario C, which uses the short cycle storage approach, the reservoir levels can be kept within their physical limits.

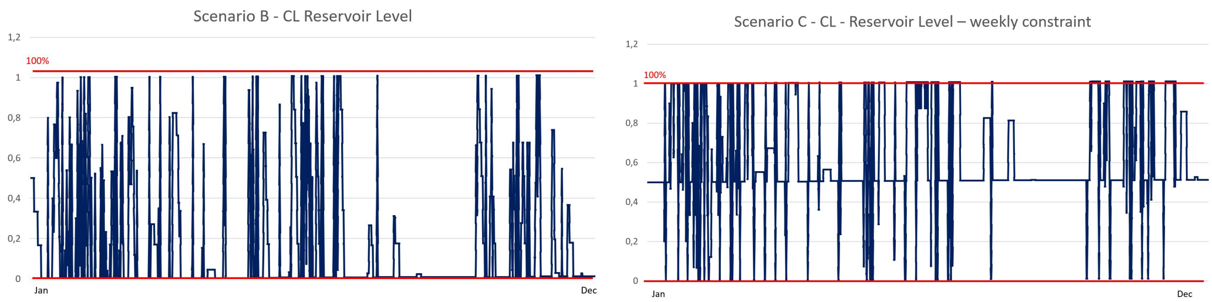


(a) (b)

**Figure 6.9:** Reservoir levels for Closed Loop representation following Scenario B and C - Target year 2025, CY 2016

Table 6.7 shows the number of hours in which CL pump storage units have turbine or pump operation during a year. The highest number can be observed for Scenario C with a total of 267 hours for turbine operation and 348 hours of pump operation. Overall, these quantities appear to be far too low for a pumped storage plant.

**Table 6.7:** Hours of Closed Loop PSP units in operation in the three scenarios in the trilateral model (Model 2 from 6.1)

| | A-2 | B-2 | C-2 |
|---|---|---|---|
| turbine | 199 h | 221 h | 267 h |
| pump | 246 h | 266 h | 348 h |

The implementation of the above approaches in the pan-European model already shows a higher utilization of the CL PSP pump and turbines compared to the trilateral test model. Table 6.8 shows the operating hours of CL turbine and pump in a pan-European model, with operating hours of up to 1700 hours in case of using the short cycle approach. For Scenario B where the water value functionality is usage of CL PSP remains with 505 hours for turbine and 652 hours for pump operation comparably low.

**Table 6.8:** Hours of Closed Loop PSP units in operation in the pan-European model (Model 3 from Table 6.1)

| | A-3 | B-3 | C-3 |
|---|---|---|---|
| turbine | | 505 h | 1262 h |
| pump | | 652 h | 1653 h |

Implementing the two developed scenarios in the pan-European model and performing an adequacy calculation for 350 Monte Carlo simulations leads to a LOLE reduction of up to 55 % for both scenarios and EENS is reduced to 0.5 GWh for the average results. If only the climate year 1985 is assessed, a reduction of 70 % can be achieved for LOLE. In the case of the EENS indicator, the implementation of the two approaches already shows an EENS decrease from 71.2 GWh to 0.483 GWh for Scenario B and 0.517 GWh for Scenario C for the average over all 350 Monte Carlo years. The results for the climate year 1985 show a decrease from 21.67 GWh to 6.517 GWh in Scenario B and 6.75 GWh in Scenario C. Table 6.9 shows the results for both scenarios for the average over all 350 Monte Carlo simulations as well as the individual adequacy results for the climate year 1985.

**Table 6.9:** Adequacy results after implementing CL PSP in the pan-European model (Model 3 from Table 6.1)

| | Base | B-3 | C-3 |
|---|---|---|---|
| avg 350 | | | |
| LOLE | 1.17 h | 0.43 h | 0.52 h |
| EENS | 71.2 GWh | 0.483 GWh | 0.517 GWh |
| CL 1985 | | | |
| LOLE | 19 h | 6 h | 6 h |
| EENS | 21.67 GWh | 6.517 GWh | 6.75 GWh |

In scenarios B and C, the minimum and maximum reservoir levels of the closed loop reservoir can be tracked, which is an improvement compared to the approach used in the ENTSO-E processes following the introduction of the new PEMMDB 3.0 database format. The number of operating hours for CL pumped storage in the developed trilateral test models remains very low. Scenario B remains at 221 hours and scenario C at 267 hours for turbine operation in the trilateral model. Applying the two approaches developed to the pan-European model already leads to an increased use of CL pumps of 1653 hours and turbines of 1262 hours in the case of of the short cycle approach (Scenario C) and a use of CL pumps of 652 hours and turbines of 505 hours in the case of the water value approach (Scenario B). The implementation of the two scenarios developed in a pan-European model shows a reduction of the adequacy indicators by more than half for the LOLE indicator in the case of the averaged results of 350 Monte Carlo simulations for both scenario B using the water value approach and scenario C using the short cycle approach.

**Proposed approach:** Scenario C, due to the following findings of the analysis:

- reservoir limits can be respected
- operating hours in the pan-European model (Model 3 from Table 6.1) are of similar size like for open loop PSP
- only two additional nodes in the whole perimeter are needed to implement scenario C for

all country nodes having closed loop PSP installed

## 6.3 Results of an enhanced approach for swell representation

One result of the master thesis, in which the database format PEMMDB 2.0 was compared with the PEMMDB 3.0 and the effects on the representation of hydropower [22], was the assumption that a certain flexibility is lost in the PEMMDB 3.0 representation due to the merging of the ROR and swell inflow time series and their immediate dispatch. In this chapter, the results of three different ways of separating the swell inflows and modeling swell production with a daily storage pattern are presented. The geographically reduced trilateral model with the three bidding zones Austria, Switzerland and Italy North (Model 2 from Table 6.1) is used for these investigations. This reduced test model is extracted from the ERAA 2021 model and evaluates the target year 2025. 1015 Monte Carlo simulations are carried out to assess the adequacy indicators.

**Table 6.10:** Overview of scenarios used in the representation for swell representation based on the trilateral test model (Model 2 from Table 6.1)

| Scenario | Description |
|---|---|
| A | The original representation used directly with the introduction of the PEMMDB 3.0 database: ROR and swell inflows are merged in a time series and dispatched immediately. The description of PEMMDB 3.0 hydropower representation is explained in chapter 4.1. |
| B | A first attempt to separate the swell production by introducing a separate swell node that is connected to the country node. The time series of ROR inflows are placed in the country node and dispatched immediately, and the time series of swell inflows are placed as energy to be produced in a supporting hydro node. The energy flow on the link between the country node and the swell node is constrained as explained in chapter 4.4.1. |
| C | With the introduction of Antares version 7, the water value functionality is available. This functionality is used to represent the daily storage pattern of swell reservoirs: a swell node is connected to the country node. The ROR inflow time series are placed in the country node and dispatched immediately, and the swell inflows are placed in the swell node as inflow to a hydro reservoir. This hydro reservoir is specified with its size and a water value matrix that separates the filling level below 50 % with high water values and filling levels above 50 % with low water values. A detailed explanation can be found in chapter 4.4.3. |
| D | The third representation used for the swell generation representation applies the short cycle storage approach using a weekly cycle (as with the CL PSPs). This approach is described in chapter 4.4.2. |

The geographical reduced trilateral model can be run for 1015 Monte Carlo years in a reasonable (< 4 hours) computing time. The adequacy indicators of the different scenarios from the simulation are shown in the tables 6.11 and 6.12:

**Table 6.11:** LOLE Indicator for the different Swell representation

| Country | A-2 | B-2 | C-2 | D-2 |
|---|---|---|---|---|
| AT | 18.2 h | 23.6 h | 14.6 h | 11.4 h |
| | | 30 % | −20 % | −37 % |
| CH | 15.4 h | 17.2 h | 16.1 h | 15.6 h |
| | | 15 % | 6 % | 1 % |
| ITN | 91.6 h | 102.2 h | 91.3 h | 91.7 h |
| | | 14 % | 0 % | 0 % |
| Total | 125.2 h | 143.0 h | 122.0 h | 118.7 h |
| | | 15 % | −1 % | −1 % |

**Table 6.12:** EENS Indicator for the different Swell representation

| Country | A-2 | B-2 | C-2 | D-2 |
|---|---|---|---|---|
| AT | 18.3 GWh | 24.6 GWh | 14.6 GWh | 15.8 GWh |
| | | 34 % | −20 % | −14 % |
| CH | 41.8 GWh | 48.2 GWh | 44.1 GWh | 42.4 GWh |
| | | 15 % | 6 % | 1 % |
| ITN | 193.7 GWh | 220.0 GWh | 193.2 GWh | 193.9 GWh |
| | | 14 % | 0 % | 0 % |
| Total | 253.8 GWh | 143.0 GWh | 521.9 GWh | 252.1 GWh |
| | | 15 % | −1 % | −1 % |

Table 6.11 shows the LOLE adequacy indicator and Table 6.12 shows the EENS adequacy indicator for the three bidding zones evaluated. It can be seen that scenario B leads to a worse situation with regard to the adequacy indicators for Austria. The situation worsens with an EENS deterioration of 34 % for Austria, 15 % for Switzerland and 14 % for Italy North. Scenarios C and D improve the situation in terms of adequacy indicators for Austria (up to 37 % less LOLE in approach D), while scenario B and C slightly worsen the adequacy situation for Switzerland and remain constant in terms of EENS and LOLE for Italy North for scenario C and D.

The adequacy indicators for the entire perimeter show a minimal improvement in terms of LOLE in scenario C and D, while scenario B leads to a significant deterioration in the adequacy indicators: 50 % LOLE and EENS.

If only the LOLE adequacy indicator is considered, scenario D with the short cycle storage representation can be recommended for Austria, since it leads to the lowest LOLE indicator which is the indicator for result comparison in the European framework of resource adequacy (also known as Reliability Standard). This approach forces the reservoir to reach 50 % of its filling level at the end of a weekly cycle. The approach with a simplified water value matrix (scenario C) can also be recommended if EENS and LOLE are considered together. Scenario B leads to a deterioration of the adequacy indicators for all nodes and can therefore be omitted.

An additional way to compare the results of the three scenarios is to examine the hourly dispatch of run of river and swell production. For this purpose, a comparison is made with the historical values of the year 2021 of two rivers that contain most of the swell units installed in Austria, namely Drau and Enns. Figure 6.10 shows the hourly dispatch for one week in winter (January 11 to 17, 2021) and Figure 6.12 one week in summer (July 5 to 11, 2021) of the measured ROR and swell production. The measured values (source: APG) of the historical year 2021 for ROR and swell are scaled up to the installed generation capacity in 2025, which is used in the modeling approaches. The results of the three modeling approaches originate from the climate year 1985, a very cold and dry year that led to stress conditions in Western Europe.

Looking at the behavior of the swell production of the two rivers Drau and Enns (light blue in Figure 6.10), the swell production shows a certain indicative daily behavior with a morning and an evening peak, but without reaching a production of zero during the whole week (a constant minimum production of swell units is present during the whole week).

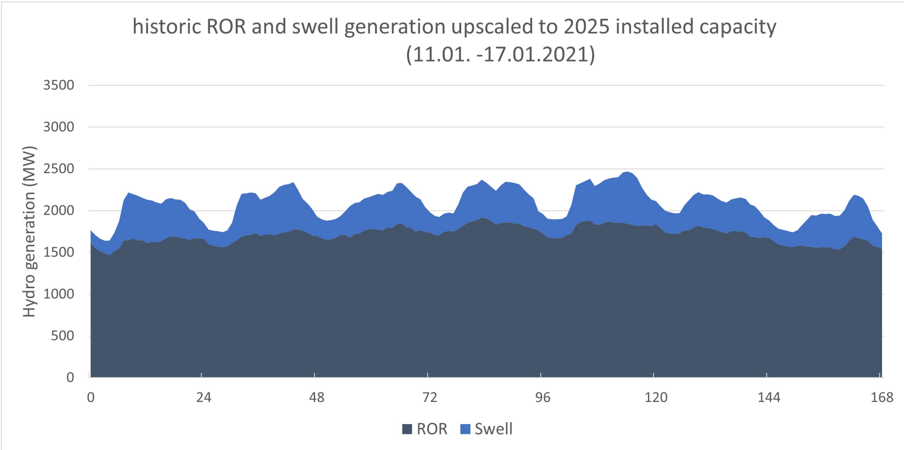


**Figure 6.10:** Historic swell production January 11 to 17, 2021 scaled up to 2025

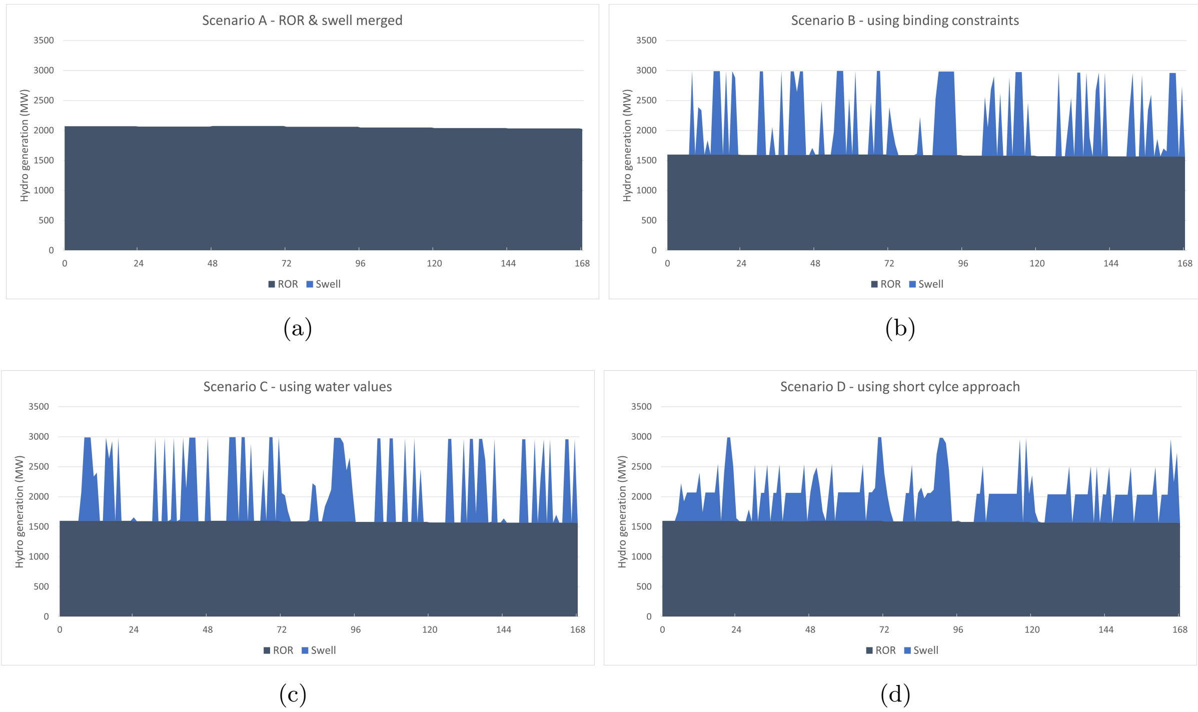


**Figure 6.11:** Hourly dispatch of one week in January (11 - 17 Jan) for the target year 2025 extracted from climate year 1985

Comparing the hourly dispatch results of the four models for the same winter week (see Figure 6.11), the results of scenarios B, C and D show a high fluctuating behavior in swell production. The maximum production is reached several times during the day in scenarios B and C, whereby the swell production also drops to zero for a significant amount of hours of the day. Scenario D shows slightly less fluctuating behavior between 0 and 50 % production from swell and also reaches maximum production less often over the week.

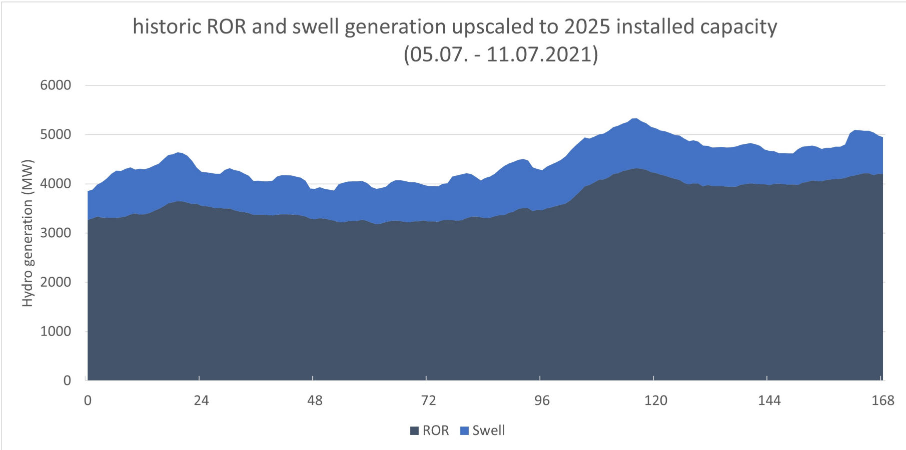


**Figure 6.12:** Historic swell production July 05 to 11, 2021 scaled up to 2025

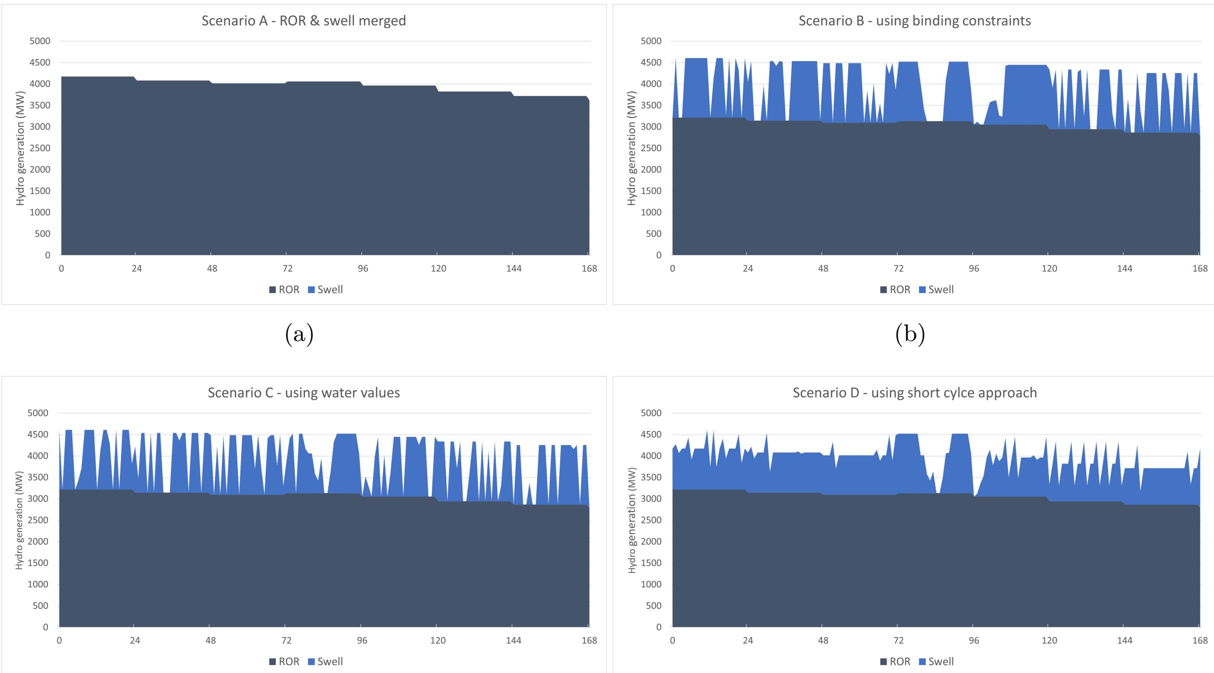


(a)

(b)

(c)

(d)

**Figure 6.13:** Hourly dispatch of one week in July (5 - 11 July) for the target year 2025 extracted from climate year 1985

Compared to the historical swell production of the winter week, the summer week (see Figure 6.12) shows a generally higher band production of run of river, and the swell production also appears to be flatter than in the historical winter week. The peak hours of swell production in the morning and evening hours are lower, but still present.

When comparing the historical swell production in the summer week with the result of the four modeling attempts (as shown in Figure 6.13), it becomes clear that scenario B and C also show fluctuations between zero and maximum swell production in summer. Scenario D provides a behavior with some band production and a daily reservoir utilization in summer.

Looking at the results of the comparison of the adequacy indicators, scenario C or D can be recommended as the best option for the swell representation. Combining this finding with the result of the hourly dispatch, the approach that uses the short cycle storage approach for the swell representation (Scenario D) can be suggested as the preferred representation.

Table 6.13 shows the correlation parameters and the values of the normalized root mean square error (nRMSE) for the three approaches developed for the swell representation.

**Table 6.13:** Statistical interpretation of results

| Statistical Indicator | B-2 | C-2 | D-2 |
|---|---|---|---|
| correlation | 0,344 | 0,339 | 0,424 |
| nRMSE | 0,866 | 0,841 | 0,583 |

The results of the statistical analysis of the time series for the swell generation in conjunction with the comparison of the hourly results with historical measured values leads to the conclusion that scenario D is the most suitable representation for the swell generation. However, the correlation coefficient is still far too low and the nRMSE relatively high, so that these parameters cannot be considered a useful tool for hourly time series comparison.

**Proposed approach:** Scenario D using the approach for short cycle representation, due to the following findings of the analysis:

- decrease of the LOLE indicator of 37 %
- graphical interpretation with the highest share of constant production and few daily peaks
- graphical interpretation with the lowest fluctuating behavior between zero and maximum peak swell power
- highest correlation and lowest nRMSE statistical value.

## 6.4 Results of an approach to introduce a cascade representation for OL PSP Kaprun

Combining all hydropower plants per plant type into one common cluster per country node is the methodological approach used in the European process. The question of whether a separation of larger hydropower plant groups operated in a cascade affects the results of the adequacy calculation is addressed in this chapter. Cascade operation means that turbined water from an upper reservoir increases the inflow to the lower reservoir and can therefore be used by the turbine units connected to the lower reservoir. Austrian pumped storage power plants in the Austrian Alps in the western part of Austria often operate in cascade mode. This chapter therefore attempts to separate the Kaprun power plant group from the category of Austrian open loop pump storage power plants. The representation of the Kaprun pump storage power plant, as described in chapter 4.5, and its implementation in Antares is first tested in an isolated model, in which only the country node of Austria with all its characteristics is used.

The input data of the ERAA 2021 model is used, whereby only Austria is extracted in an isolated model and the adequacy simulation run for 1015 Monte Carlo years.

To start with the results of climate year 2016 are extracted from the isolated model comparing the annual energy quantities for the different categories traditional reservoir, open loop as well as the individual turbine and pump units of the Kaprun power plant group. Table 6.14 shows the annual energy volumes of the various hydropower categories.

**Table 6.14:** Individual annual results of the isolated test model (Model 1 from Table 6.1) for the separation of the Kaprun power plant group for the target year 2025- extracted values for climate year 2016

| AT isolated | Traditional Reservoir | Open Loop Turb | Open Loop Pump | Kaprun Turb | Kaprun Pump | Kaprun Unterstufe |
|---|---|---|---|---|---|---|
| Base | 2.18 TWh | 6.70 TWh | −2.27 TWh | | | |
| Kaprun detailed | 1.72 TWh | 5.59 TWh | −1.71 TWh | 0.66 TWh | −0.81 TWh | 1.24 TWh |
| Delta | −21.2 % | −16.5 % | −24.8 % | | | |

Table 6.14 shows the annual energy volumes of the various hydropower pump storage categories once for the isolated case in which all units of a type are aggregated in a cluster, and compares these values with the results obtained when the Kaprun power plant cascade is separated from the aggregated Austrian cluster. It can be seen that the total generation from the traditional reservoir and open loop PSP category decreases by 21.2 % for the traditional reservoir and 16.5 % for the open loop PSP category. The turbine of the OL PSP part of the Kaprun power plant group has an annual generation of 0.66 TWh and 0.81 TWh for pump consumption in the model. The turbines connected to the lower reservoir of the cascade generate a total of 1.24 TWh.

**Table 6.15:** Annual results of the isolated test model (Model 1 from Table 6.1 for the separation of the Kaprun power plant group for the target year 2025 - extracted values for climate year 2016 - total turbine and pump generation

| annual | Sum Turbine | Sum Pump |
|---|---|---|
| AT isolated | 8.88 TWh | −2.27 TWh |
| AT isolated with separation of cascade Kaprun | 9.21 TWh | −2.51 TWh |
| Delta | 3.7 % | 10.7 % |

The total sum of reservoir and OL turbine generation is 9.21 TWh which is 3.7 % higher than in the isolated model with the aggregated units, and the pump consumption is 2.51 TWh, which is 10.7 % higher than in the isolated model with aggregated units.

Figure 6.14 shows the hourly dispatch of the hydropower plant types traditional reservoir, open loop pump storage and Kaprun power plant group for one week in July (5 to 11 July) of the target year 2025 extracted from the climate year 2016. It can be seen that due to the fact that an isolated model is run, the pumping behavior of the open loop category as well as the pumping of the Kaprun power plant appears to be higher than the extracts for the OL pumping category when the full European model is examined.

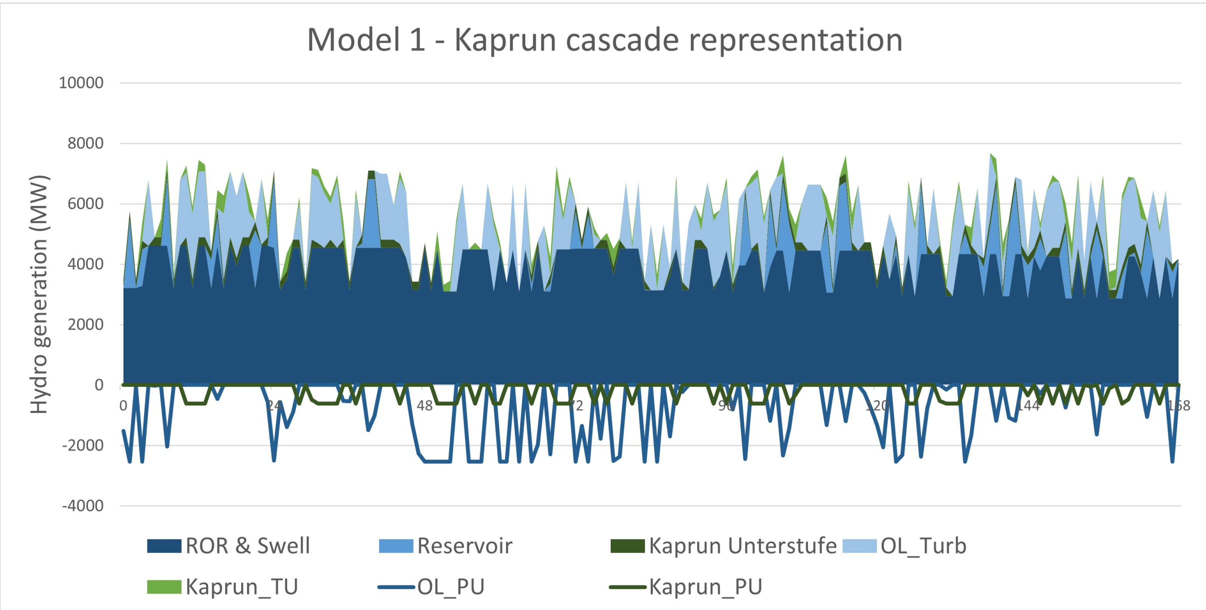


**Figure 6.14:** Hourly results of reservoir and OL production separating Kaprun power plant group for the week July 05 to 11 in target year 2025 - Model 1 of Table 6.1

Summarizing the above, the test calculations showed, that

- a more detailed representation of the hydropower fleet is of value
- the total yearly used hydro energy amount increases when separating the power plant group from the aggregated Austrian cluster
- increasing the model complexity and the amount of data collection increases, but can be applied for more detailed national sensitivities
- due to the increased amount of data which needs to be collected, this approach needs to be weighted in case of european-wide deployment

## 6.5 Results of an approach for the representation of additional storage components

In addition to the storage options resulting from large hydro reservoirs, this chapter discusses the storage capacities of market-participating batteries and flexible demand components such as heat pumps and electric vehicles and their impact on the adequacy results.

In a first step, the estimated quantity of market-participating batteries in the trilateral test model is estimated based on the ERAA 2022 input data. As already described in chapter 3.2.3, the development of market participating batteries is difficult to predict and two sources of development targets are discussed in this work. The estimate of the AIT study with a total amount of 68 MW and 102 MWh in 2030 compared with the estimates of the OENIP [2] with an estimated battery storage charge and discharge power of 1284 MW and 2568 MWh storage size.

Table 6.16 provides an overview of the different quantities of market participating batteries implemented in the trilateral test model. The amount is gradually increased until the targets published in the OENIP are reached.

**Table 6.16:** Installed capacities of market participating batteries for the target year 2025

| | target 2025 | target 2030 | 10 × target 2030 | OENIP 2030 |
|---|---|---|---|---|
| charge-/discharge | 33 MW | 68 MW | 680 MW | 1284 MW |
| storage size | 50 MWh | 102 MWh | 1020 MWh | 2568 MWh |
| total AT demand | 76 TWh | 90 TWh | | |

First the impact of this stepwise increase of market-participating batteries and their impact on adequacy indicators for Austria is compared based on the average of 700 Monte Carlo simulations executed[2]. Table 6.17 lists the adequacy indicators as an average over all 700 Monte Carlo simulations performed with the geographically reduced trilateral test model. In this trilateral test model, which is based on the ERAA data set from 2022, the scarcity situation varies due to different processing of the input data from the transmission system operators. The scarcity indicators in the trilateral model are higher than in previous test models based on ERAA input data from 2021 and earlier. In any case, the model serves as the basis for academic test calculations and is therefore used for the models evaluated in this chapter.

**Table 6.17:** Adequacy results of the trilateral test model (Model 2 from Table 6.1) using ERAA 2022 input data for the implementation of market participating batteries for the target year 2025 - average values of 700 Monte Carlo simulations -battery developments used as targets defined in Table 6.16

| | target 2025 | target 2030 | 10 × target 2030 | OENIP 2030 |
|---|---|---|---|---|
| LOLE | 228.3 h | 228.1 h | 226.0 h | 223.7 h |
| delta LOLE | | −0.1 % | −1.0 % | −2.0 % |
| EENS | 371 GWh | 371 GWh | 368 GWh | 366 GWh |
| delta EENS | | −0.1 % | −1.0 % | −1.3 % |

In the various penetration scenarios of the market-participating batteries, the charge and discharge power of batteries is gradually increased. The AIT estimates for the target year 2025 with a charge and discharge power of 33 MW and a storage size of 50 MWh are taken as a starting point. In this base model, the LOLE is 228,3 hours with an EENS of 371 GWh. Gradually, charge and discharge power is increased until the OENIP estimates are reached, resulting in a LOLE of 223,7 hours for the trilateral test model. This reduction in LOLE corresponds to approximately −2.0 % and an EENS reduction of approximately −1.3 % in the evaluation of the trilateral test models. These figures from the average adequacy results appear low, so the results for the individual climate year 1985 are extracted and compared and presented in Table 6.18.

**Table 6.18:** Adequacy results of the trilateral test model (Model 2 from Table 6.1) for the implementation of market participating batteries for the target year 2025 - excerpts from the Climate Year 1985

| | target 2025 | target 2030 | 10 × target 2030 | OENIP 2030 |
|---|---|---|---|---|
| LOLE | 841 h | 840 h | 829 h | 821 h |
| delta LOLE | | −0.1 % | −1.4 % | −2.4 % |
| EENS | 1487 GWh | 1487 GWh | 1487 GWh | 1487 GWh |
| delta EENS | | 0.0 % | −0.5 % | −0.8 % |

[2]The adequacy indicators of the test models must not be compared with the real adequacy results from the European process, as the geographical scope of the models is reduced, thus enabling the comparison of different modeling attempts with their effects on adequacy indicators

A similar distribution of the adequacy indicators is retrieved when only comparing results of the climate year 1985. In this case the absolute LOLE for the base model lays at 841 hours decreases to 821 hours in the case of OENIP targets, which corresponds to a LOLE reduction of −2.4 %. EENS reduction results in −0.8 % compared to the base model. The figures for the climate year 1985 remain in the order of magnitude of LOLE and EENS reduction as for the average results.

In a second test case, the modeling approach for short cycle storage is also applied to the demand components electric vehicles and heat pumps, whereby the initial value of a 5 % flexible share of EVs and HPs is gradually increased to 50 % in a scenario framework. Table 6.19 lists the applied charging and discharging power as well as the storage capacity for the test cases performed. The flexible share of electric vehicles and heat pumps is applied to the model as described in chapter 5.2. To represent the flexible share of electric vehicles and heat pumps, a 6-hour interval is used in which the storage size is forced to reach 50 % of the filling level again at the end of the 6-hour cycle. In between, the electric vehicles and heat pumps charge and discharge in the same way as the batteries participating in the market.

**Table 6.19:** Installed amount of charge and discharge power for market participating batteries for the target year 2025

| amount of flexible share for implicit Demand Side Response | Base 0 % | +5 % | +10 % | +20 % | +50 % |
|---|---|---|---|---|---|
| EV charge-/discharge | 0 MW | 23 MW | 45 MW | 90 MW | 226 MW |
| EV storage size | 0 MW | 135 MWh | 271 MWh | 542 MWh | 1354 MWh |
| HP charge-/discharge | 0 MW | 199 MW | 399 MW | 797 MW | 1993 MW |
| HP storage size | 0 MW | 1196 MWh | 2391 MWh | 4783 MWh | 11 957 MWh |

Table 6.20 provides an overview of the adequacy indicators that are achieved by gradually increasing the proportion of flexible HPs and EVs until a flexible share of 50 % is reached.

**Table 6.20:** Adequacy results of the trilateral test model (Model 2 from Table 6.1) for the implementation of electric vehicles and heat pumps for the target year 2025 - average values of 700 Monte Carlo simulations

| amount of flex share for iDSR | Base 0 % | +5 % | +10 % | +20 % | +50 % |
|---|---|---|---|---|---|
| LOLE | 228.3 h | 227.8 h | 227.5 h | 226.9 h | 225.9 h |
| delta LOLE | | −0.2 % | −0.4 % | −0.6 % | −1.1 % |
| EENS | 371 GWh | 370 GWh | 369 GWh | 369 GWh | 367 GWh |
| delta EENS | | −0.3 % | −0.5 % | −0.5 % | −1.1 % |

According to the results of the Table 6.20, the effects on the LOLE and EENS adequacy indicators only improve by −1.1 % if the flexible share of EV and HP is increased to 50 % and the results of 700 Monte Carlo simulations are extracted.

Summarizing the results of the two scenarios conducted in this chapter, it can be concluded that the battery amount estimated by the orientation towards the German market is a very low estimate and has no influence on the adequacy results. The battery distribution as assumed by OENIP influences the adequacy results in the trilateral test model with −2.0 % LOLE and −1.3 % EENS improvement.

The introduction of the flexible share of heat pumps and electric vehicles remains with a very small LOLE improvement of −0.2 % in the case of a 5 % flexible share and a LOLE improvement of −1.1 % in the case of a 50 % flexible share when using the geographically reduced test. These results, obtained in this geographically reduced test environment, show no significant deviation in the adequacy indicators for this model. This suggests that the trilateral test model is not the optimal test environment for the investigating short cycle storage components.

Based on these finding, the two above-mentioned test cases are combined in a final step and implemented in a pan-European model. 350 Monte Carlo simulations are performed and the adequacy indicators are compared. The base model contains the low estimated battery figures with a charging and discharging power of 33 MW and a storage size of 50 MWh combined with a 5 % flexible share of HPs and EVs. This model is compared with the implementation of the battery figures with a charging and discharging power of 1284 MW and a storage size of 2568 MWh in combination with a 50 % flexible share of HPs and EVs.

Table 6.21 shows the results of the full pan-European model - the base case is compared with the higher battery figures and the flexible share of HPs and EVs of 50 %.

**Table 6.21:** Adequacy results of the full European model (Model 3 from Table 6.1) for the implementation of a flexible share of EVs and HPs of 50 % and OENIP battery figures for the target year 2025 - average values of 350 Monte Carlo simulations

| | Base | OENIP battery & 50 % iDSR |
|---|---|---|
| LOLE | 1.17 h | 0.64 h |
| delta LOLE | | −45.3 % |
| EENS | 71.22 GWh | 0.723 GWh |
| delta EENS | | −99 % |

The average results of the adequacy indicators in the pan-European model show a reduction of the LOLE by −45.3 %, with the average LOLE values decreasing from 1.17 h to 0.64 h in the case of implementing the high battery share in combination with 50 % flexible share of EVs and HPs.

Table 6.22 shows the results of the pan-European model in the base case compared to the higher battery figures and 50 % flexible share of HPs and EVs for the climate year 1985 only.

**Table 6.22:** Adequacy results of the full European model (Model 3 from Table 6.1)for the implementation of 50 % flexible share of EVs and HPs and OENIP battery figures for the target year 2025 - results of the individual climate year 1985

| | Base | OENIP battery & 50 % iDSR |
|---|---|---|
| LOLE | 19 h | 9 h |
| delta LOLE | | −52.6 % |
| EENS | 21.67 GWh | 13.14 GWh |
| delta EENS | | −39.4 % |

The results of the climate year 1985 confirm the LOLE reduction of −52.6 % for the single climate year and an EENS reduction of −39.4 % from 21.67 GWh in the base case to 13.14 GWh in the case of the implementation of the high battery share and 50 % flexible share of EVs and HPs.

**Proposed approach:** Implementing market-participating batteries and flexible share of EVs and HPs as a starting point using the developed approach for short cycle representation is a starting point, with the following findings:

- using the trilateral test model (Model 2 from Table 6.1) is not a suitable test environment for short cylce storage representation
- impact on adequacy indicator changes remain low in the trilateral test model <3 %
- using the pan-European model (M3 from Table 6.1) results in a greater reduction of Adequacy indicators with a reduction of the LOLE by −50 % and EENS by −99 %

Test calculations with the short cycle storage approach developed in this work serve as a starting point for investigations into the behavior of the flexible share of heat pumps and electric vehicles as well as market-participating batteries. In the pan-European model, an influence on the adequacy indicators can be observed, while the trilateral test model does not appear to be suitable for the test calculations.

Further research into the different behavior of batteries must be carried out in the future. In particular, the Austrian transmission grid operator is investigating the inclusion of batteries behind the meter in order to include them in the demand forecast in the future (e.g. peak load limitation, grid support, etc.).

# 7 Conclusions and Outlook

The analysis conducted in this thesis summarize the developments in the representation of hydropower in the context of resource adequacy modeling using the Antares tool, which was specifically developed for resource adequacy studies.

Following the study of the first probabilistic European resource adequacy analysis, which started with the Mid Term Adequacy Forecast 2017 models, some development streams were identified and improvements in the representation of hydropower were started. This chapter summarizes the developments proposed for the representation of hydropower and concludes with the results for short cycle storage to be implemented for the modeling of implicit Demand Side Response resulting from heat pumps and electric vehicles, as well as a representation for market-participating batteries.

1. Traditional Reservoir and Open Loop Pump Storage

In this thesis, the hydro pre-optimization approaches of Antares for the hydropower types traditional reservoir and open loop pump storage are first discussed and the results of using the Antares heuristic, as described in chapter 2.6.1, are compared with the results of a water value approach. Two possible approaches are discussed to determine the water value matrix that is entered into Antares when using the water value functionality. First, a sophisticated approach with dynamic programming according to Bellman's optimality principle (see chapter 2.6.2) is performed for an ERAA 2022 model. Secondly, a simplified approach to calculate the water values is performed by using the marginal costs of a previous calculation (e.g. by applying the Antares heuristic) and assigning them to two different cost values: the level between the lower reservoir level rule curve and the mean reservoir level is assigned a higher cost value and the level between the mean reservoir level and the upper reservoir level rule curve is assigned a lower value. This calculation can be done by hand in reasonable amount of time and is therefore faster to use compared to the dynamic programming approach. These two attempts using the water value functionality are compared with the Antares heuristic, which uses the internal pumping functionality since Antares version 7. The approach of using the Antares heuristic with the internal pump functionality is compared against the original approach where the pump functionality in Antares is implemented by two virtual nodes which imply a round-trip efficiency of the pump storage unit via binding constraints. The results of this first comparison of modeling outputs with historic values led to the realization that Antares internal pump functionality in combination with the Antares heuristic (scenario B) has the lowest consumption of hydropower pump storage.

The results of scenario B show $-33\,\%$ less pump activity in the model results of the climate year

2016 compared to historical measured values from 2016 up-scaled to installed capacity in the target year of the model. The results of the hydro pre-optimization with water values retrieved via dynamic programming lead to a turbine utilization that only deviates by 1 % compared to historical values. The pump energy deviates with 14 % less consumption compared to the historical values and leads to the recommendation that the Antares water value functionality is to be used in combination with the internal pump functionality. Since the calculation of water values using dynamic programming is very time consuming, one reservoir type per country node leads to several hours on a server machine, the results show that even the simplified approach of using marginal prices from a previous calculation is an acceptable way to model hydropower pumped storage in Antares.

**The approach in which the water values are determined on the basis of the marginal prices of a previous calculation (scenario D), leads to a deviation of −0.01 % for the turbined energy and −13.5 % for the pumped energy and can therefore be recommended for future use.**

Comparing the hourly results of the four modeling attempts, it is clear that the number of hours with zero production is very high for hydropower pumped storage and traditional reservoir (about 7400 hours per year) for all four scenarios examined. Antares seems to use hydropower pumped storage and traditional reservoir mainly for peak production, with most events occurring at maximum turbine or pump power, while the historical values show that traditional reservoirs are used in all hours of the year. This finding have to be further elaborated, initial feedback is discussed with RTE R&D. For the modeling of resource adequacy, it can be assumed that this behavior is acceptable, since the availability of hydropower with maximum available generation is given in scarcity situations.

2. Short cycle representation for Closed Loop pump storage units

The second focus of this work is on the representation of closed loop pump storage, which includes hydro reservoirs without natural inflows. In the initial representation to represent the pumping behavior with Antares, two additional virtual nodes are connected to the country node to imply the pumping behavior as described in chapter 4.1, with the disadvantage that the reservoir limits cannot be respected. Until the introduction of Antares version 7, in which the pumping functionality was officially included, an approach was established that uses thermal units and links restricted by binding constraints to mimic the pumping behavior with the possibility of tracking the reservoir size. This approach served as the basis for the representation of different types of short cycle storage and is described in chapter 4.3.1. Since the introduction of Antares version 7, the pumping functionality for closed loop pump storage plants can be used in combination with the water value functionality, making it possible to specify the size of the reservoir and thus respect the limits of the closed loop reservoir within its physical boundaries. The annual results show that the turbine and pump utilization of closed loop pump storage plants increases with the two developed scenarios, but still remains at a low level. In the trilateral test model, which includes the three country nodes Austria, Switzerland and Italy North, the operation of closed loop pump storage hydropower plants remains below 350 hours per year. This shows that the trilateral model is not be the best environment for investigating short cycle storage. Although the trilateral test model is under constant scarcity, the turbine and pump activity of closed loop pump storage remains too low. The implementation of the closed loop pump storage in the full pan-European model leads to a utilization with up to 1700 hours, which is considered more realistic. The two modeling options developed show that the boundaries of the reservoir can be considered in both scenarios. The implementation of the two approaches in the pan-European model leads to similar improvements in the LOLE and EENS adequacy indicators (reduction of LOLE by 55 % for the average of 350 Monte Carlo simulations).

**Since the implementation of short cycle storage (scenario C) can be modeled for the entire European perimeter with only two additional nodes, it is recommended that this approach be used in future adequacy calculations to represent closed loop pump storage.**

3. Swell Representation

When the new database format PEMMDB 3.0 was introduced in 2019, initial assessments of the new format showed that the inflow time series of run of river and swell were merged in a common time series. This resulted in the implementation in the tool dispatching the merged time series immediately without providing any kind of storage option. In reality, swell units follow a daily storage behavior and amount to about 22 % of the total run of river and swell hydropower turbine power in Austria. For this reason, APG showed great interest in an appropriate modeling of this type of hydropower plant. This thesis discusses three possible representations of how the separation of run of river and swell inflows can be incorporated into resource adequacy modeling.

At the beginning, the combined inflow is divided proportionally to the installed turbine capacity. The three described modeling approaches represent the storage potential of swell units once with an additional swell node connected to the country node and including binding constraints. These constraints are used to allocate the daily energy for swell generation based on the inflow split (see chapter 4.4.1). A second approach applies the attempt for short cycle storage as developed for the closed loop pump storage, but additionally considers the inflow for swell (see chapter 4.4.2). A third approach uses the water value functionality, where water values in the matrix below 50 % get a high water value and above 50 % a low water value. This approach is described in chapter 4.4.3. The three modeling attempts are tested and compared in a trilateral test model using ERAA 2021 input data.

The first approach, which uses binding constraints and implies daily energy amounts, leads to a deterioration of the adequacy indicators with 30 % for LOLE and 34 % for EENS. The approach with the water value functionality improves the LOLE and EENS indicator by -20 % and the approach with the short cycle storage improves the LOLE indicator by -37 % and EENS by -14 %. The hourly dispatch of one week in January and one week in July is compared with historical measured values from 2021. This historical data was available in APG, but does not go back to the year 2016, thus no direct comparison with climate years extracted from the model is possible. The graphical visualization shows, that the behavior of the approach with the short cycle representation comes closest to reality, with some band production during the day and few peak hours, which is also confirmed by the highest correlation index and the lowest nRMSE value.

**It is therefore recommended that the approach developed for the short cycle representation is also applied to the swell representation.**

After discussing the results of this work, which were also presented at a CIGREE SEERC conference [84], ENTSO-E was asked to separate the inflow time series for run of river and swell inflows. This reintroduction of the split was achieved in 2021 for the ERAA 2022 data collection.

4. Cascade Representation

Due to Austria's unique location in the center of Europe, but also in the middle of the Alps, both the traditional reservoirs and the open loop pump storage power plants are located in the mountainous region of the Austrian Alps. This fact raises the question of whether it is sufficient to model all Austrian pumped storage units in a common cluster. This question applies to all European countries, but is discussed in detail in this thesis for the Austrian open loop power plant cascade Kaprun. Most of the open loop pump storage plants in Austria operate in a cascade system, i.e. the water from an upper reservoir basin is turbined by the upper turbine units, enters the lower reservoir basin and is then further utilized by the turbine units connected to the lower reservoir. The level of the lower basin depends on the pump and turbine activities of the upper units, is fed by a natural inflow and the stored hydro energy is utilized by the turbine units connected to the lower reservoir. Despite the fact that industrialized market modeling tools already contain predefined objects for modeling a cascade system, chapter 4.5 describes an approach how to model a cascade system in Antares using the available features. The representation is tested in an isolated test model based on ERAA 2021 input data, where only the country node of Austria is specified, and leads to a 50 % reduction in LOLE when the Kaprun cascade is separated.

**This is a clear indication that the separation of larger cascade systems is reasonable in resource adequacy assessments.**

5. Additional storage components

After discussing the modeling attempts for an improved representation of hydropower, the question arises whether a representation is available to also consider the future storage components resulting from market-participating batteries or a flexible share of implicit demand side response by electric vehicles or heat pumps. These can change their charging or discharging behavior according to the price signals. The short cycle approach developed for closed loop pump storage plants, as discussed in chapter 4.3.1, is applied to the representation of market-participating batteries. Instead of a weekly cycle forcing an initial reservoir level of 50 % at the end of a cycle, a daily cycle is assumed for batteries and a 6 hour cycle for electric vehicle and heat pumps. Determining the future penetration rates is a challenge upfront the modeling. Therefore, different penetration rates of market-participating batteries are discussed and for electric vehicle and heat pumps a variation of the flexible share is discussed between 5 % to 50 % of the total electric vehicle and heat pump demand. In the official European procedures, a flexible share of 5 % is currently used for these components. In this work, the proportion is gradually increased and the adequacy indicators compared. In the case of the trilateral test model based on the ERAA

2022 input data, increasing the flexible share of EVs and HPs does not have a large impact on the averaged LOLE and EENS of 700 Monte Carlo simulations. The LOLE indicator decreases by −1.1 % if 50 % instead of 5 % flexible shares of EVs and HPs are assumed for Austria. This is not a significant change compared to the test model in the trilateral test model setup. A range of 33 MW and 50 MWh to 1284 MW and 2568 MWh is determined for the various penetration rates of the market-participating batteries. With regard to adequacy indicators, a reduction in the average LOLE of −2 % and EENS of −1.3 % can be achieved, which is in the same order of magnitude as the individual results for the climate year 1985.

If the geographical scope is extended to the pan-European model, and the two test cases are combined, assuming a flexible share of 50 % for electric vehicle and heat pumps and the OENIP penetration rates for batteries, the results show a larger effect. For the average over 350 Monte Carlo simulations in the pan-European model, the LOLE values decrease by about −50 % in the average results. This example shows that the test calculations performed in the trilateral test model are not an adequate test environment for investigating the short cycle storage. The results of the pan-European model show a significant impact on the adequacy indicator with −50 % for the average over all 350 Monte Carlo simulations. **As a result of the work carried out as part of this thesis, it is recommended that the calculations for future penetration rate tests be carried out over a larger geographical area, such as the pan European model.**

**Summary**

To summarize the above findings, it can be said that a precise representation of hydropower generation is important for Austria. A first achievement was the introduction of splitting the hydro run of river and swell inflows and its modeling attempt introduced in ERAA 2022. The Antares pre-optimzation using water values (simplified calculation using the marginal price of a previous calculation) and internal pumping functionality is an acceptable way to move forward with Antares hydro representation and the hydro pre-optimization. The short cycle storage representation shows too few pump and turbine hours in the geographical reduced test model. Investigations are underway at the french transmission system operator, while the closed loop representation is not the highest priority for the Austrian transmission system operator, as only one project with a comparably small turbine and pump power is listed until 2030. No closed loop pump storage plant is in operation in Austria in 2024. However, the developments in modeling the different types of short cycle storage are not yet completed and must be continued, as the same representation is used for the storage components coming from the demand side.

Estimates for the penetration of the flexible share of electric vehicle and heat pumps are discussed in this thesis and the results of the geographically reduced test models show little impact on the averaged adequacy results for Austria. A larger impact is seen when comparing the results of the pan-European model, which combines the two extreme penetration cases. However, penetration rates are difficult to predict, which is why further research is recommended to present the flexible demand components for the European system. In addition to the estimates on the penetration of these components, also the way they are implemented in the system also needs to be discussed further.

### Outlook and open questions

Advanced methods for representing hydropower in resource adequacy assessments are discussed in this thesis and some of them are already implemented in the operational European processes. The separation of the modeling of swell units as one example, advanced hydro pre-optimization as a second.

There are still some unanswered questions, which are summarized below and can be clarified in further research activities:

1. The amount of turbine and pump hours in the category of traditional reservoirs and open loop PSP in the model remains low compared to the historical measured values.

2. The representation of short cycle storage, as used for closed loop PSPs, with high turbine and pump power in combination with a comparatively small reservoir size leads to results with a low number of operating hours.

3. The separation of the larger hydropower cascades from the aggregated cluster has an impact on the adequacy results:

    - The round-trip efficiency for the individual Austrian units appears to be higher than the value estimated across Europe. Discussions must be initiated with the power plant owners so that individual efficiency values can be used for national adequacy assessments for the larger units.

    - The question of splitting the inflow in relation to the size of the reservoir must be assessed. In real operation, the estimation of inflows is a very complex part. Further ideas for the estimation of inflows based on the European approach needs to be discussed for the Austrian adequacy models.

The following investigations have already been reported to and are being investigated by RTE:

- Antares hydro pump consumption, which is comparably low when using the Antares heuristic in combination with the internal pump functionality.

- The high number of zero production hours for storage units compared to historical measured values, where Antares has a comparable low number of utilization hours.

- The developed approach for short cycle storage is implemented as an object for Antares users in order to avoid the manual procedure described in this thesis.

# Bibliography


[1] "Antares", Accessed: 2024-4-18. [Online]. Available: https://antares-simulator.org/.

[2] Bundesministerium für Klimaschutz, Umwelt Energie, Mobilität, Innovation und Technologie, "Integrierter österreichischer Netzinfrastrukturplan", Wien, 2023.

[3] E. Commission and D.-G. for Energy, "Clean energy for all Europeans", Brussels, 2019. [Online]. Available: https://energy.ec.europa.eu/topics/energy-strategy/clean-energy-all-europeans-package_en.

[4] E. Parliament, "Regulation (EU) 2019/943 OF THE EUROPEAN PARLIAMENT AND OF THE COUNCIL of 5 june 2019 on the internal market for electricity", Brussels, 2019.

[5] E. Parliamant, "Regulation (EU) 2019/941 OF THE EUROPEAN PARLIAMENT AND OF THE COUNCIL of 5 june 2019 on risk-preparedness in the electricity sector and repealing directive 2005/89/EC", Brussels, 2019.

[6] ENTSO-E, "Methodology for the European resource adequacy assessment in accordance with Article 23 of Regulation (EU) 2019/943 of the European Parliament and of the Council of 5 june 2019 on the internal market for electricity", Brussels, 2020.

[7] ENTSO-E, "Methodology for calculating the value of lost load, the cost of new entry and the reliability standard", Brussels, 2020.

[8] ENTSO-E, "Short-term and Seasonal Adequacy Assessments Methodology Proposal in accordance with Article 8 of the REGULATION (EU) 2019/941 of 5 June 2019 on risk-preparedness in the electricity sector and repealing directive 2005/89/EC", Brussels, 2020.

[9] ENTSO-E, "Ten Year Network Development Plan 2020", Brussels, 2020. [Online]. Available: https://tyndp.entsoe.eu/.

[10] ENTSO-E, "ENTSO-E target methodology for adequacy assessment", Brussels, 2014.

[11] ENTSO-E, "Mid Term Adequacy Forecast 2020", Brussels, 2020. [Online]. Available: https://www.entsoe.eu/outlooks/midterm/.

[12] ENTSO-E, "European Resource Adequacy Assessment 2021 Edition", Brussels, 2021. [Online]. Available: https://www.entsoe.eu/outlooks/eraa/2021/.

[13] "Plexos", Accessed: 2024-4-18. [Online]. Available: https://www.energyexemplar.com/plexos.

[14] "GRARE", Accessed: 2024-4-18. [Online]. Available: https://www.cesi.it/app/uploads/2020/01/GRARE_brochure.pdf.

[15] "BID3", Accessed: 2024-4-18. [Online]. Available: https://bid3.afry.com/.

[16] "PowrSym", Accessed: 2024-4-18. [Online]. Available: http://www.powrsym.com/PSM_Feb_2012%20RAB.pdf.

[17] "RTE france", Accessed: 2024-4-18. [Online]. Available: https://www.rte-france.com/en/home.

[18] "ELIA", Accessed: 2024-4-18. [Online]. Available: https://www.elia.be/.

[19] "Austrian Power Grid AG", Accessed: 2024-4-18. [Online]. Available: https://www.apg.at/.

[20] "Adequacy and flexibility study for Belgium 2024 - 2034", Accessed: 2024-7-14. [Online]. Available: https://issuu.com/eliagroup/docs/adequacy_flexibility_study_for_belgium_2024-203?fr=sOTBhNDYxOTUwMTY.

[21] "Les bilans prévisionnels", Accessed: 2024-7-14. [Online]. Available: https://www.rte-france.com/analyses-tendances-et-prospectives/les-bilans-previsionnels.

[22] G. Iotti, "Hydropower modelling in Mid-Term adequacy forecasts the peculiar case of Austria", M.S. thesis, Politecnico de Milano, 2020.

[23] "Tennet tso", Accessed: 2024-5-5. [Online]. Available: https://www.tennet.eu/de.

[24] "Das ist 50hertz", Accessed: 2024-5-5. [Online]. Available: https://www.50hertz.com/de/unternehmen.

[25] "PSE", Accessed: 2024-5-5. [Online]. Available: https://www.pse.pl/web/pse-eng.

[26] "Terna Driving Energy - Terna spa", Accessed: 2024-5-5. [Online]. Available: https://www.terna.it/en.

[27] "Eirgrid", Accessed: 2024-5-5. [Online]. Available: https://www.eirgrid.ie/.

[28] Pentalateral Energy Forum, "Generation adequacy assessment 2015", Brussels, 2015.

[29] Pentalateral Energy Forum, "Generation adequacy assessment 2018", Brussels, 2018.

[30] Pentalateral Energy Forum, "Generation adequacy assessment 2020", Brussels, 2020.

[31] Pentalateral Energy Forum, "Scientific support on methodological improvements of resource adequacy assessments prepared by the pentalateral energy forum", Brussels, 2022.

[32] ENTSO-E, "Mid term adequacy forecast 2019, appendix 2: Methodology", Brussels, 2019. [Online]. Available: https://www.entsoe.eu/outlooks/midterm/.

[33] ENTSO-E, "Mid term adequacy forecast 2019 - executive summary", Brussels, 2019.

[34] A. J. Wood, *Power Generation Operation and Control*. Wiley-Interscience Publication, 1996.

[35] "Mathworks", Accessed: 2023-4-8. [Online]. Available: https://www.mathworks.com/help/optim/ug/mixed-integer-linear-programming-algorithms.html#btwyo05.

[36] RTE, "Antares simulator 8.0.0 general reference guide", Paris, 2021.

[37] ENTSO-E, "Data collection guidelines for market data for ERAA 2021", Brussels, 2020.

[38] D.-E. Gharsallaoui, "Optimisation de la gestion des stocks hydrauliques dans un outil d'équilibre offre-demande", M.S. thesis, Mines ParisTech, Paris, 2021.

[39] K. Frauendorfer, H. Glavitsch, and R. Bacher, "Optimization in planning and operation of electric power systems", Thun, Switzerland, 1992.

[40] ENTSO-E, “European Resource Adequacy Assessment 2023 Edition”, 2023. [Online]. Available: https://www.entsoe.eu/outlooks/eraa/2023/.

[41] Bundesministerium für Klimaschutz, Umwelt, Energie, Mobilität, Innovation und Technologie, “ENTWURF zur öffentlichen Konsultation Integrierter nationaler Energie- und Klimaplan für Österreich Periode 2021-2030”, Wien, 2023.

[42] “DTU”, Accessed: 2024-4-18. [Online]. Available: https://data.dtu.dk/articles/dataset/Solar_PV_generation_time_series_PECD_2021_update_/19727239?file=35039788.

[43] ENTSO-E, “Hydropower modelling - new database complementing PECD”, Brussels, 2019.

[44] “Die Donau”, Accessed: 2024-4-23. [Online]. Available: https://www.verbund.com/de-at/ueber-verbund/kraftwerke/gewaesser/donau.

[45] “Speicherkraftwerk Gerlos”, Accessed: 2024-4-23. [Online]. Available: https://www.verbund.com/de-at/ueber-verbund/kraftwerke/unsere-kraftwerke/gerlos.

[46] “VERBUND-Pumpspeicherkraftwerk Malta Hauptstufe”, Accessed: 2024-4-23. [Online]. Available: https://www.verbund.com/de-at/ueber-verbund/kraftwerke/unsere-kraftwerke/malta-hauptstufe.

[47] “Energiespeicher Bernegger GmbH”, Accessed: 2024-4-23. [Online]. Available: https://esb.bernegger.at/.

[48] “Pumpspeicherwerk Goldisthal”, Accessed: 2024-5-21. [Online]. Available: https://www.hydroprojekt.de/projekte/wasserkraftanlagen/ansicht/pumpspeicherwerk-goldisthal/.

[49] “SMHI”, Accessed: 2024-5-5. [Online]. Available: https://www.smhi.se/en/q/Stockholm/2673730.

[50] M. Petz, G. Achleitner, B. Mihic, and R. Schürhuber, “Modelling of resource adequacy in the mid term adequacy forecast using a new europe wide database format - impact on hydro usage and its flexibility”, CIGRE SEERC, Vienna, 2021.

[51] S. Bauchinger, “Vergleich unterschiedlicher Modellierungsansätze zur Abbildung von Lauf- und Schwellkraft in europäischen Lastdeckungsanalysen”, University of Technology, Vienna, 2022.

[52] ENTSO-E, “Winter Outlook Report 2017/2018”, Brussels, 2017. [Online]. Available: https://www.entsoe.eu/outlooks/seasonal/.

[53] ENTSO-E, “Demand forecasting methodology v1.1. TF trapunta”, Brussels, 2019.

[54] European Commission and Directorate-General for Energy, “Stepping up europe’s 2030 climate ambition”, Brussels, 2020. [Online]. Available: https://eur-lex.europa.eu/legal-content/EN/TXT/HTML/?uri=CELEX:52020DC0562.

[55] W. Austria, “Wärmepumpe Austria”, Accessed: 2023-4-9. [Online]. Available: https://www.waermepumpe-austria.at/die-waermepumpe/kostenlose-umgebungswaerme.

[56] M. A. Lagler, “Influence of optimising prosumers on rural distribution networks”, Ph.D. dissertation, Graz University of Technology, 2021.

[57] M. Petz, J. Spreitzhofer, J. Hierzer, G. Achleitner, K. Misak, and A. Bres, “Wärmepumpenzuwachs in Österreich bis 2030 und dessen Auswirkung auf Lastprofile – Evaluieren von Sensitivitaeten am Beispiel eines Testmodells für europäische Lastdeckungsanalysen”, e&i Elektrotechnik und Informationstechnik, Springer-Verlag, 2020.

[58] Hartl, M., Biermayr, P., Schneeberger, A., Schöfmann, P., “Österreichische Technologie-Roadmap für Wärmepumpen. Bundesministerium für Verkehr, Innovation und Technologie. Berichte aus Energie- und Umweltforschung”, Vienna, 2016.

[59] “Meteonorm”, Accessed: 2023-4-8. [Online]. Available: `https://meteonorm.com/`.

[60] “Eurostat”, Accessed: 2023-4-8. [Online]. Available: `https://ec.europa.eu/eurostat/de/web/nuts/local-administrative-units`.

[61] “Idm Wärmepumpen”, Accessed: 2023-4-8. [Online]. Available: `https://www.idm-energie.at/myidm-energy`.

[62] “KNV Wärmepumpen”, Accessed: 2024-1-7. [Online]. Available: `https://www.knv.at/technologie/smart-price-adaption/`.

[63] “aWATTar”, Accessed: 2022-1-3. [Online]. Available: `https://www.awattar.at/services/`.

[64] F. Lehfuss, D. Meier, J. Hierzer, M. Petz, K. Misak, and D. Stahleder, “The electrification of transportation and ist impact on the austrian electricity demand curve with a special emphasis on european resource adequacy studies”, 17. Symposium EnergieInnovation, 16.-18.02.2022, Graz, 2022.

[65] I. E. Agency, “Global EV outlook 2021”, Paris, 2021. [Online]. Available: `https://www.iea.org/reports/global-ev-outlook-2021`.

[66] AGGM, “ONE100 - Österreichs nachhaltiges Energiesystem - Studie zur Identifikation der optimierten Zielinfrastruktur für ein 100 Prozent klimaneutrales Energiesystem in Österreich”, Austria, 2020.

[67] D. Stahleder, “Implementation of a real time capable, flexible and accurate electric vehicle model to holistically evaluate charging services and methods”, English, in *Proceedings of 7th Transport Research Arena TRA 2018*, Transport Research Arena TRA 2018 ; Conference date: 16-04-2018 Through 19-04-2018, 2018.

[68] “EV database”, Accessed: 2022-1-8. [Online]. Available: `https://ev-database.de/`.

[69] K. Liu, W. Jiangbo, Y. Toshiyuki, and T. Morikawa, “Exploring the interactive effects of ambient temperature and vehicle auxiliary loads on electric vehicle energy consumption”, in *Applied Energy*, 2018.

[70] B. für Verkehr Innovation und Technologie, “Österreich unterwegs 2013/2014”, Wien, 2016.

[71] P. Biermayr, S. Aigenbauer, C. Dißauer, *et al.*, “Innovative Energietechnologien in Österreich Marktentwicklung 2022”, Bundesministerium für Klimaschutz, Umwelt, Energie, Mobilität, Innovation und Technologie (BMK), 2023.

[72] “Wien Energie Positionen”, Accessed: 2024-1-21. [Online]. Available: `https://positionen.wienenergie.at/grafiken/energiespeicher-europa/`.

[73] Regelleistung-Online, “Update 2020: Weiteres Wachstum der Batteriespeicher im PRL markt”, 14.01.2021. [Online]. Available: https://www.regelleistung-online.de/update-2020-weiteres-wachstum-der-batteriespeicher-im-prl-markt/.

[74] Bundesnetzagentur für Elektrizität, Gas, Telekommunikation, Post und Eisenbahnen, “Genehmigung des Szenariorahmens 2019 to 2030”, 2018.

[75] Bundesnetzagentur für Elektrizität, Gas, Telekommunikation, Post und Eisenbahnen, “Genehmigung des szenariorahmens 2021-2035”, 2020.

[76] International Renewable Energy Agency, “Electricity storage and renewables: Costs and markets to 2030”, 2017.

[77] “DKE - VDE verband der elektrotechnik elektronik informationstechnik e.v”, Accessed: 2024-1-21, 2023. [Online]. Available: https://www.dke.de/de/arbeitsfelder/energy/netzintegration-von-speichern#:~:text=Im%20April%202023%20waren%20in,Prim%C3%A4rregelleistung%20zur%20Netzstabilisierung%20genutzt%20werden..

[78] “Eraa downloads”, Accessed: 2024-7-14. [Online]. Available: https://www.entsoe.eu/outlooks/eraa/2022/eraa-downloads/.

[79] ENTSO-E, “Europen Resource Adequacy Assessment 2023 - Annex 2 Methodology”, Brussels, 2023.

[80] F. Verrier, M. Doquet, R. Gonzalez, S. Lepy, and E. Momot, “A new tool for adequacy reporting of electric systems: ANTARES”, in *42nd International Conference on Large High Voltage Electric Systems 2008, CIGRE 2008*, 2008.

[81] “Kraftwerksgruppe kaprun”, Accessed: 2024-7-12. [Online]. Available: https://de.wikipedia.org/wiki/Kraftwerksgruppe_Kaprun.

[82] “ENTSO-E Transparency Platform - installed capacity per production type”, Accessed: 2014-1-24. [Online]. Available: https://transparency.entsoe.eu/.

[83] A. Haas, G. Iotti, M. Petz, and K. Misak, “Methodological developments for European Resource Adequacy Assessments”, 17. Symposium EnergieInnovation, 16.-18.02.2022, 2022.

[84] M. Petz, G. Achleitner, B. Mihic, and R. Schürhuber, “Modelling of resource adequacy in the mid term adequacy forecast using a new europe wide database format – impact on hydro usage and its flexibility”, Vienna, 2021. [Online]. Available: https://energy.ec.europa.eu/topics/energy-strategy/clean-energy-all-europeans-package_en.